



TRIBHUVAN UNIVERSITY
INSTITUTE OF ENGINEERING
PULCHOWK CAMPUS

B-06-BAS-2018/23

**AERIAL MAPPING OF PARTICULATE MATTERS (PM 2.5 AND PM 10)
USING UNMANNED AERIAL SYSTEM (UAS)**

by

Abhimanyu Khadka (PUL075AER001)

Ashma Karki (PUL075AER007)

Kalbina Shrestha (PUL075AER016)

A PROJECT REPORT

SUBMITTED TO THE DEPARTMENT OF MECHANICAL AND AEROSPACE
ENGINEERING IN PARTIAL FULFILLMENT OF THE REQUIREMENTS FOR
THE DEGREE OF BACHELOR IN AEROSPACE ENGINEERING

DEPARTMENT OF MECHANICAL AND AEROSPACE ENGINEERING
LALITPUR, NEPAL

MARCH, 2023

COPYRIGHT

The author has agreed that the library, Department of Mechanical and Aerospace Engineering, Pulchowk Campus, Institute of Engineering may make this project report freely available for inspection. Moreover, the author has agreed that permission for extensive copying of this project report for scholarly purpose may be granted by the professor(s) who supervised the work recorded herein or, in their absence, by the Head of the Department wherein the thesis was done. It is understood that the recognition will be given to the author of this project report and to the Department of Mechanical and Aerospace Engineering, Pulchowk Campus, Institute of Engineering in any use of the material of this project report. Copying or publication or the other use of this project report for financial gain without approval of the Department of Mechanical and Aerospace Engineering, Pulchowk Campus, Institute of Engineering, and author's written permission is prohibited.

Request for permission to copy or to make any other use of this project report in whole or in part should be addressed to:

Head of Department

Department of Mechanical and Aerospace Engineering


Pulchowk Campus, Institute of Engineering

Lalitpur, Nepal

**TRIBHUWAN UNIVERSITY
INSTITUTE OF ENGINEERING
PULCHOWK CAMPUS**

DEPARTMENT OF MECHANICAL AND AEROSPACE ENGINEERING

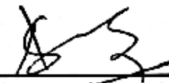
The undersigned certify that they have read, and recommended to the Institute of Engineering for acceptance, a project report entitled "**Aerial Mapping of Particulate matters (PM2.5 AND PM10) Using Unmanned Aerial System (UAS)**" submitted by Abhimanyu Khadka, Ashma Karki and Kalbina Shrestha in partial fulfillment of the requirements for the degree of Bachelor of Aerospace Engineering.



Supervisor, Dr. Nawraj Bhattarai

Associate Professor

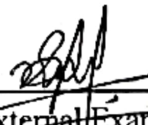
Department of Mechanical and Aerospace Engineering



Supervisor, Ashish Karki

Assistant Professor

Department of Mechanical and Aerospace Engineering



External Examiner, Er Siddhartha Paudel

Lecturer, Everest Engineering College



Committee Chairperson, Assoc. Prof. Dr. Surya Prasad Adhikari

Head

Department of Mechanical and Aerospace Engineering



16th March 2028

Date:

ABSTRACT

Air pollution has become one of the largest threats to the environment and human health globally. However, the conventional approach of measuring air quality relies on a limited number of stationary monitoring stations. This project aims to address this issue and proposes building an air pollution measurement system based on an Unmanned Aerial System (UAS). The project is divided into three parts: UAS design and fabrication, sensor integration and testing. Firstly, a fixed-wing UAS was designed and fabricated. The design and analysis were performed respectively and after the analysis a detailed CAD model was developed, and the fabrication process was started. After its construction, manual and autonomous flight tests were performed to ensure its functionality. Secondly, the PMS5003 sensor was selected for measuring the particulate matter while DHT-22 was selected for temperature and humidity measurement. The sensors were calibrated using the reference device Laser-egg 201 with the assumption that the data provided by laser-egg are accurate. A single-point calibration method, which just adjusts the offset, was implemented. The final test was performed with the sensor integrated into the UAS and the results obtained demonstrates the potential of using UAS for air pollution measurement.

Keywords: Fixed-Wing UAS, Particulate Matter (PM_{2.5}, PM₁₀), PMS5003T, DHT22

ACKNOWLEDGMENT

First of all, we would like to begin by expressing our deepest gratitude to the Department of Mechanical and Aerospace Engineering, IOE, Pulchowk Campus, Lalitpur, for providing us with the opportunity to work on this project and gain invaluable experience in the field.

Similarly, we would like to extend our heartfelt thanks to our supervisors, Associate Prof. Dr. Nawraj Bhattarai and Asst. Prof. Ashish Karki, for their continuous support, guidance, and motivation throughout the project. Their invaluable insights and constant encouragement have been instrumental, and we are deeply indebted to them for their contributions. It certainly wouldn't have been possible without them. We would also like to extend our sincere appreciation to Dr. Prateek Shrestha, our mentor, for providing us with his invaluable support and guidance.

We would also like to express our gratitude to Asst. Prof. Dr. Sudip Bhattarai for his invaluable advice and insightful suggestions throughout the project. We are also grateful to the head of Incubation, Innovation and Entrepreneurship Center (IIEC) for providing us with the workspace for the project. Additionally, we extend our thanks to the Director of Centre for Energy Studies (CES) for providing us with the Laser-Egg air pollution monitoring device, which was used for the calibration of the sensors.

Finally, we would like to thank our friends and both seniors/ juniors, for their support, encouragement, and suggestions throughout the project.

Abhimanyu Khadka (075AER001)

Ashma Karki (075AER007)

Kalbina Shrestha (075AER016)

TABLE OF CONTENTS

COPYRIGHT.....	ii
APPROVAL PAGE.....	iii
ABSTRACT.....	iv
ACKNOWLEDGMENT.....	v
TABLE OF CONTENTS.....	vi
LIST OF FIGURES	ix
LIST OF TABLES	xii
ABBREVIATIONS	xiii
SYMBOLS.....	xiv
CHAPTER 1: INTRODUCTION	1
1.1. Background	1
1.2. Problem Statement.....	2
1.3. Objectives	3
1.3.1. Main Objective.....	3
1.3.2. Specific Objectives	3
1.4. Applications	3
1.5. Features	3
1.6. Feasibility Analysis.....	4
1.6.1. Economic Feasibility	4
1.6.2. Technical Feasibility	4
1.6.3. Operational Feasibility.....	5
1.7. System Requirements.....	5
1.7.1. Software Requirements.....	5
1.7.2. Hardware Requirements.....	8
CHAPTER 2: LITERATURE REVIEW	10
2.1. History.....	10
2.2. Research Gap	10
CHAPTER 3: METHODOLOGY	14
3.1. Project Detail Flowchart	14
3.2. Sensors and Data Acquisition	15
3.3. UAS Design	16
CHAPTER 4: RESULTS AND DISCUSSION.....	19

4.1 UAS Design.....	19
4.1.1. Conceptual Design	19
4.1.1.1. Mission Requirements	19
4.1.1.2. Mission Profile	20
4.1.1.3. Weight Approximation / Maximum Takeoff Weight.....	20
4.1.1.4. Configurations Selection	21
4.1.1.4.1. Wing Location	21
4.1.1.4.2. Empennage.....	22
4.1.1.4.3. Propulsion System	24
4.1.1.4.4. Fuselage	25
4.1.2. Preliminary Design	26
4.1.2.1. Airfoil Selection	26
4.1.2.2. Wing loading (W/S) and Power loading (W/P) Estimation	27
4.1.3. Detail Design	28
4.1.3.1. Wing Design.....	28
4.1.3.2. Horizontal Tail Design	29
4.1.3.3. Vertical Tail Design	30
4.1.3.4. Control Surface Sizing	30
4.1.3.4.1. Aileron Sizing	30
4.1.3.4.2. Elevator and Rudder Sizing	31
4.1.3.5. Stability Analysis	31
4.1.3.5.1. Static Stability Analysis	31
4.1.3.5.2. Dynamic Stability Analysis	34
4.1.3.6. Final Design Specifications:.....	44
4.1.3.7. CAD Modelling.....	45
4.1.3.8. Manufacturing Process	47
4.1.4. Flight Test	51
4.2. Sensors & its System Development	53
4.2.1. Circuit Diagram	54
4.2.2. Sensor Housing and Setup	55
4.2.3. Sensors Calibration	57
4.2.3.1. PM2.5 and PM10 Calibration analysis.....	59
4.2.3.2. Temperature and Humidity Calibration Analysis	61

4.2.3.3. Sensors Field Validation	63
4.3. Data Acquisition and Processing.....	65
4.3.1. Working Mechanism.....	65
4.3.2. Setup	66
4.3.3. Data Processing and Analysis.....	67
4.4. Limitations.....	72
4.5. Problems Faced	72
4.6. Budget Analysis	73
CHAPTER 5: CONCLUSION AND FUTURE ENHANCEMENT.....	74
5.1. Conclusion	74
5.2. Scope for Future Enhancement	75
REFERENCES	76
BIBLIOGRAPHY	80
APPENDIX A.....	81
APPENDIX B	87

LIST OF FIGURES

- Figure 1.1: Graphical user interface of QgroundControl
- Figure 1.2: Pixhawk and its components
- Figure 3.1: Detail flowchart of the project methodology
- Figure 3.2: Detail flowchart for sensors methodology
- Figure 3.3: Detail flowchart of the project methodology
- Figure 4.1: Design process for the UAS design
- Figure 4.2: Mission profile for the UAS
- Figure 4.3: Thrust measurement of the selected motor
- Figure 4.4: Conceptual design from the initial configuration selection
- Figure 4.5: Constraint diagram
- Figure 4.6: Aileron sizing
- Figure 4.7: Elevator and rudder Sizing
- Figure 4.8: Pitching moment coefficient (C_m) Vs AOA (α) curve
- Figure 4.9: Rolling moment coefficient (C_l) Vs sideslip angle (β) curve
- Figure 4.10: Yaw moment coefficient (C_n) Vs sideslip angle (β) curve
- Figure 4.11: Root locus plot for longitudinal dynamic stability
- Figure 4.12: Root locus plot for lateral-directional dynamic stability
- Figure 4.13: Spiral mode at 15 deg (Bank angle VS time)
- Figure 4.14: Spiral mode at 15 deg (Altitude VS time)
- Figure 4.15: Spiral mode at 19 deg (Bank angle VS time)
- Figure 4.16: Spiral mode at 19 deg (Altitude VS time)
- Figure 4.17: Spiral mode at 25 deg (Bank angle VS time)
- Figure 4.18: Spiral mode at 25 deg (Altitude VS time)
- Figure 4.19: Dutch roll (Yaw Angle VS time)
- Figure 4.20: Short period (Pitch Angle VS time)
- Figure 4.21: Phugoid mode (Pitch Angle VS time)
- Figure 4.22: Phugoid mode (Altitude VS time)
- Figure 4.23: Wing structure
- Figure 4.24: Wing assembly
- Figure 4.25: Horizontal stabilizer
- Figure 4.26: Vertical stabilizer

Figure 4.27: Boom assembly

Figure 4.28: Fuselage structure

Figure 4.29: Fuselage assembly

Figure 4.30: Empennage

Figure 4.31: Sensor box

Figure 4.32: Final CAD model

Figure 4.33: Laser cutting plywood for fuselage

Figure 4.34: Final assembled fuselage

Figure 4.35: Cutting airfoil shape in CNC hot wire cutter

Figure 4.36: Empennage assembled with servo attached

Figure 4.37: Wing and motor mounted on fuselage

Figure 4.38: Final assembled UAS before test flight

Figure 4.39: Initial flight plan for UAS in QGroundControl interface

Figure 4.40: UAS path behavior w.r.t. to set waypoint

Figure 4.41: Circuit diagram for sensors operation

Figure 4.42: Final sensor setup for measurement

Figure 4.43: Variation of PM_{2.5} concentration w.r.t. speed

Figure 4.44: Variation of PM₁₀ concentration w.r.t. speed

Figure 4.45: Calibration setup

Figure 4.46: Comparison plot for PM_{2.5}

Figure 4.47: Corrected plot for PM_{2.5}

Figure 4.48: Comparison plot for PM₁₀

Figure 4.49: Corrected plot for PM₁₀

Figure 4.50: Comparison plot for temperature

Figure 4.51: Comparison plot for humidity

Figure 4.52: Comparison plot for PM_{2.5} after correction

Figure 4.53: Comparison plot for PM₁₀ after correction

Figure 4.54: Absolute error of PM_{2.5} vs Time

Figure 4.55: Absolute error of PM₁₀ vs Time

Figure 4.56: Wind speed profile on 7th March

Figure 4.57: Flight profile set for autonomous final flight test

Figure 4.58: Flight profile followed in autonomous final flight test

Figure 4.59: Variations of PM_{2.5} (a) and PM₁₀ (b) w.r.t. to UAS position

Figure 4.60: Variations of Humidity (a) and Temperature (b) w.r.t. to UAS position
Figure 4.61: Variations of PM2.5 (a) and PM10 (b) w.r.t. to UAS position
Figure 4.62: Variations of Humidity (a) and Temperature (b) w.r.t. to UAS position
Figure 4.63: Variation of PM2.5 concentration w.r.t. altitude (autonomous)
Figure 4.64: Variation of PM10 concentration w.r.t. altitude (autonomous)
Figure 4.65: Variation of PM2.5 concentration w.r.t. altitude (manual)
Figure 4.66: Variation of PM2.5 concentration w.r.t. altitude (manual)
Figure A1: W/S Vs W/P as a function of stall speed
Figure A2: W/S Vs W/P as a function of maximum velocity
Figure A3: W/S Vs W/P as a function of takeoff distance
Figure A4: W/S Vs W/P as a function of ROC
Figure A5: Constraint diagram form T/W approach
Figure A6: Drag required curve
Figure A7: Power required curve
Figure A8: Circuit diagram
Figure B1: Batch analysis of NACA 0012 airfoil
Figure B2: Batch analysis of SG6042 airfoil
Figure B3: Mass distribution from XFLR5
Figure B4: Aileron sizing guidelines
Figure B5: Laser-Egg 2+ model LE201

LIST OF TABLES

- Table 3.1: Methodology for the project
- Table 4.1: Weight distribution
- Table 4.2: Wing location decision matrix
- Table 4.3: Empennage configuration decision matrix
- Table 4.4: Propulsion system decision matrix
- Table 4.5: Comparing different airfoils for wing
- Table 4.6: Wing dimensions
- Table 4.7: Longitudinal stability derivatives
- Table 4.8: Lateral stability derivatives
- Table 4.9: Details of aircraft design
- Table 4.10: Material selection and manufacturing process
- Table 4.11: List of electronic for sensor setup
- Table 4.12: Statistics of data used for calibration process
- Table 4.13: Budget estimation
- Table B1: Power to weight ratio
- Table B2: Typical values of aspect ratio
- Table B3 Typical values of aspect ratio
- Table B4: Typical values of tail volume coefficient

ABBREVIATIONS

ABS	:	Acrylonitrile Butadiene Styrene
AQHI	:	Air Quality Health Index
AQI	:	Air Quality Index
CAD	:	Computer Aided Design
CAE	:	Computer Aided Engineering
CAM	:	Computer Aided Manufacturing
CNC	:	Computer Numerical Control
CO	:	Carbon Monoxide
COPD	:	Chronic Obstructive Pulmonary Disease
DHT	:	Digital Humidity and Temperature
ESC	:	Electronic Speed Controller
GPS	:	Global Positioning System
GUI	:	Graphical User Interface
MSL	:	Mean Sea Level
PLA	:	Polylactic Acid
PM	:	Particulate Matter
PTA	:	Purified Terephthalic Acid
UAS	:	Unmanned Aerial System
UAV	:	Unmanned Aerial Vehicle

SYMBOLS

AOA , α	:	Angle of attack
b	:	Span
C or c	:	Chord
Cd or C_d	:	Coefficient of drag.
CFx	:	Component integrated X force coefficient
CFy	:	Component integrated Y force coefficient
CFz	:	Component integrated Z force coefficient
c_{HT}	:	Coefficient for horizontal tail
Cl or C_l	:	Coefficient of lift
C_m	:	Coefficient of pitching moment
C_{mx}	:	Component integrated X moment coefficient
C_{my}	:	Component integrated Y moment coefficient
C_{mz}	:	Component integrated Z moment coefficient
c_{VT}	:	Coefficient for vertical tail
L	:	Rolling moment
L/D	:	Lift to drag ratio.
L_{VT}, L_{HT}	:	Distance between wing and vertical and horizontal tail MAC
M	:	Pitching moment
MAC	:	Mean aerodynamic chord
N	:	Yawing moment
Re	:	Reynolds number
ROC	:	Rate of climb
S	:	Area of wing
T	:	Thrust
W/S	:	Wing loading
X_{cg}	:	Distance of center of gravity from leading edge
X_{np}	:	Distance of neutral point from leading edge
β	:	Sideslip angle
ξ	:	Damping ratio
λ	:	Taper ratio
μ	:	Viscosity of air
ρ	:	Density of air

CHAPTER 1: INTRODUCTION

1.1. Background

Air pollution has become one of the largest threats to environment and human health globally, being 4th leading factor for early death worldwide [1] and responsible for death of 7 million people annually [2]. Air pollution has great impact on human health and according to the State of Global Air 2020 report, air pollution has contributed significantly to an increase in the risks of Chronic Obstructive Pulmonary Disease (COPD), ischemic heart disease, stroke, lung cancer, type 2 diabetes, and lower-respiratory infections.

Very minute particles and liquid droplets suspended in the atmosphere pose a significant health danger to humans. When inhaled, these particles can harm the heart and lungs, resulting in catastrophic health consequences. Particle size is closely related to their ability to cause health concerns. A combination of liquid droplets and solid particles present in the air is referred to as particulate matter (PM). Some particles are large enough or dark enough to be visible to the naked eye, such as dust, dirt, or smoke while others are so tiny that they can only be seen with an electron microscope. PM_{2.5} is defined as particulate matter with a diameter of less than 2.5 microns, such as combustion particles. PM₁₀ is particulate matter smaller than ten microns in diameter, such as dust, pollen, and mold. Particles smaller than 10 micrometers (PM₁₀) in diameter create the most issues since they may penetrate deep into the lungs and, in some cases, enter the bloodstream.

The climate and ecosystem of earth is also strongly influenced by air quality. Air pollution has quite an effect on environment and global climate causing acid rain, low visibility, global warming, ozone layer depletion etc. The measurement and monitoring of air pollution levels are essential for the health and safety of people, as it can help protect them from harmful effects caused by air pollution. Moreover, air pollution also directly affects the environment, making it crucial to take different measures to measure air quality.

In Nepal, the Air Quality Index (AQI) is used to assess the degree of air pollution in different regions. Nepal, being one of the most polluted countries has only 27 measuring stations to determine AQI of which there are only 7 stations inside the Kathmandu valley operated by The Ministry of Forests and Environment, Nepal [3]. Among the monitoring stations almost more than half are inoperable. There are also a number of monitoring stations in Nepal as part of the World Air Quality Project, but these are also insufficient for measuring air quality throughout the country. As a result, the measurement of air pollution relies on a limited number of fixed monitoring stations.

This project aims to address this issue and proposes building an air pollution measurement system based on an Unmanned Aerial System (UAS). An Unmanned Aerial System (UAS) is an aircraft flown without a pilot onboard and can be controlled remotely by a person or be fully autonomous. UAS have a wide range of applications, including aerial photography and videography, wildfire monitoring, surveillance, delivery, military applications, and so on. A fixed-wing UAS is used in this project because of its high endurance and payload capacity and greater stability compared to drones. Fixed wing UAS is similar to conventional plane and flies using the lift created by its wings. In contrast to the measurement of pollution that is limited to certain number of fixed monitoring stations, this system will cover more ground and will estimate air quality in areas without monitoring stations.

1.2. Problem Statement

Air pollution is a significant global challenge, posing serious threats to human health and the environment so, it is essential to measure and monitor its level accurately. However, the conventional approach of measuring air quality relies on a limited number of stationary monitoring stations. Additionally, while satellite mapping is also available and offers a more comprehensive approach, it can be complex and are not accessible to all. As a result, aerial mapping using UAS, equipped with low-cost sensors can present a viable alternative for the measurement of air pollution.

1.3. Objectives

1.3.1. Main Objective

The main objective of this project is:

- Design, fabricate and test a fixed wing UAS based air pollution measurement system.

1.3.2. Specific Objectives

The specific objectives of this project are:

- To design and fabricate a physical model of the fixed wing UAS.
- To select a feasible sensor for the project.
- To fabricate a suitable sensor box for the selected sensors.
- To develop and test the integrated system to acquire air quality data.

1.4. Applications

This project can be applied in various areas:

- Industrial sites where pollution measurement is more important.
- Research based where sensor box can be replaced with other applications.
- Heavily polluted areas where tracking air pollution is more urgent for the human health.
- Areas where monitoring stations are not available.
- Remote mapping of air pollution data

1.5. Features

The proposed system has following features:

- Fixed wing UAS
 - Wingspan: 1.6m, Weight: 2kg, Endurance: 2-3min, Max altitude: 50m
- Pollution measurement system
 - PMS5003T Sensor - PM1.0, PM 2.5, PM 10.0 (@ ± 10%)
 - DHT-22 Sensor - Temperature (@ ± 0.5 °C) and Humidity (@ ±2-5%)

1.6. Feasibility Analysis

1.6.1. Economic Feasibility

Several electronic components, including the transmitter, PX 4 controller, GPS module, telemetry, servo, and ESC, along with the necessary propulsion system components like brushless motors, were provided by the department which were essential for the project. Furthermore, the primary dust sensor (PM 2.5) was also supplied by our external mentor. As a result, the budget for this project was significantly reduced, and the cost of structural components and miscellaneous items such as tape, cutters, glue guns, adhesive bonds, and other small materials, were only to be managed which were affordable.

This project aims to use low-cost sensors that demonstrate an average correlation with reference to monitoring stations and other pollution measuring instruments that can be expensive. Additionally, the fabrication cost of the Unmanned Aerial System (UAS) is also very reasonable. Consequently, the UAS-based pollution measurement system represents an economical and cost-effective solution when compared to the high cost of reference instruments.

1.6.2. Technical Feasibility

The technological requirements of this project were both software and hardware for design, analysis, and flight testing, as well as fabrication tools. This project involved the design and fabrication of a fixed wing Unmanned Aerial System (UAS) and sensor box. For design and analysis tasks, software like XFLR 5, CATIA V5, and X-PLANE were utilized, which proved to be sufficient. Furthermore, there was the access to a flight simulator that facilitated the testing of the designed UAS. Regarding the fabrication process, several tools and machines were utilized, including a CNC laser cutting machine which was used to cut plywood into ribs and a CNC Hot wire cutter machine for shaping Styrofoam into the central structural part's required airfoil shape. Along with these machines, a 3D printer was also utilized to print various items such as servo connectors, boom mounts, tail mounts, and other miscellaneous components.

1.6.3. Operational Feasibility

The purpose of the project is to build a fixed wing UAS based pollution measurement system. It cannot, however, be commercialized until a proper regulation is established as there are no established guidelines and regulations specifically for operating UAS for air pollution measurement in Nepal.

1.7. System Requirements

1.7.1. Software Requirements

➤ XFLR5

XFLR is a free open-source tool for analyzing airfoils, wings, and planes at low Reynolds numbers. It incorporates direct and indirect airfoil, wing, and plane design analysis. With its assistance, we can generate numerous graphs and values to test an aircraft's static and dynamic stability.

➤ X-Plane

X-Plane is a tool used to predict the flight characteristics of fixed- and rotary-wing aircraft. It is an excellent tool for engineers to forecast the flight characteristics of their new planes and for aviation enthusiasts to investigate the field of aircraft flight dynamics. It can be used for a variety of tasks, including concept design and flight testing as well as flight training.

➤ Plane Maker

Plane Maker is software in cooperated with X-plane that lets the user design their own aircraft. It allows the detailed modeling of an aircraft from fuselage to instrumentation. You can input all the physical details, such as the weight, control deflections, wingspan, engine nacelles, landing gears, airfoil sections, engine power, airfoil sections, etc.

➤ **MATLAB**

MATLAB is a programming language software package designed especially for engineers and scientists to analyze and design systems and products. Its applications include data analysis, data exploration and visualization, mathematics and computation, algorithm development, simulation and prototyping, modeling, application development, including Graphical User interface (GUI) building, etc.

➤ **Arduino IDE**

Arduino IDE is open-source software designed and created by Arduino.cc used to write and upload codes to the Arduino boards. It runs on the Java Platform, which is compatible with all operating systems, including MAC, Windows, and Linux, and has built-in functions and commands that are necessary for debugging, editing, and compiling the code.

➤ **CATIA**

Computer Aided Three-Dimensional Interactive Application (CATIA) is product design and engineering software created by Dassault system. It cooperates Computer Aided Design (CAD), Computer-Aided Engineering (CAE) and Computer Aided Manufacture (CAM). It is mostly used in automotive, defense, aerospace, and industrial sector.

➤ **RD Works**

RD works is a tool that allows user to perform laser cutting and engraving operations. The software exports in “. rd" format for laser cutting and uses the "rld" file format to save graphic information, layer parameters, and the processing of graphic elements.

➤ **GRBL Hotwire Mega 5X**

Hotwire Mega 5X is Controller Software for 4-axis CNC Foam Cutters. It runs on the Arduino Mega 2560 with a RAMPS board. The working principle of GRBL consists of converting G-code motion commands into electromechanical signals to drive stepper motors according to the pre-defined motion and speed.

➤ UP Studio

UPSTUDIO is software used for several functions like model showing, model editor, model generator and model printing. It allows user for 3D printing.

➤ QGroundControl

QGroundControl provides full flight control and vehicle setup for PX4 or ArduPilot powered vehicles. It has a better graphic user interface. It provides easy and straightforward usage for beginners. A major advantage of QGroundControl that the real time data from telemetry can be easily plotted and visualized. Since QGroundControl has more features and an easy-to-use interface, it was selected for ground control station.

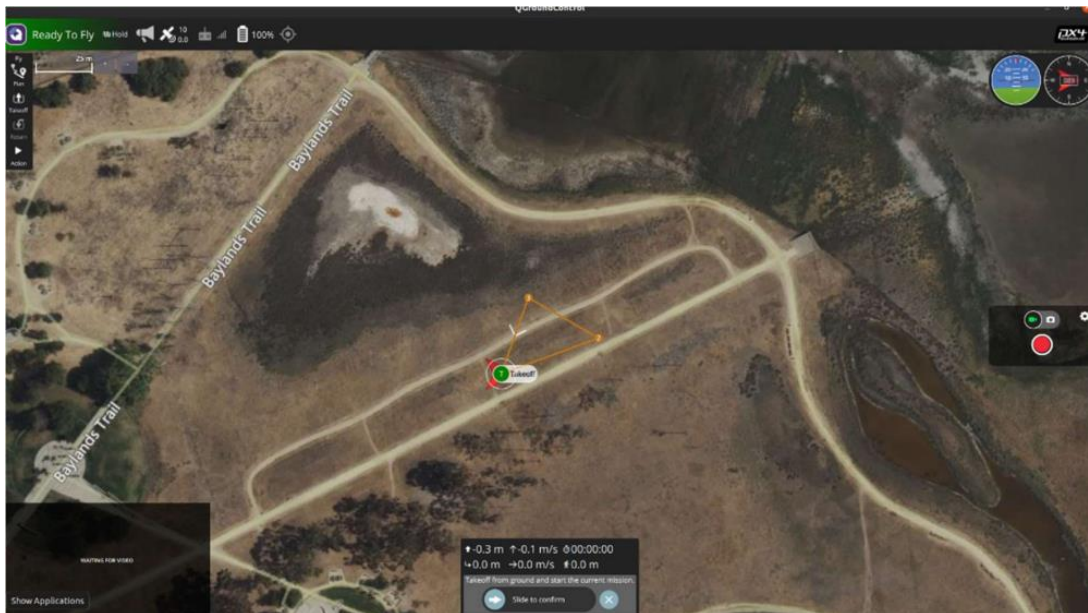


Figure 1.1: Graphical user interface of QGroundControl (Source: px4.io)

1.7.2. Hardware Requirements

➤ CNC Laser Cutter

CNC is a computerized manufacturing process in which pre-programmed software and code controls the movement of production equipment. In a CNC laser cutter, a material is marked, cut, or engraved to create specific shapes using a concentrated, powerful laser beam.

➤ CNC Hot Wire Cutter

CNC Hot Wire is a machine used to cut the Styrofoam into a desired shape. It is programmed using GRBL Hotwire Mega 5X.

➤ 3D Printer

3D Printer is a construction tool used to obtain three-dimensional object from a CAD model or a digital 3D model. It allows for the construction of more complex designs than traditional manufacturing processes. Materials like ABS, PLA, PTA can be used for its operations as required.

➤ Flight Simulator

A flight simulator is a device that artificially re-creates the experience of flying an aircraft. It is employed in the fields of education, research, and entertainment. There are different kinds of flight simulators, including desktop simulators, professional-grade simulators, full motion simulators, fixed base simulators, simulators for basic training, and virtual reality flight simulators.

➤ Control Stick

A control stick is a handheld device that is used to control movement in a computer game or simulation. Typically, it consists of a stick that may travel in various directions and a base with one or more buttons. A control stick functions by converting physical stick motion into computer-interpretable electrical impulses.

➤ **Mechanical Tools**

Normal hand tools like hammer, scale, drill machine, paper cutter, grinder, plier, etc.

➤ **Pixhawk (PX4)**

PX4 is an open-source flight control software for drones and other unmanned vehicles. It's a great piece of equipment that can transform any fixed-wing, rotary-wing, multirotor, or even boats and automobiles into a completely autonomous vehicle capable of executing a broad range of activities, including pre-programmed GPS missions with waypoints. It has compatible GPS module, Telemetry module, power management board and various other hardware's for the operation.



Figure 1.2: Pixhawk and its components (Source: alitools.com)

CHAPTER 2: LITERATURE REVIEW

2.1. History

Many researchers and organizations are interested in employing rotor wing UAV to collect data, while others are interested in employing fixed-wing UAVs, communication and mapping systems, sensor dependability, and so on. Although fixed-wing UAVs offer greater endurance, stability, and flexibility for sensor mounting points, they cannot hover and have low operating heights, whereas rotor-winged UAV have a slower speed, but allow for discontinuous routes, such as hovering, for obtaining close-proximity inspections and facilitates downwash effect due to rotor blade [4]. However, this downwash effect also disturbs the onboard measurement of the sensor data. It has been demonstrated that fixed-wing UAVs can also be employed for atmospheric measurements. The study focused on assessing the horizontal, vertical, and temporal variations of particulate matter (PM) within a 150m range from the ground [5]. To validate this approach, four test flights were conducted using a 3m fixed-wing model aircraft equipped with an aerosol spectrometer and the intake probe was installed in a cowl to ensure undisturbed air sample collection [6].

An AQI monitoring and mapping system was developed based on the MQ-9, MQ-135, and MQ-2 gas sensors using drone as the aerial vehicle platform [7]. Similarly, another study focused on measuring particulate matter using low-cost sensors placed on a drone, specifically examining the relationship between PM_{2.5} concentration and altitude [8]. In addition, combining an air quality sensor with an autopilot aboard a UAV system was proposed to be viable. The author demonstrated this concept by monitoring dust particles in open-pit mines after blasting with both fixed-wing and multi-rotor UAVs [9]. An autonomous flight control system was implemented in a fixed-wing UAV for spatiotemporal analysis of PM_{2.5} using a low-cost OPC R1 sensor. This approach aimed to identify pollution hotspots in urban areas, industrial regions, and smart cities, as well as locate burning sites [10].

Similarly, the most popular sensor for drones is a low-cost chemical sensor, which includes amperometric gas sensors (AGS), and metal oxide semiconductor (MOX or

MOS) sensors, non-dispersive infrared (NDIR) sensors, and photoionization detectors (PIDs) [11]. Moreover, another study explored the potential of using low-cost sensors to develop a real-time air pollutant monitoring system. The system focused on monitoring PM_{2.5}, PM₁₀, Carbon Monoxide (CO) gas, as well as temperature and humidity and sensors such as Figaro TGS 2600 for CO, SHARP DN7C3CA006 for PM_{2.5}, and SHARP GP2Y1010AU0F for PM₁₀ were used in the developed real-time system [12].

In a comparative analysis of three light scattering low-cost particle sensors, namely GP2Y1010AU0F (GP2Y), PPD42NS (PPD), and DSM501A (DSM), their performance was evaluated and compared to Side Pak measurements. The results showed that the GP2Y sensor exhibited the highest linearity throughout the experiments and the PPD and DSM sensors had relatively lower limits of detection compared to the GP2Y sensors [13]. Furthermore, the performance of the dust sensor GP2Y1010 can be enhanced through optimization of the capacitor and resistor in the external circuit, dark painting of the internal chamber of the dust sensor and focusing on the shielding of the dust sensor and circuit. Considering all these parameters resulted in a noise equivalent limit of detection of 3 gm⁻³ for PM detection [14].

Similarly, the use of the low-cost sensor PMS5003 was tested in two real-life settings: urban and suburban. The study demonstrated that when used correctly, low-cost sensors can provide remarkably good correlation with expensive reference instruments. The hourly average correlation of PM₁₀ concentrations was similar in both locations, while the daily average values achieved 90% correlation at the suburban location, indicating even better performance [15]. Additionally, the performance of two low-cost sensors, Plant tower PMS A003 and Shinyei PPD42NS, was evaluated and was observed that there was a sudden rise in concentrations of PM_{2.5} values due to the warming up of the sensors while developing the calibration model [16].

Further, the calibration process of the PMS3003 sensor was studied and discovered that PMS3003 can measure the PM_{2.5} concentrations within ~ 10% of ambient values if a proper RH correction factor from non-linear equations is embedded. Similarly, an 11% reduction in error is achieved if a quadratic fit is implemented rather than a linear fit

when the PM_{2.5} concentrations exceed 125 µg/m³ [17]. Likewise, the calibration strategy of SDS011 sensor was proposed with the Grimm1.108 as a reference instrument and presented that the ratio between PM₁₀/PM_{2.5} predicts the proper particle mass distribution [18]. Moreover, the portable measurement system for dust particles was proposed and they forwarded the idea of calibration and validation of sensors considering the temperature and humidity measured from the DHT22 sensor [19]. Among the various regression models like simple linear, non-linear, robust linear, etc. used for the calibration of low-cost sensors, robust linear regression using the Talwar method had the highest correlation of $R^2 = 0.8634$ with the Dustrak as a reference instrument [20].

The three available sensors, namely PMS5003 (Plantower), SPS30 (Sesirion), and SM-UART-04L (Amphenol) were studied. The study employed single-point calibration, two-point calibration, and multi-point curve correction methods and it was concluded that the PMS5003 sensor exhibited a relatively small standard error, measuring less than 15 µg/m³, across all parameter measurements [21]. Additionally, an offset and gain calibration model were utilized for pollution measurement, employing the ordinary least squares method [22]. The findings of their work were further supported by suggesting that a minimum of three months of field evaluation is necessary for the calibration of the setup [23].

Many efforts have been made in data acquisition, data presentation, and it plays a significant role in the visualization of the overall work. A handheld real time-based Arduino multi-sensor device was developed to measure different atmospheric pollutants, utilizing a Nova sense SDS011 sensor to acquire PM_{2.5} and PM₁₀ concentrations and the device was Bluetooth-connected to an Android smartphone app interface to transfer and display the data [24]. Furthermore, a system was introduced where air data is measured, collected, and transmitted to a ground station via radiofrequency and the ground station then processes the data and sends it to the internet [25]. Similarly, a LoRa and web UI-based approach was opted for data transfer and processing using the PMS5003T sensor, which measures PM_{2.5}, PM₁₀, temperature, and humidity [26]. Moreover, LabVIEW was also used to generate a graphical user interface (GUI) that allows users to easily visualize and saves real-time air quality data,

and Oasis Montaj software was also incorporated to create color contour plots which gives more in-depth visualization [27]. Lastly, a GIS/GPS-based pollution monitoring system was developed, allowing the evaluated data to be integrated into a map and viewed by relevant authorities in real-time [28].

2.2. Research Gap

Despite the growing interest in the use of Unmanned Aerial Systems (UAS) for air pollution monitoring, there is still a limited number of studies exploring the potential of fixed-wing UAS for air quality assessment. Although some research has been conducted on the use of drones for air quality monitoring, there is a lack of comprehensive studies that examine the effectiveness of fixed-wing UAS, so more research is needed to evaluate the feasibility and effectiveness of using fixed wing UAS for air pollution measurement. Additionally, there is a need for more research in using low-cost sensors in UAS for air pollution assessment.

CHAPTER 3: METHODOLOGY

3.1. Project Detail Flowchart

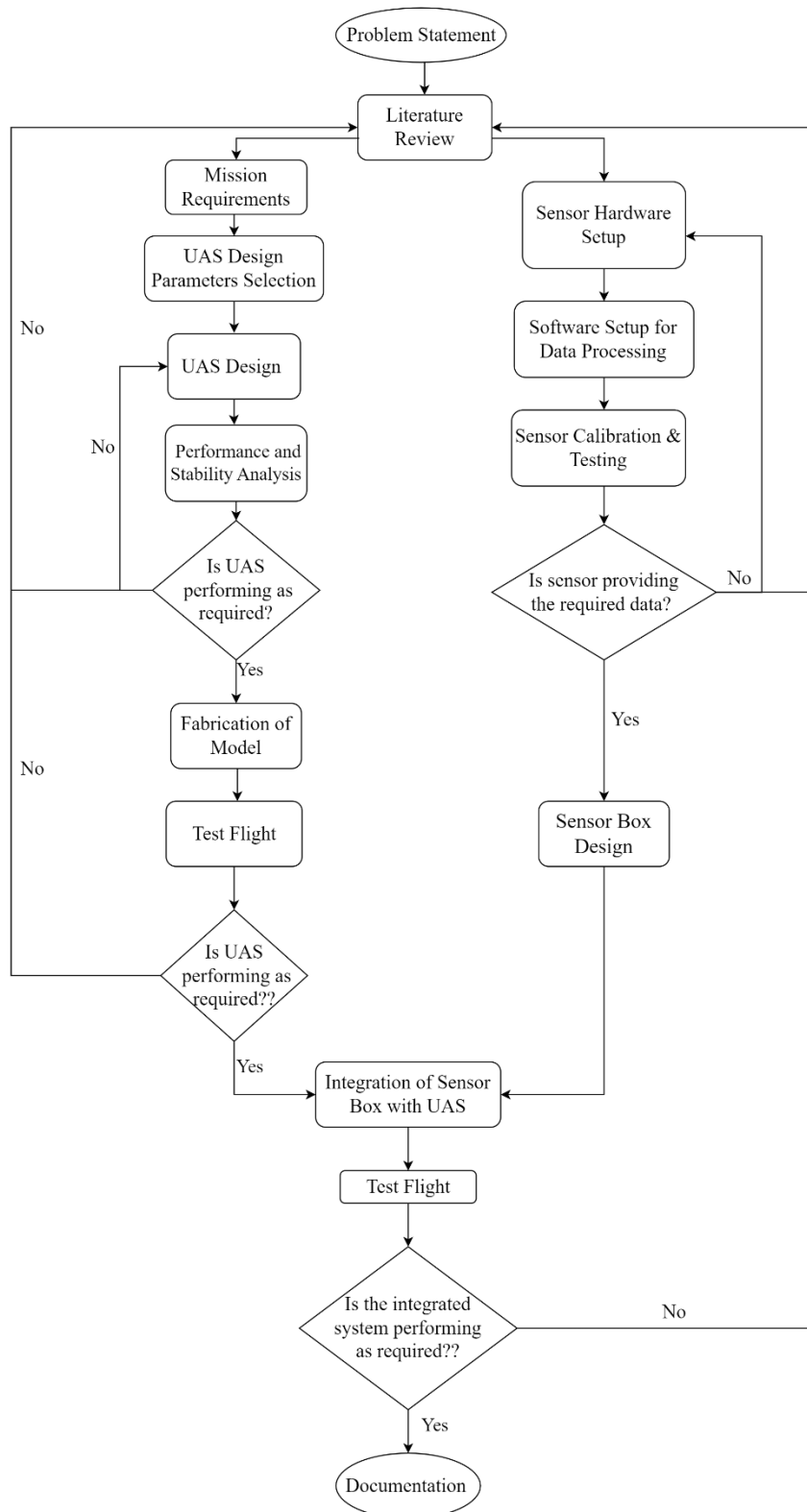


Figure 3.1: Detail flowchart of the project methodology

The methodology section is a crucial part of any project, as it outlines the approach to completing the project. The methodology section of this project encompasses various aspects such as sensor hardware and software setup, data processing methods, sensor housing, UAS configuration, and its geometrical parameters. This section will explain the details of the methods we employed throughout the project's duration.

3.2. Sensors and Data Acquisition

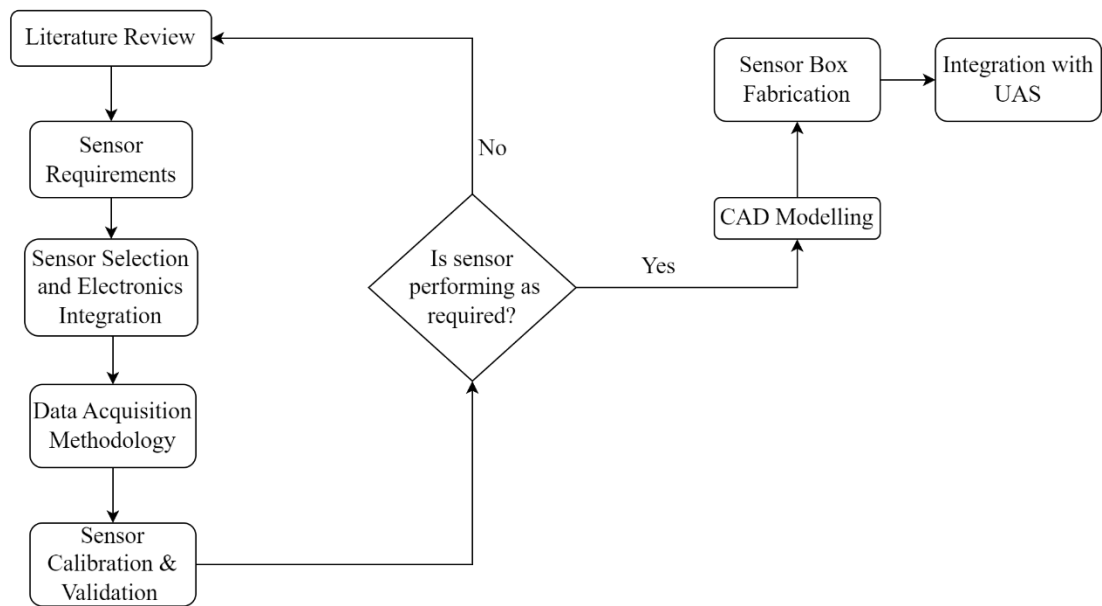


Figure 3.2: Detail flowchart for sensors methodology

Sensors and their instrumentation are a crucial component of this project, as they play a vital role in achieving the main objective of pollution measurement. For this purpose, the PMS5003T was selected as the primary sensor to measure the particulate matter (PM2.5 and PM10). Additionally, temperature and humidity sensor (DHT-22) was also integrated into the system. For this project, the preferred microcontroller was Arduino Uno, which is compatible with the selected sensors. The primary goal of the project was to establish the entire sensor array to enable the acquisition and transmission of required signals.

3.3. UAS Design

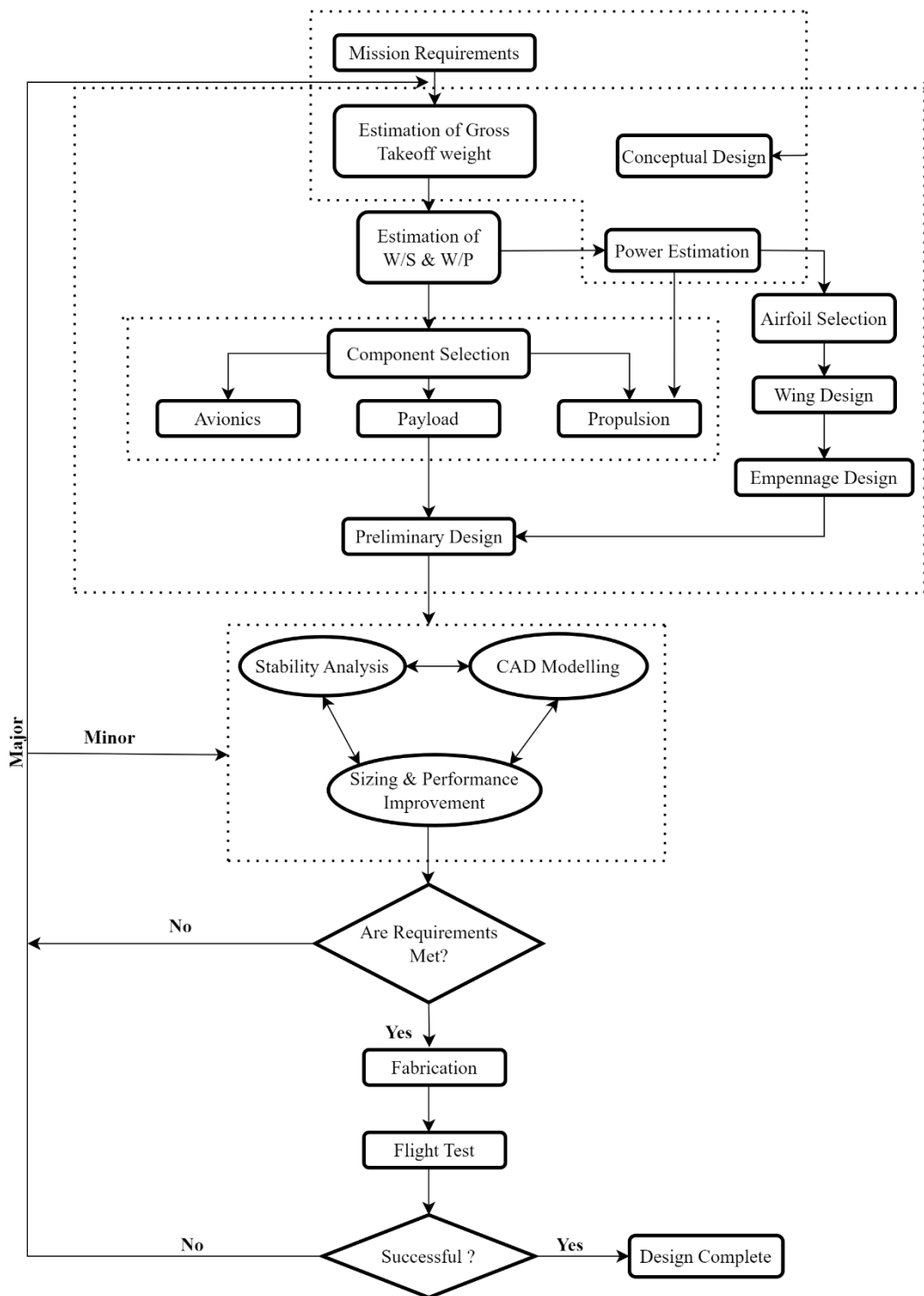


Figure 3.3: Detail flowchart of the UAS design

The conceptual design, preliminary design and detail design followed for the UAS is shown in above flowchart (Figure 3.3).

The methodology implemented in this project is summarized in the table below:

Table 3.1 Methodology for the project

	Objective	Methodology	Resources Utilized
UAS Design and Fabrication			
1.	Conceptual Design	Mission requirements, approx. weight, and configuration selection etc.	Books, articles and other resources mentioned in references. Studied the related articles, books and available resources to understand the related concepts.
		Motor selection	Thrust measurement and manufacturer's datasheet.
2.	Preliminary Design	Airfoil selection	Decision matrix and theoretical calculation.
		Calculation of W/P and W/S	MATLAB and theoretical calculations.
3.	Detail Design	Based on the parameters calculated, a CAD model was developed.	CATIA V5 R21
		Wing and empennage design.	Theoretical calculation and modification according to the stability analysis.
		Stability and performance analysis.	Initial stability analysis in XFLR5 and final dynamic stability analysis in XPLANE 11.
4.	UAS Fabrication	Based on a designed CAD model the UAS was manufactured.	CNC laser cutter, CNC hot wire cutter, 3D Printer, mechanical tools.

Sensor Integration			
1.	Sensor Selection	Studied the related articles, research papers, data sheets and available resources. Comparison of shortlisted PM sensors.	Articles, research papers, data sheet and other resources mentioned in references.
2.	Sensor Box Design	Designed a CAD model of sensor box.	CATIA V5 R21
3.	Sensor Box Fabrication	Manufacturing the sensor box according to the designed CAD model.	3D printer/ laser cut
4	Sensor Calibration	Determining the best calibration model and calibration factor for measurement.	Comparison with reference instrument, literature review of past studies for calibration process.
5	Data Processing	3D plot of the pollutant measured, temperature and humidity. Statistical analysis of data obtained.	MATLAB for the plot and analysis.
Flight Test			
1	Preliminary Test	Manual flight	Radio Controller
2	Autonomous Test	Integration of flight control system and its component with the UAS.	QGroundControl for flight plan, PX4 and its components as flight controller.
3	Final Flight Test	Integration of flight controller and sensor module.	QGroundControl, PX4 and designed sensor setups.

CHAPTER 4: RESULTS AND DISCUSSION

4.1 UAS Design

Aircraft design is an iterative process that includes various disciplines like aerodynamics, flight stability and dynamics, performance, propulsion, and control, etc. It is always a trade-off between all those fields. A good design is the combination of all these elements and fulfills the mission requirements.

The aircraft design is divided into 3 phases. They are:

- Conceptual design
- Preliminary design
- Detail design

The simple flow cycle is shown below in figure 4.1, which shows the typical approach for the aircraft design, starting from the requirements for the design phase to the final design for the fabrication stage.

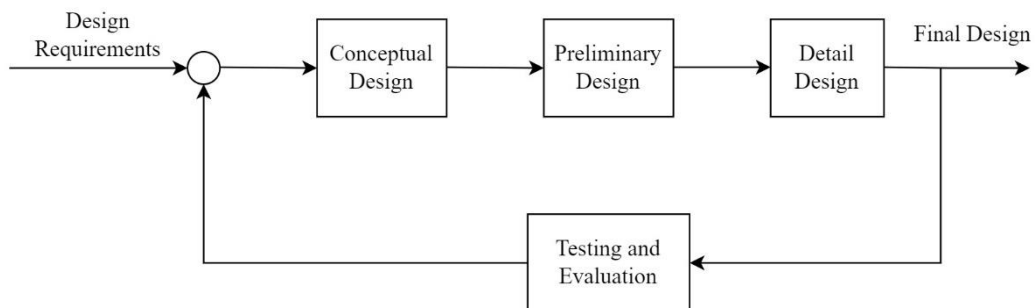


Figure 4.1: Design process for the UAS Design

4.1.1. Conceptual Design

4.1.1.1. Mission Requirements

The project should accomplish following requirements:

- Must provide stable platform for the sensor box and have an undisturbed air for the measurement.
- Maximum takeoff weight of 2kg.

- Must be able to carry a payload i.e., sensor box of approximately 200 grams.
- Climb to altitude of around 50m (visual line of sight).
- Must be able to loiter for around 5 minutes at cruise speed of 13-15m/s.
- Maximum speed of 20m/s.

4.1.1.2. Mission Profile

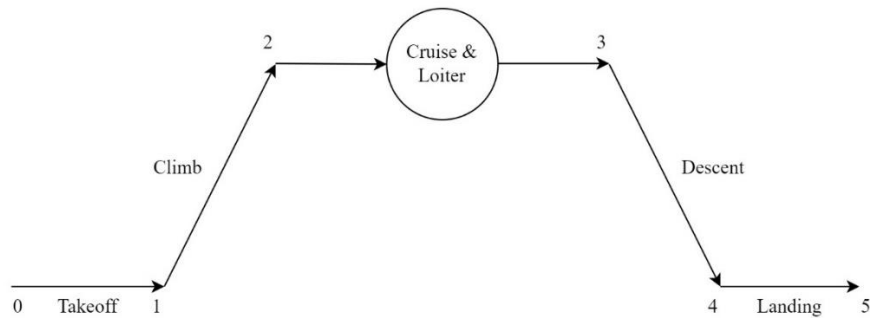


Figure 4.2: Mission Profile for the UAS

A simple cruise and loiter mission was selected, as it is feasible for collecting the data from the sensor.

4.1.1.3. Weight Approximation / Maximum Takeoff Weight

Table 4.1: Weight distribution

Description	Weight(g)
Wing	500
Vertical stabilizer	100
Horizontal stabilizer	150
Body (fuselage+ structure)	400
Sensor box	50
Servo + Linkages	50
Motor + Prop + Mount	100
Px4+GPS+ESC	100
Sensors + Arduino	150
Battery and accessories	250
Total	1850 g

It is given that some weight will be added in the manufacturing process and if a battery with a higher capacity is used, the extra weight will be added. Therefore, considering all, the **maximum takeoff weight of the UAS was decided to be 2kg.**

4.1.1.4. Configurations Selection




General outlook of the UAS was discussed where different components like wings configuration, placement, empennage configuration, motor placement etc. were considered for design. The components were compared on the basis of decision matrix as shown below. All the characteristics were given weightage and compared with one another.

Note: All the weightage are in % and desirable properties are given higher number and undesirable properties are given lower number. (Multiples of 5 for convenience). Example: high wing has less weight which is most desirable property, so it has high marking whereas roll rate is slow, so it has lowest marking.

4.1.1.4.1. Wing Location

The placement of wing plays an important role in the performance of the aircraft. It has direct relation to the roll rate and stability of the aircraft. In addition to the performance, weight and manufacture ease also plays great role in the wing position.

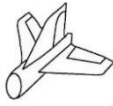



Table 4.2: Wing location decision matrix

Weightage				
		Low Wing	Mid Wing	High Wing
Weight	20	15	15	20
Stability	20	5	10	20
Control surface requirement	20	15	15	10
Roll rate	20	20	20	10
Complexity/Manufacturability	20	10	10	15
	100	65	70	75 (opted)

- **Stability:** Moderate stability is favorable considering the aircraft handling qualities. High wing is inherently stable configuration compared to mid wing and low wing.
- **Roll rate:** Higher roll rate provides less performance time i.e., higher roll rate will take little input and time for rolling, making control surfaces smaller, which in turn reduces the weight.
- **Weight:** High wing is simple for attachment to the fuselage as compared to low wing and mid wing. Low wing and mid wing need more additional support for the attachment, which in turn increases the weight. High wing offers comparatively less weight compared to low and mid wing.
- **Control surface requirement:** High wing has slow roll rate, slower roll rate takes higher input and time for rolling, making the size of control surfaces larger. Similarly, low wing and mid wing has slightly higher roll rate which in turn decreases the size of control surfaces.
- **Manufacturing feasibility:** In comparison to low and mid wings, the high wing is easier to attach to the fuselage which makes it easier for fabrication. Low wing and mid wing need additional support which makes them more difficult for manufacturing.

4.1.1.4.2. Empennage

Table 4.3: Empennage configuration decision matrix

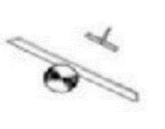

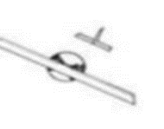

Weightage					
		Conventional Tail	T-Tail	V-Tail	H-Tail
Weight	25	20	15	25	10
Stability	25	20	20	15	20
Drag	10	5	5	10	0

Feasibility	20	10	20	0	15
Complexity/ Manufacturability	20	15	10	5	15
	100	70	70 (opted)	55	60

- **Weight:** V-tail has only two surface which makes it lightest of all, whereas H-tail is heavier. Both Conventional and T-tail has similar surfaces, but T-tail weighs slightly more than conventional because vertical tail needs more stiffeners to support the horizontal tail. However, T-tail frequently has compensating advantages. Additionally, T-tail offers a reduced vertical tail due to endplate effect.
- **Stability:** V-tail has less stability, and it is difficult for the control. All other configurations provide good stability. The conventional tail provides adequate stability at the lightest weight.
- **Manufacturing ease:** Conventional and H-tail is easier for the construction than T-tail. T-tail is comparatively difficult to manufacture as horizontal surface requires more structure support. V-tail is complex for the manufacture, so it is least used in common homebuilt projects.
- **Feasibility:** T-tail is more feasible for this project as prop-wash enhances the effectiveness of horizontal tail. Also, in the case of tail strike T-tail is less likely to be damaged. Conventional Tail could have been another best option for the project.
- **Drag:** V-tail offers the least drag, since it has reduced wetted area and also has less interference drag. Both Conventional and T-tail has similar surface, so offers similar drag.

4.1.1.4.3. Propulsion System

Table 4.4: Propulsion system decision matrix

Weightage					
		Single Puller	Dual Puller	Single Pusher	Dual Pusher
Weight	25	25	15	25	15
Cost	25	25	15	25	15
Complexity/ Manufacturability	25	20	10	20	10
Feasibility	25	0	0	20	15
	100	70	40	90 (opted)	55

- **Weight:** Dual pusher and dual puller means more motor accessories which in turn means more weight. Single puller and pusher offer same weight.
- **Cost:** Dual pusher and dual puller are more expensive while single pusher and puller are of same cost.
- **Complexity:** Dual pusher and dual puller are not feasible as double motor means more motor accessories more weight which in turn increases the complexity.
- **Feasibility:** Dual pusher and dual puller configurations are not feasible for the UAS design because having two motors will increase the number of motor accessories, overall weight, and cost of the system, which adds more complexity. While a single puller is a viable option, it is not suitable as the sensor needs a clean air, the puller configuration can disturb the air in front of the propeller, compromising the integrity of the air quality measurements.

➤ **Motor Selection:**

Motor brand: Avionic 2812

Motor KV: 1120 RPM/Volt

No load current: 1.8 Amps

Max continuous current: 16 Amps

Max continuous power: 270 Watt

Max Lipo cell: 4S

Propeller used: 10" * 4.5."



Figure 4.3: Thrust measurement of the selected motor

Thrust obtained: 1.75 Kg (approximately) with the 80% throttle.

4.1.1.4.4. Fuselage

A simple rectangular box with rounded fillets was selected for the UAS design. This box is easy to construct and provides ample volume for the avionics and payload. However, the box's larger cross-sectional area results in a higher drag coefficient, which is a disadvantage. To address the issue of space limitations, a boom configuration was adopted for the half portion of the fuselage. This configuration helped to save weight and simplify the manufacturing process.

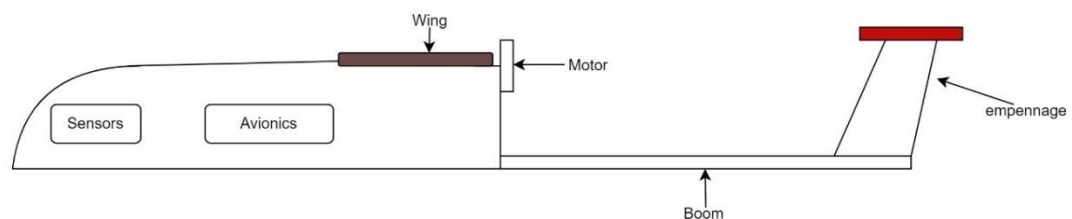


Figure 4.4: Conceptual design from the initial configuration selection

4.1.2. Preliminary Design

4.1.2.1. Airfoil Selection

The best approach for selecting the suitable airfoil is preparing a list of commonly used low-speed airfoils and comparing their behavior under similar conditions (Same Reynolds number). Some of the selected airfoils for wings were Clark X, Clark Y smooth, Clark Z, NACA 2414, NACA 4412, SA 7035, SD 7037, SD 7062, SD 7080, SG 6042, etc.

The analysis of the airfoils was conducted at the average Re of 200000 as the velocity of the aircraft would be in between 10-20 m/s. The chord was assumed to be around 20-25cm. From the shortlisted airfoils, three airfoils were selected for comparison. All the relevant data was obtained from Xfoil (airfoils.com).

Table 4.5: Comparison of different airfoils for wing

Re = 200000	Clark Y 11.7%	SG6042	SD7037
Thickness ratio (High is best)	11.7 % @ 30.9%	10% @ 33.5%	9.2% @ 26.1%
$C_{l_{max}}$ (Highest is best)	1.3584	1.4735	1.3267
AOA at $C_{l_{max}}$ (Highest is best)	15.75	14.75	13.75
Stall characteristics	B	A	B
$C_{d_{min}}$ (Lowest is best)	0.01034	0.01083	0.00899
(Cl/Cd) max (Highest is best)	74.36	88.96	74.75
Cl of (Cl/Cd) _{max} (Lowest is best)	0.9057	1.008	0.8708
Point summation	2	3(opted)	2

The horizontal tail and vertical tail have roughly around the same chord length as wing, so airfoils were analyzed at average $Re = 200000$. In general, stabilizers have symmetrical airfoils, but unsymmetrical airfoils can also be used for horizontal stabilizers. Based on the similar decision matrix as of airfoils for wing selection, historical data's and convenience for the manufacturing, NACA 0012 was opted for the horizontal and vertical tail.

4.1.2.2. Wing loading (W/S) and Power loading (W/P) Estimation

Typically, cruise, climb and takeoff are the most governing parameters. So, W/S vs. W/P graphs was plotted for four performance parameters.

- As a function of stall speed
- As a function of maximum velocity
- As a function of takeoff distance
- As a function of rate of climb

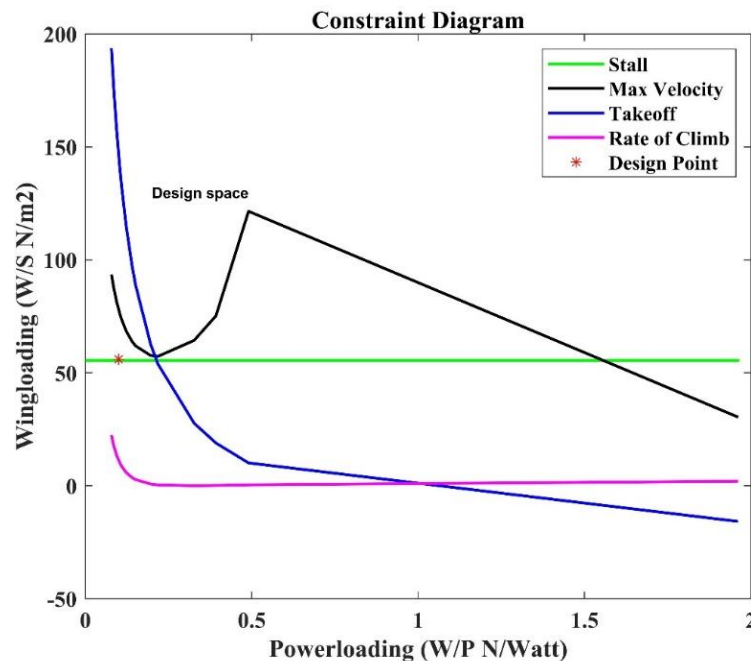


Figure 4.5: Constraint diagram (Appendix A)

Some of the important interpretation from the constraint diagram are:

- Wing loading of 50 N/m^2 to 80 N/m^2 would be feasible. So, wing loading of **55 N/m²** was considered for the preliminary design.

- Corresponding power loading was **0.0935 N/Watt**, which yields the power consumption of **209.83 Watt**. (Suggested W/P = 12lb/hp = 0.0716 N/ Watt- Appendix B -Table B1-homebuilt)
- If ROC is considered, wing loading of about 20-25 N/m² must be obtained that would yield wing area of 0.981m²- 0.79m² which is not feasible.

4.1.3. Detail Design

4.1.3.1. Wing Design

Wing was designed considering all wing parameters such as aspect ratio, taper ratio, manufacturability constraints, etc. The lift and load distribution on the wing should remain elliptical from root to tip.

Airfoil selected for wing was SG6042.

Wing loading (W/S) = 55N/m²

Aspect Ratio (A.R) = 6.0 (assumed for homebuilt-Appendix B-Table B2)

Tapered ratio = 1.0

$$\begin{aligned}
 \text{Area (S)} &= \frac{W}{W/S} && \text{Equation 4.1} \\
 &= \frac{2*9.81}{55} \\
 &= \mathbf{0.3567 \text{ m}^2}
 \end{aligned}$$

$$\begin{aligned}
 \text{Wingspan (b)} &= \sqrt{S * A.R} && \text{Equation 4.2} \\
 &= \sqrt{0.3567 * 6.0} \\
 &= \mathbf{1.4629 \text{ m}}
 \end{aligned}$$

$$\begin{aligned}
 \text{Chord (c)} &= \frac{2S}{b(1+\lambda)} = \frac{2*0.3567}{1.4629(1+1)} && \text{Equation 4.3} \\
 &= \mathbf{0.2438 \text{ m}}
 \end{aligned}$$

For the performance and other considerations, parameters are often overestimated for the small UAS. So, the final parameters for the detail analysis is summarized in the tabulated form:

Table 4.6: Wing dimensions

Area	0.4 m ²
Root chord	250mm
Tip chord	250mm
Span	1.6
Aspect ratio	6.4
MAC	250mm

4.1.3.2. Horizontal Tail Design

The tail volume coefficient method is a highly efficient technique for initial sizing. However, to carry out the calculations, firstly the moment arm must be determined, which can be estimated using various early estimation methods like:

- Percentage of fuselage length: For an aft mounted aircraft, the moment arm is generally taken 45%-50% of fuselage length.
- 2-3 times the wing chord.
- 40% of wingspan.

Considering all the parameters, the average value for moment arm was taken (L) = **0.65m**

Horizontal tail coefficient (C_{HT}) = 0.50 or 0.475 (5% reduction can be done in coefficient if T-tail is used- Appendix B-Table B4)

$$\begin{aligned} \text{Area (S}_{HT}) &= \frac{0.475 * 0.25 * 0.4}{0.65} \\ &= \mathbf{0.0731 \text{ m}^2} \end{aligned}$$

$$\text{Aspect ratio} = 3 \text{ (assumed-Appendix B-Table B3)}$$

$$\begin{aligned} \text{Span (b)} &= \sqrt{S * A.R} \\ &= \sqrt{0.0731 * 3.0} \\ &= \mathbf{0.468m} \end{aligned}$$

$$\text{Chord (c)} = \frac{2S}{b(1+\lambda)} = \frac{2*0.0731}{0.468(1+1)} = \mathbf{0.156m}$$

4.1.3.3. Vertical Tail Design

The process of designing the vertical tail was similar like the horizontal tail.

Vertical tail coefficient (C_{VT}) = 0.04 or 0.038 (5% reduction can be done in coefficient if T-tail is used-Appendix B-Table B4)

$$\begin{aligned} \text{Area (S}_{VT}) &= \frac{0.038*0.25*0.4}{0.65} \\ &= \mathbf{0.0374 \text{ m}^2} \end{aligned}$$

$$\text{Aspect ratio} = 1.2 \text{ (assumed for T-tail)}$$

$$\begin{aligned} \text{Span (b)} &= \sqrt{S * A.R} \\ &= \sqrt{0.0374 * 1.2} \\ &= \mathbf{0.212m} \end{aligned}$$

$$\text{Taper ratio (} \lambda \text{)} = 0.6 \text{ (assumed-Appendix B-Table B3)}$$

$$\begin{aligned} \text{Root chord (C}_{root}) &= \frac{2S}{b(1+\lambda)} = \frac{2*0.0374}{0.212(1+0.6)} \\ &= \mathbf{0.220m} \end{aligned}$$

$$\text{Tip chord (C}_{tip}) = \lambda * C_{root} = 0.6*0.220 = \mathbf{0.132 \text{ m}}$$

4.1.3.4. Control Surface Sizing

4.1.3.4.1. Aileron Sizing

Ailerons are typical 15% - 25% of wing chord (Source: Raymer)

Aileron chord / wing chord = 0.25 (Appendix B-Figure B4)

Aileron chord = 63 mm

Aileron span / wingspan = 0.4(Appendix B-Figure B4)

Aileron Span = 320 mm (350mm was taken for over estimation)

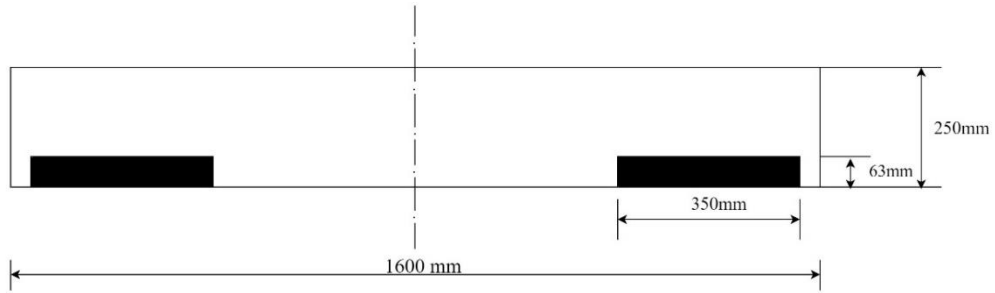


Figure 4.6: Aileron sizing

4.1.3.4.2. Elevator and Rudder Sizing

Elevators and Rudders are typically about 25%-50% of tail chord (Source: Raymer)

In span wise, it is taken 90% of full span. (Source: Raymer)

Elevator chord = 50 mm

Rudder chord = 50 mm

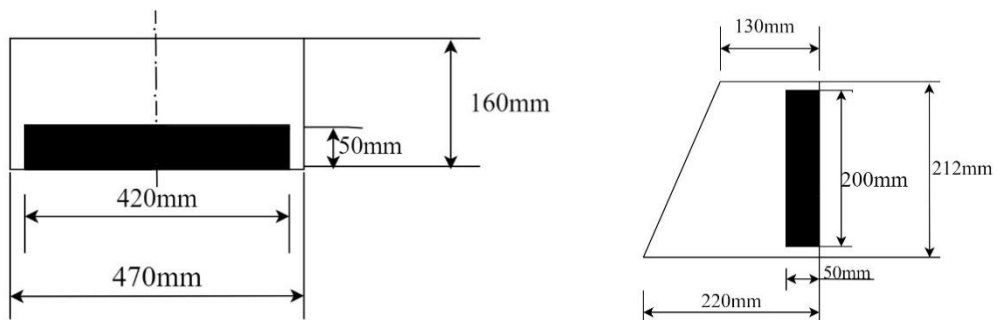


Figure 4.7: Elevator and rudder sizing

The final size of tail will be determined after the stability analysis is done.

4.1.3.5. Stability Analysis

4.1.3.5.1. Static Stability Analysis

The neutral point of the aircraft was found to be at 131cm from the leading edge and the C.G of the aircraft was approximated to be around 80.36cm. With mean aerodynamic chord (MAC) of 250 cm, the static margin is obtained as below:

$$S.M = (X_{np} - X_{cg}) / MAC \quad \text{Equation 4.4}$$

$$S.M = 0.20256 = 20.26 \%$$

The positive static margin shows that the aircraft is statically stable in longitudinal direction. This can also be seen from the figure 4.8 which shows the graph of coefficient of pitching moment (C_m) versus Angle of attack (AOA). The slope of C_m vs AOA curve is negative which is the criteria for longitudinal static stability.

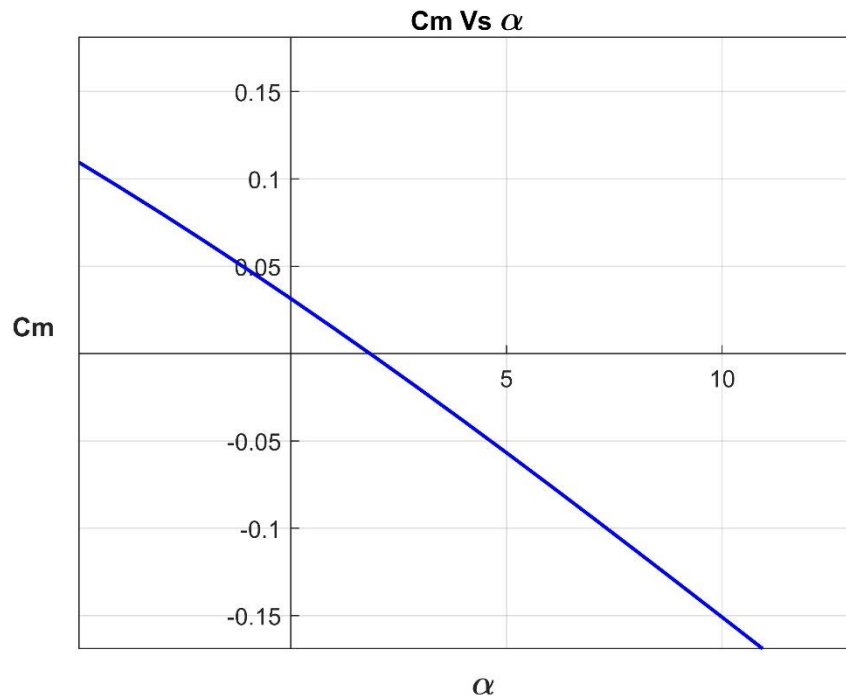


Figure 4.8: Pitching moment coefficient (C_m) Vs AOA (α) curve

Similarly, from the figure 4.9 i.e., graph of coefficient of rolling moment versus beta it can be seen that the slope is decreasing which simply indicates the fulfillment of the criteria for lateral static stability.

Mathematically, the criteria can be represented as:

If $C_{l\beta} > 0$ then the aircraft is laterally unstable.

If $C_{l\beta} < 0$, then the aircraft is laterally stable.

If $C_{l\beta} = 0$, then the aircraft is laterally neutral.

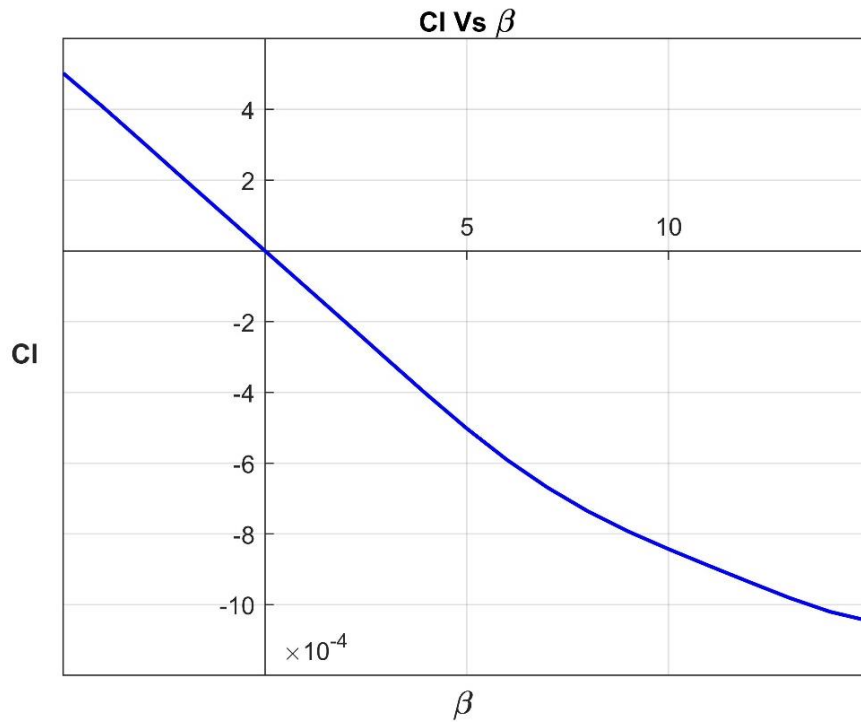


Figure 4.9: Rolling moment coefficient (C_l) Vs sideslip angle (β) curve

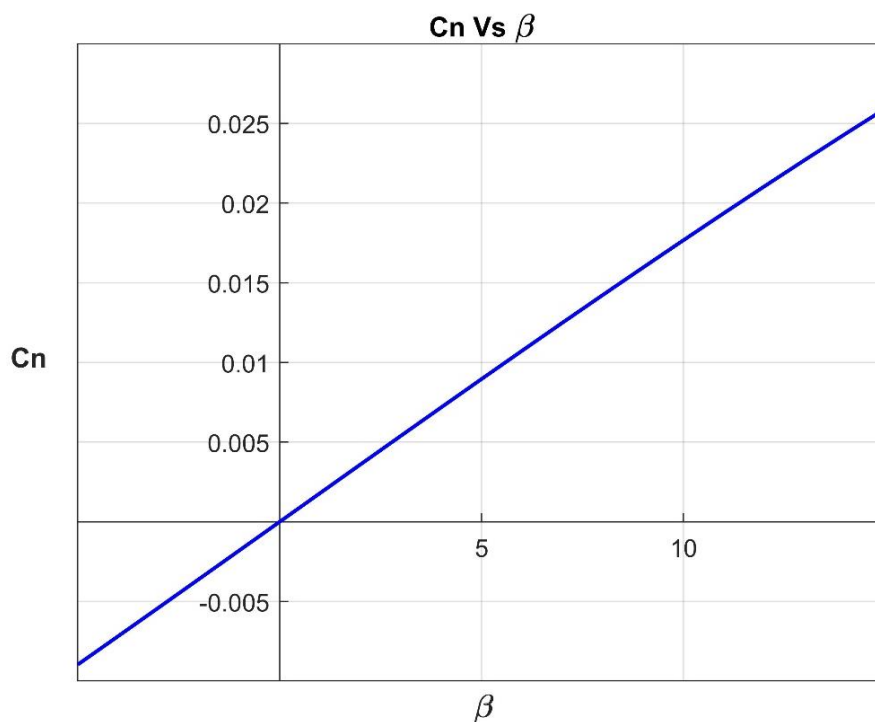


Figure 4.10: Yaw moment coefficient (C_n) Vs sideslip angle (β) curve

In the figure 4.10, the value of slope is positive.

Mathematically, the criteria for directional stability can also be expressed below:

If $C_{n\beta} > 0$, then the aircraft is directionally stable.

If $C_{n\beta} < 0$, then the aircraft is directionally unstable.

If $C_{n\beta} = 0$, then the aircraft is directionally neutral.

This indicates that the vehicle inherits directional stability.

4.1.3.5.2. Dynamic Stability Analysis

The figure 4.11 shows the root locus plot of the longitudinal stability obtained from the XFLR5 computation. Both short period and long period (Phugoid) have roots in the negative plane, which signifies that the aircraft is dynamically stable in longitudinal motion.

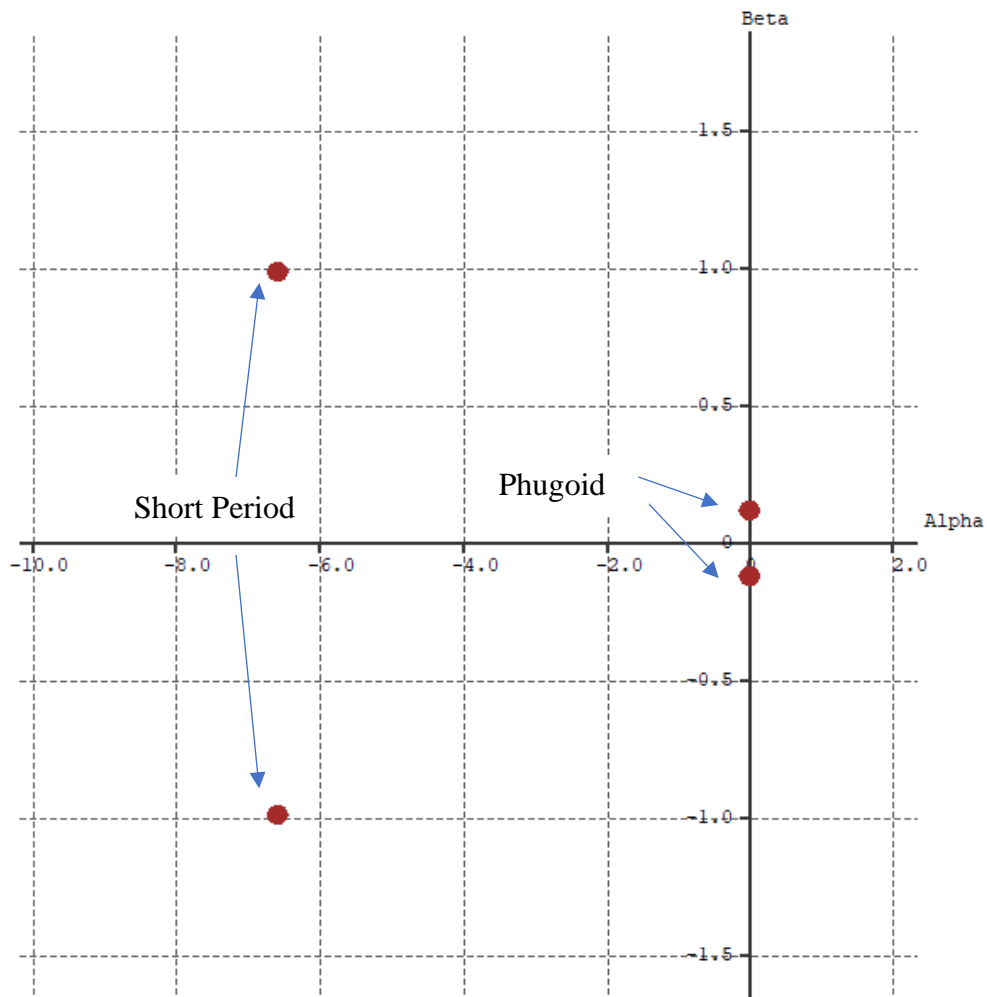


Figure 4.11: Root locus plot for longitudinal dynamic stability

Longitudinal state matrix obtained from the XFLR5 dynamic analysis are:

$$\begin{pmatrix} -0.0667624 & 0.432456 & 0 & -9.81 \\ -1.44465 & -7.71709 & 11.886 & 0 \\ -0.0098682 & -3.29836 & -5.38043 & 0 \\ 0 & 0 & 1 & 0 \end{pmatrix}$$

From the matrix, Eigen value of the stability are:

Short period = -6.574 ± 6.183i

Long period = -0.007855 ± 0.7514i

Since, the real part of the roots are negative which signifies the aircraft is dynamically stable in longitudinal direction. Similarly, the imaginary part is non-zero which indicates that it is oscillatory, decaying sinusoidal motion.

Table 4.7: Longitudinal stability derivatives

Longitudinal derivatives			
Xu	-0.12017	Cxu	-0.042007
Xw	0.77842	Cxa	0.2721
Zu	-2.6004	Czu	0.0041771
Zw	-13.891	Cla	4.8556
Zq	-2.9394	CLq	8.2198
Mu	-0.002023	Cmu	-0.0028281
Mw	-0.67604	Cma	-0.94526
Mq	-1.1028	Cmq	-12.336

From the relation between dynamic and static longitudinal stability,

$$M_{\alpha}Z_u - Z_{\alpha}M_u > 0$$

$$(-0.67604 \times -13.881) - (-0.0020226 \times -2.6004) > 0$$

9.39087 > 0.005259 (It further signifies the dynamic longitudinal stability.)

Similarly, figure 4.12 shows the root locus plot for the lateral-directional stability. Here, root locus of roll subsidence and dutch roll lies in left half plane which signifies that the aircraft is dynamically stable in lateral direction. The root of spiral mode is in right plane which signifies that the spiral mode is divergent in nature.

Lateral state matrix obtained from the XFLR5 dynamics analysis.

$$\begin{pmatrix} -0.404893 & 0.00875316 & -13.2257 & 9.81 \\ -0.106333 & -14.0019 & 3.73468 & 0 \\ 1.45135 & -1.76698 & -0.769704 & 0 \\ 0 & 1 & 0 & 0 \end{pmatrix}$$

From the matrix Eigen value of the stability are:

Roll subsidence = -13.58 ± 0i

Dutch roll = -0.8902 ± 4.515i

Spiral mode = 0.1821 ± 0i

The real part of the roots are negative which signifies it is dynamically stable whereas imaginary part is non-zero which indicates it is oscillatory, decaying sinusoidal motion. Similarly, the spiral is unstable and divergent in nature since it has positive real roots.

Table 4.8: Lateral stability derivatives

Lateral derivatives			
Yv	-0.7288	Cyb	-0.2548
Yp	0.01576	Cyp	0.00688
Yr	0.52786	Cyr	0.23065
Lv	-0.0462	Clb	-0.0101
Lp	-1.7135	Clp	-0.4679
Lr	0.48516	Clr	0.13249
Nv	0.46772	Cnb	0.10219
Np	-0.2491	Cnp	-0.068
Nr	-0.3314	Cnr	-0.0905

From the relation between dynamic and static lateral-directional stability,

$$L_{\beta}N_r - N_{\beta}L_r > 0$$

$$(-0.0133077 \times -0.3314) - (0.03464 \times 0.48516) > 0$$

-0.012395 < 0 (Spiral mode is unstable in nature).

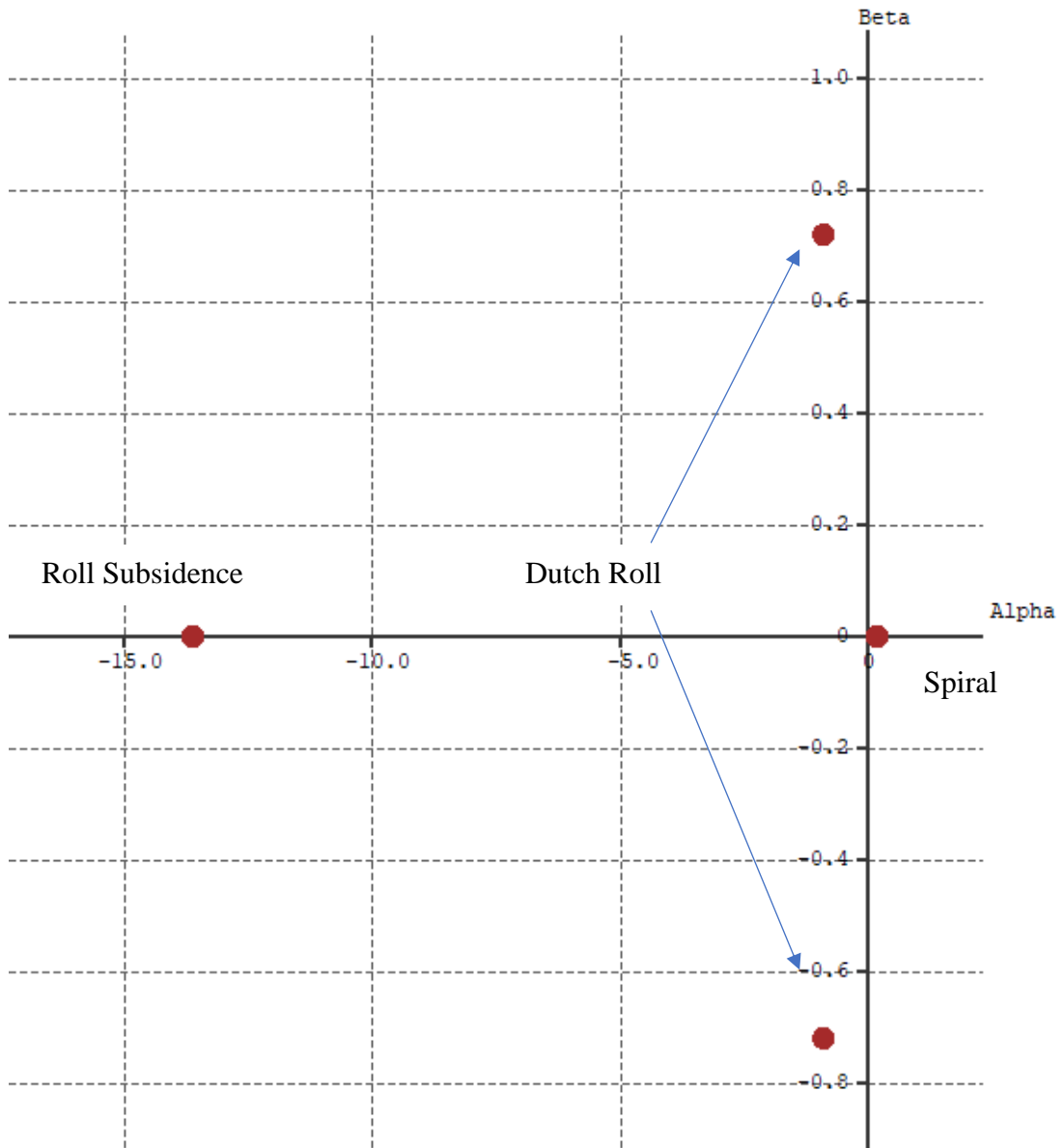


Figure 4.12: Root locus plot for lateral-directional dynamic stability

The detail dynamic analysis was done in XPLANE. The results are discussed as below:

a) Spiral mode:

Airspeed: 29 knots

Altitude: 5740 ft above MSL

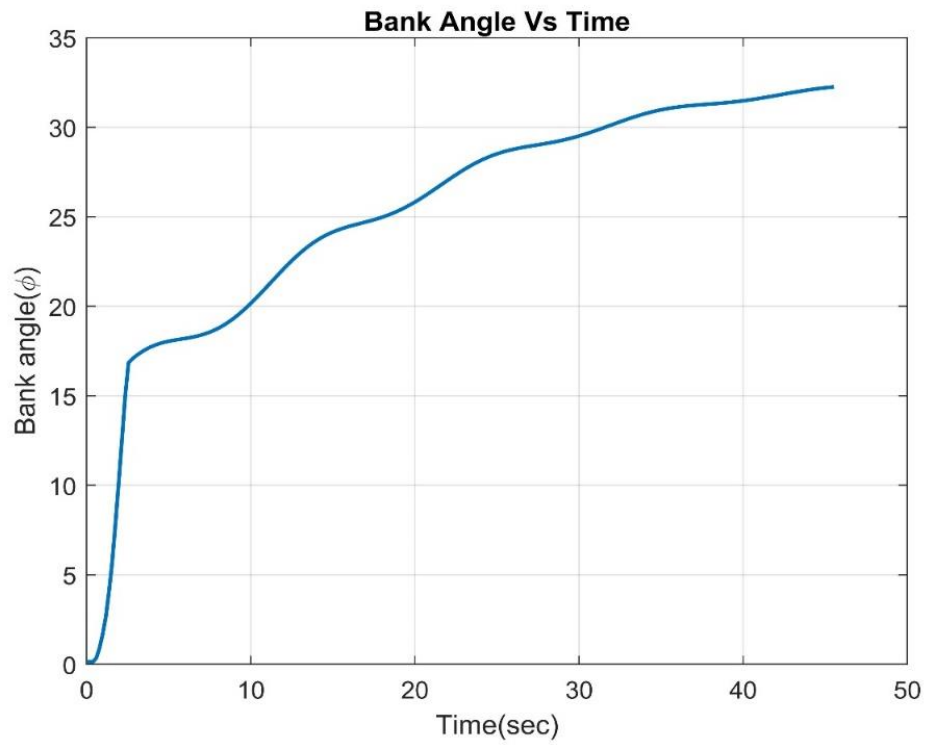


Figure 4.13: Spiral mode at 15 deg (Bank angle VS time)

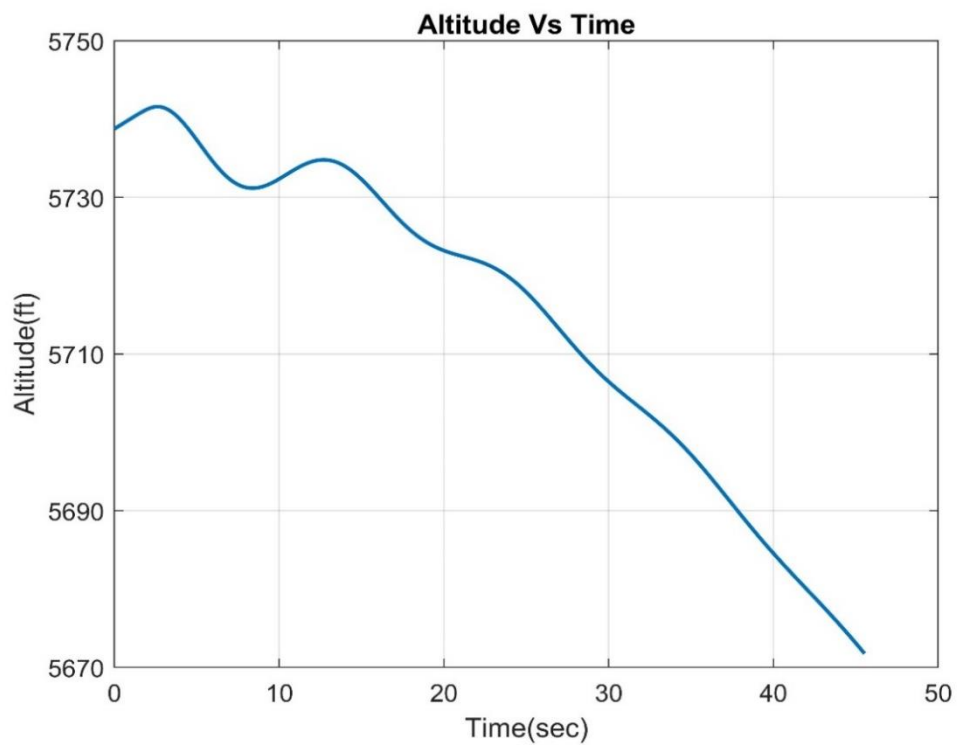


Figure 4.14: Spiral mode at 15 deg (Altitude VS time)

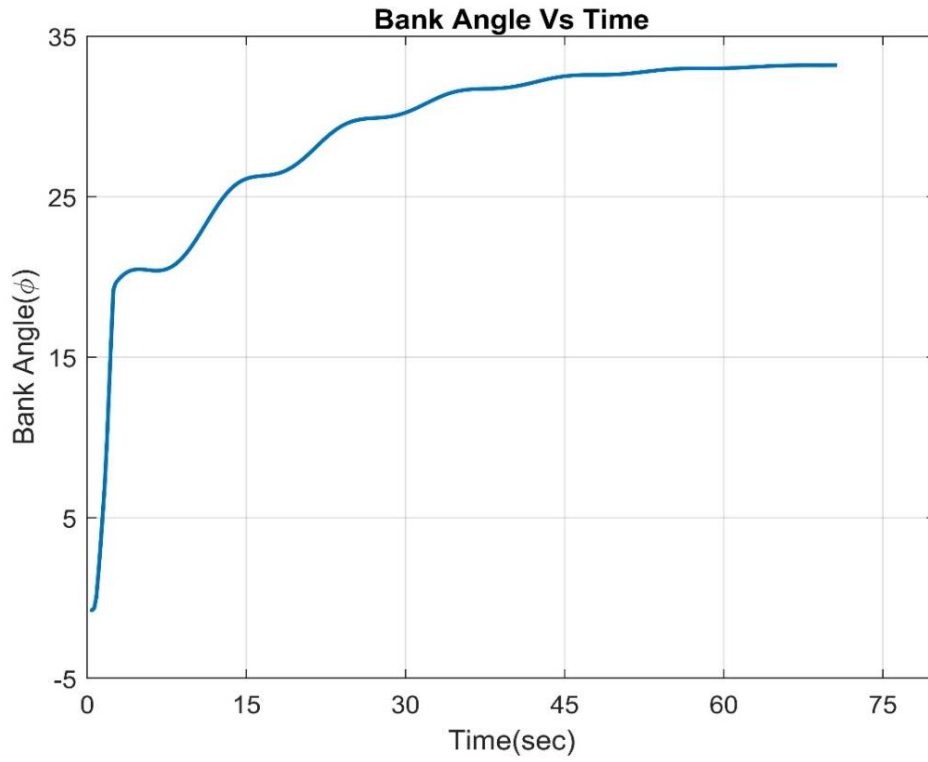


Figure 4.15: Spiral mode at 19 deg (Bank angle VS time)

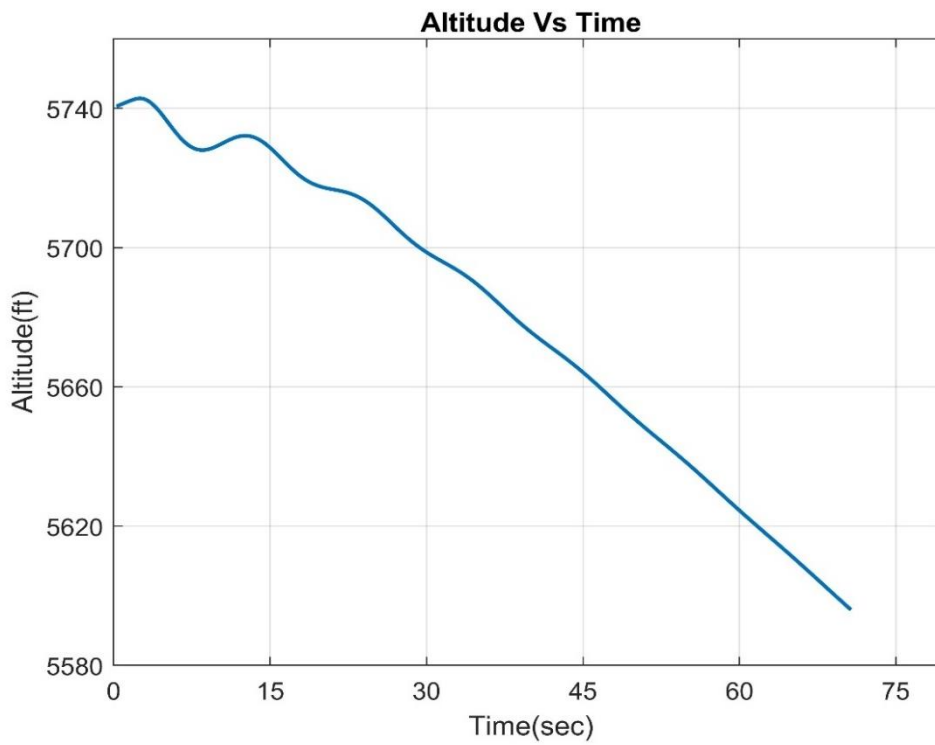


Figure 4.16: Spiral mode at 19 deg (Altitude VS time)

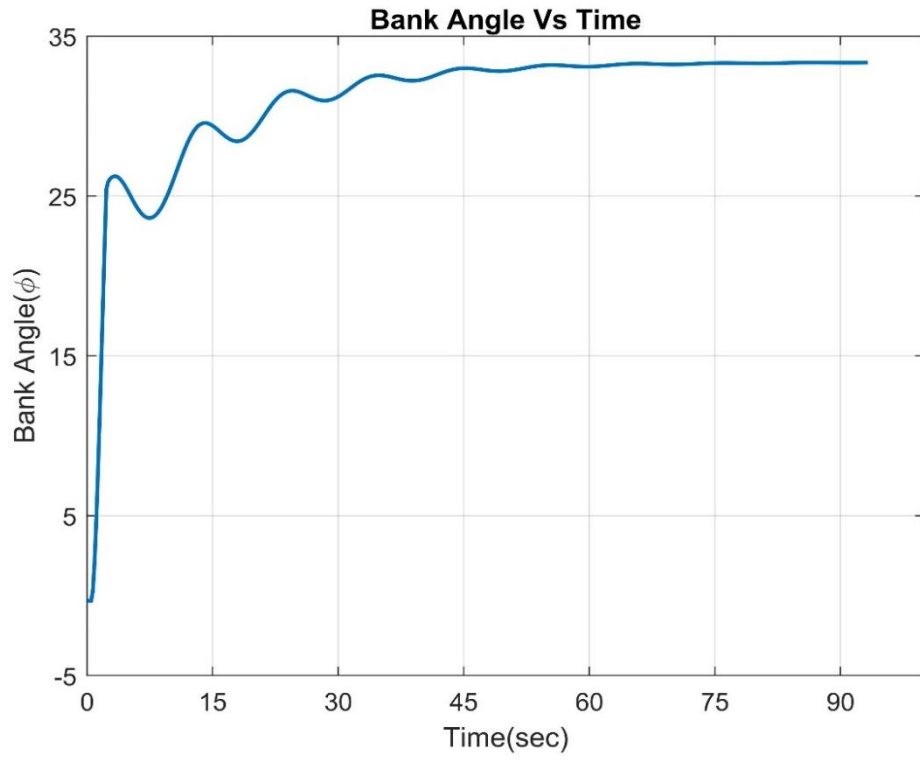


Figure 4.17: Spiral mode at 25 deg (Bank angle VS time)

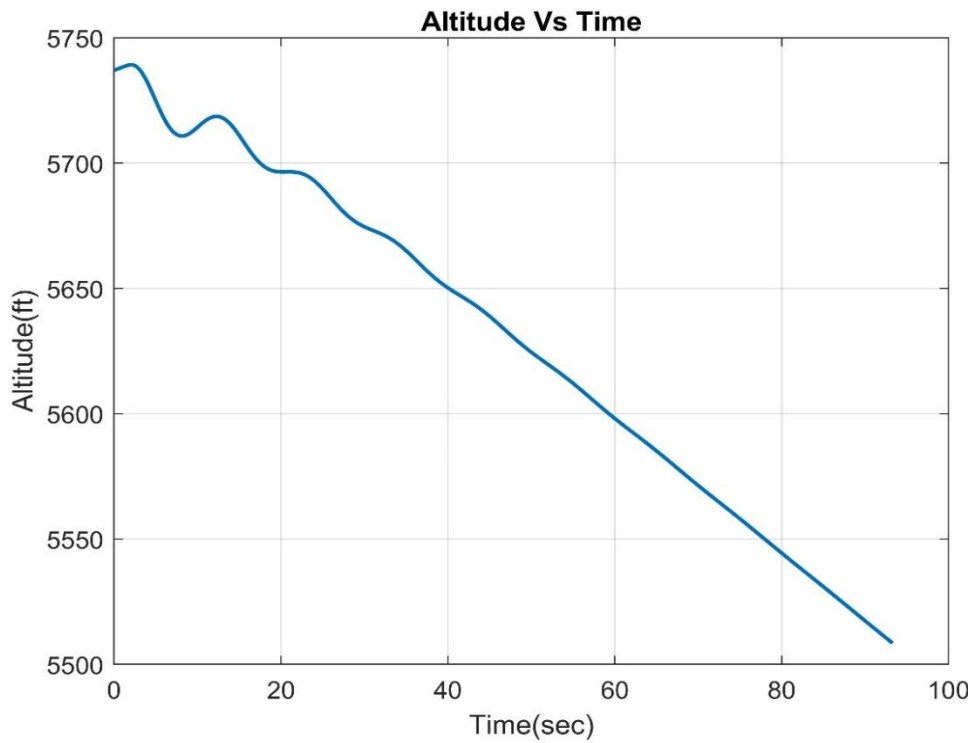


Figure 4.18: Spiral mode at 25 deg (Altitude VS time)

- Bank angle increases with time (Figure13, Figure 15 and Figure 17).
- Aircraft loses altitude with time (Figure 14, Figure 16 and Figure 18).
- Indication of gradual descent of the aircraft in a convergent spiral path.
- Reason behind this instability: higher directional stability and less lateral stability.
- Evident even in aircrafts that are inherently stable in all other parameters.
- Easily corrected by pilot.

b) Dutch roll

Airspeed: 29 knots

Altitude: 5740 ft above MSL

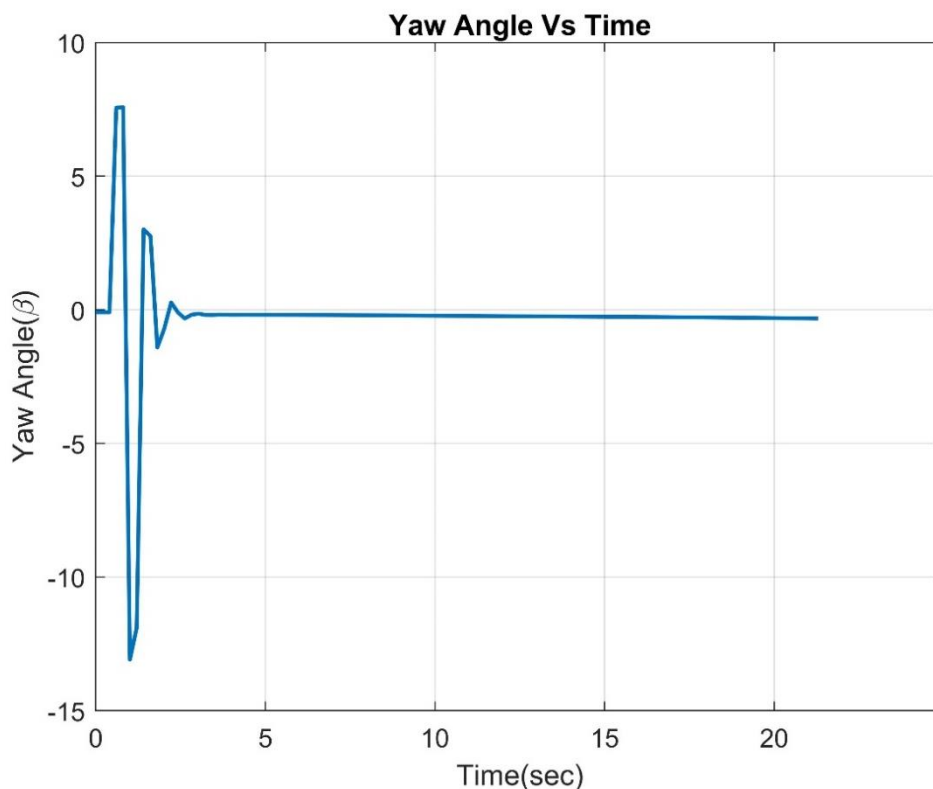


Figure 4.19: Dutch roll (Yaw Angle VS time)

- Full deflection of 7.5 degrees on positive axes and 13 degrees on negative axes.
- At t=2 second (approx.), we observed a nose-down response indicating that it is statically stable.
- The aircraft regained a stable flight condition at t=5 seconds (approx.) which shows dynamically stable nature.

- Reason behind this instability: less directional stability and high lateral stability ($\xi_L > \xi_H$).

c) Short period

Airspeed: 29 knots

Altitude: 5740 ft above MSL

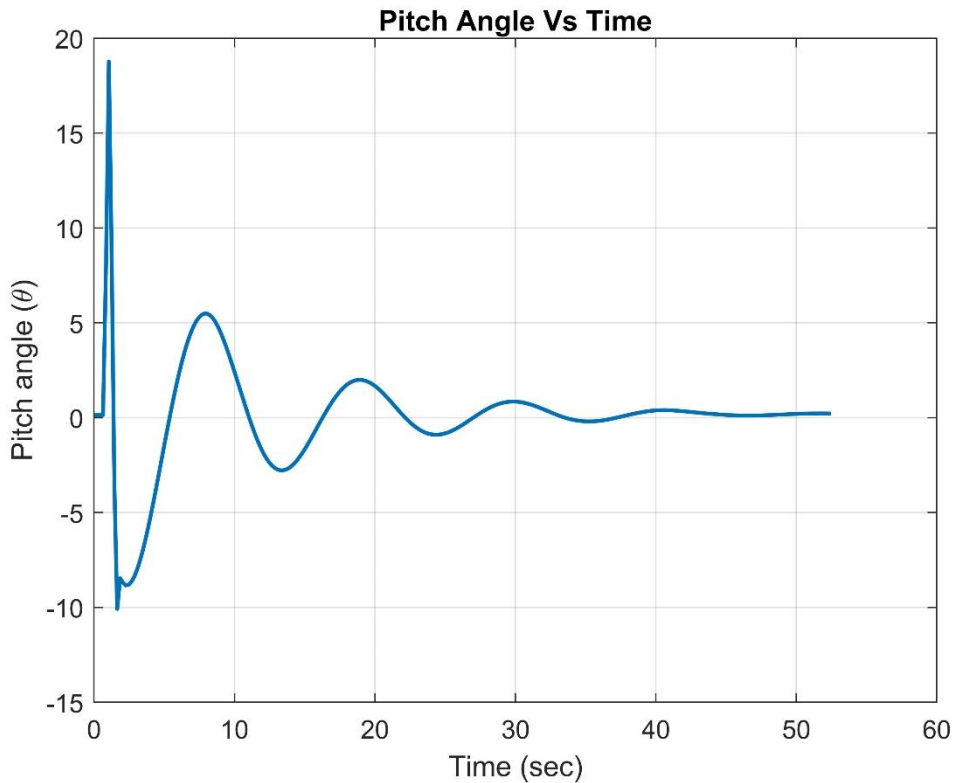


Figure 4.20: Short period (Pitch Angle VS time)

Pitch up response to pitch doublet shows that aircraft is statically stable. Pitch oscillations showed a damped tendency with time.

d) Phugoid mode

Airspeed: 29 knots

Altitude: 5740 ft above MSL

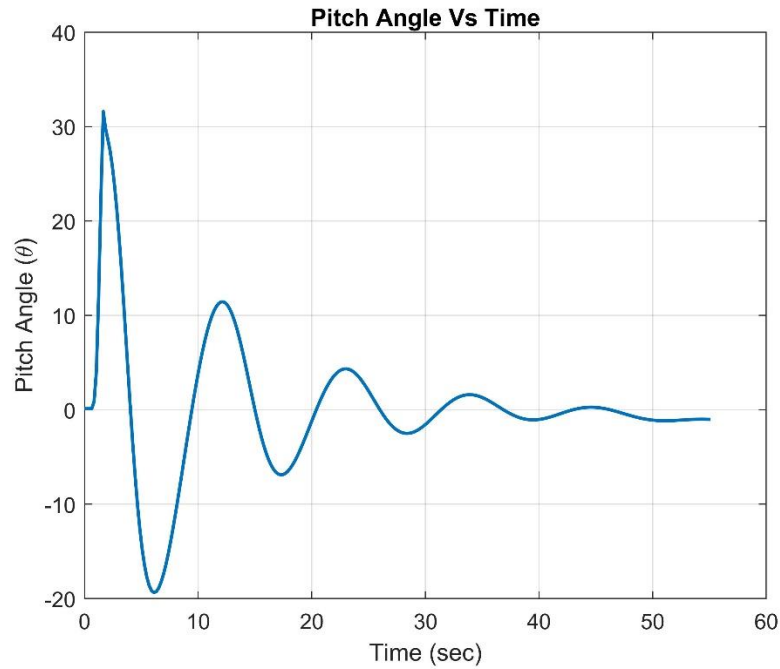


Figure 4.21: Phugoid mode (Pitch Angle VS time)

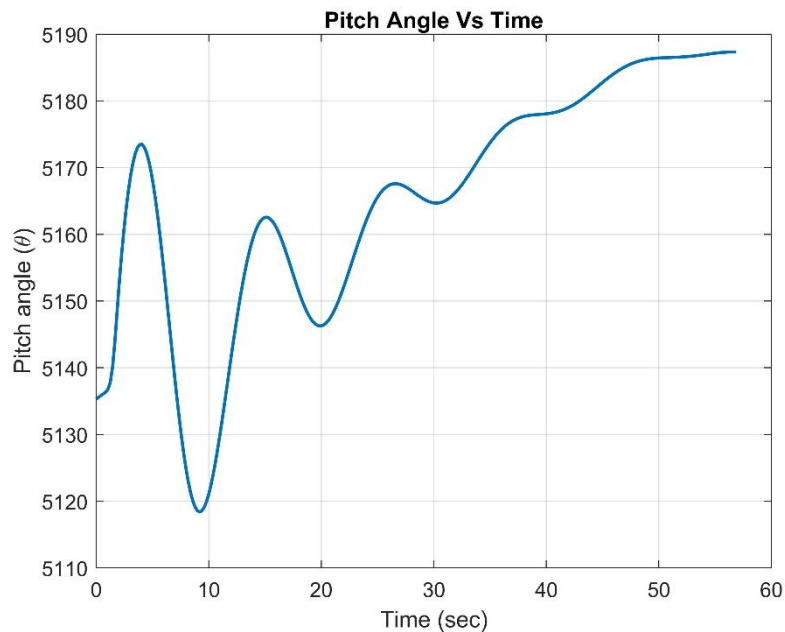


Figure 4.22: Phugoid mode (Altitude VS time)

- As the aircraft goes "downhill" and "uphill," energy is continuously exchanged.
- At $t=12$ seconds approximately a nose-down response can be observed, indicating that it statically stable.
- The aircraft regained its level flight at approximately $t=50$ sec indicating dynamic stability. ($\xi_L > \xi_H$).

4.1.3.6. Final Design Specifications:

Table 4.9: Details of aircraft design

General Specifications		Horizontal Stabilizer	
Weight	2 kg	Airfoil	NACA 0012
Length	1.02 m	Aspect ratio	1.25
Fuselage configuration	Twin boomed	Span	0.5 m
Tail configuration	T-tail	Chord	0.2 m
Wing loading	4.5 kg/m ²	Area	0.1 m ²
Stall velocity	12 m/s		
Cruise velocity	15 m/s		
Propulsive System		Vertical Stabilizer	
Type	Pusher	Airfoil	NACA 0012
Motor	Brushless	Span	0.5 m
Motor RPM	1120 rpm/Volt	Chord	0.2m, 0.12m
Propeller	10"x4.5"	Area	0.04 m ²
Battery voltage	14.8 V	Root to tip sweep	13.5°
Wing		Control Surfaces	
Airfoil	SG 6042	Aileron span	0.06 m
Aspect ratio	6.4	Aileron chord	0.35 m
Taper ratio	1	Elevator span	0.4 m
Wing area	0.4 m ²	Elevator chord	0.05 m
Wing chord	0.25 m	Rudder span	0.4 m
Wingspan	1.6 m	Rudder chord	0.019 m

4.1.3.7. CAD Modelling

The CAD modeling was done using CATIA V5. The design process for the aircraft involved extracting the airfoil geometry for the wing and tail from <http://airfoiltools.com>. Once the airfoil geometries were established, the rest of the aircraft's geometry was designed according to the required specifications mentioned in the above table. This included designing the fuselage, empennage, and other structural components. Then all of the individual components were assembled together to create the complete aircraft.

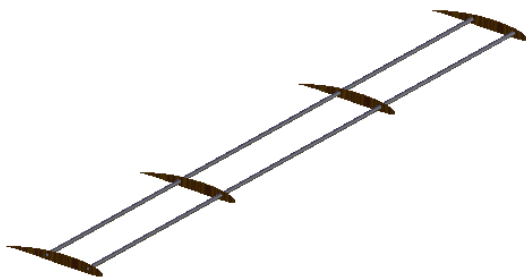


Figure 4.23: Wing structure

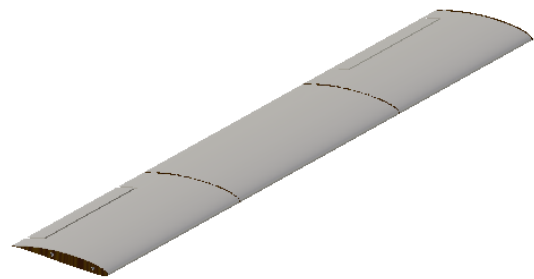


Figure 4.24: Wing assembly

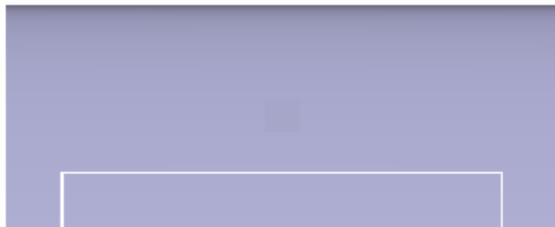


Figure 4.25: Horizontal stabilizer



Figure 4.26: Vertical stabilizer

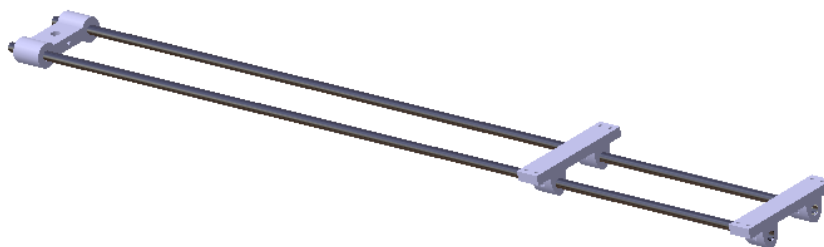


Figure 4.27: Boom assembly

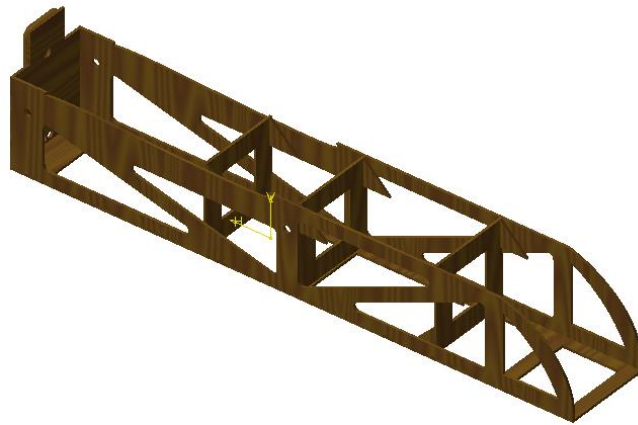


Figure 4.28: Fuselage structure

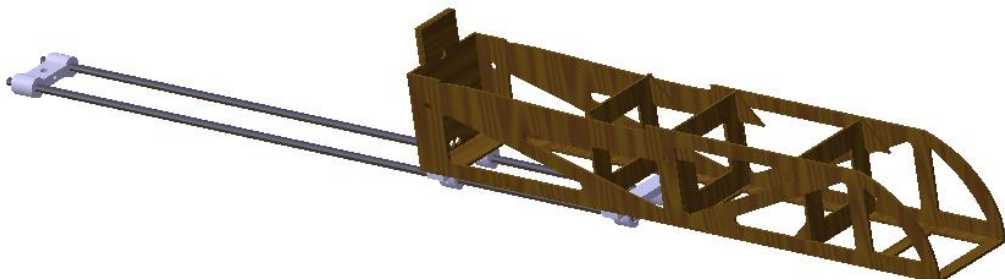


Figure 4.29: Fuselage assembly



Figure 4.30: Empennage

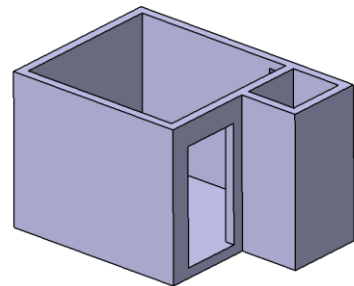


Figure 4.31: Sensor box

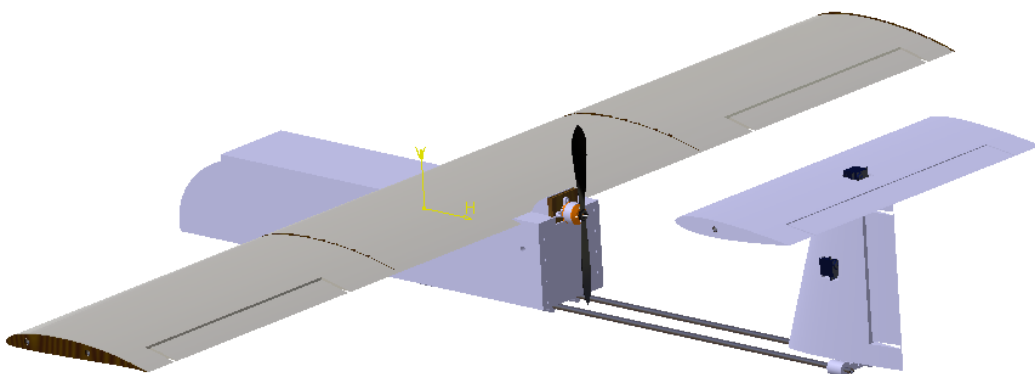


Figure 4.32: Final CAD model

4.1.3.8. Manufacturing Process

In general, the final step of the design process is the manufacturing stage. After conducting the necessary analysis and calculations, decisions regarding manufacturing design are made. One of the most crucial decisions made during the manufacturing is the selection of materials. The materials used must be strong while also being as lightweight as possible.

To ensure ease of manufacturing, a shortlist of available materials were created and evaluated which are listed in the tabular form:

Table 4.10: Material selection and manufacturing process

S.No	Description	Materials	Process	Remarks
1	Wing and tail ribs	Ply board	Laser Cut	3mm thick-590 kg/m ³
2	Wing and tail spar	Aluminum rod	-	9mm rod
3	Wing and tail surface	Styrofoam	CNC hot wire cutter	Approx. 45kg/m ³
4	Tail boom	Aluminum rod	-	9mm rod
5	Motor mount	Ply board	Laser cut	5mm thick
6	Fuselage structure	Ply board	Laser cut	3mm thick-590 kg/m ³
7	Fuselage surface	Styrofoam	CNC hot wire cutter	Approx. 45kg/m ³
8	Boom connector	ABS, PLA	3D printer	-
9	Tail connector	ABS, PLA	3D printer	-
10	Sensor box	ABS, PLA	3D printer	-

When considering the manufacturing of a Fixed Wing UAS, it can be broken down into several major components for the ease of construction and assembly. These components include:

➤ Fuselage

The process of fabricating a fuselage involved the use of laser cutting for the jig spar and bulkhead. In order to decrease the weight of the structure, plywood with a thickness of 3mm was utilized for both the jig and bulkheads. The incorporation of avionics,

including the battery, ESC, autopilot system, and payload, was achieved by covering them with a layer of 6-7mm Styrofoam. Additionally, the fuselage was strengthened by creating compartments for the batteries and control systems using plywood.

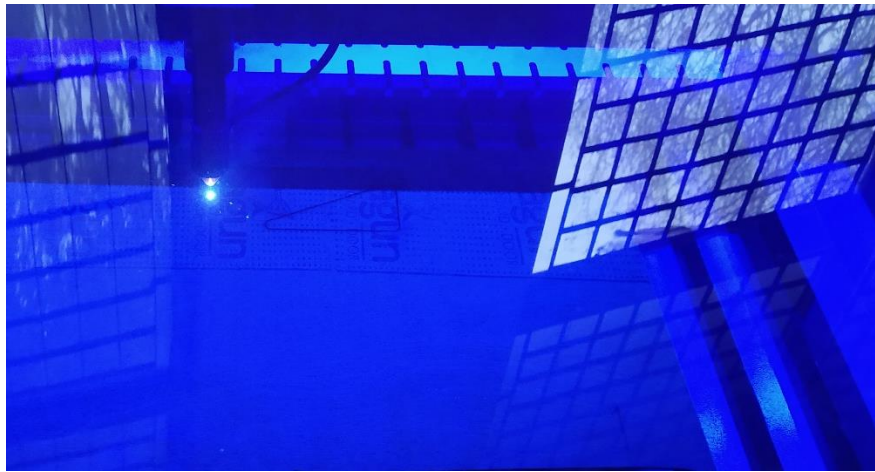


Figure 4.33: Laser cutting plywood for fuselage



Figure 4.34: Final assembled fuselage

➤ **Wing**

For the UAS, a high wing configuration was opted and the wing was designed to be detachable, simplifying transportation. The wing was constructed from Styrofoam, while a CNC hot wire cutter was utilized in the fabrication process. The spars were made of plywood and were produced using CNC laser cutting technology. Then all these components were assembled in accordance with the final CAD design. Servo bases were attached to the wings lower surface and the ailerons were attached using

tape, while the servo linkage was made using 2mm rod. To integrate the control surfaces, 3D printed servo linkage was utilized.



Figure 4.35: Cutting airfoil shape in CNC hot wire cutter

➤ **Tail**

The manufacturing process for the horizontal tail was similar to that of the wing. A CNC hot wire cutter was used to shape the Styrofoam, while the ribs were cut using a laser. Tapes were used as hinges to attach the elevator and rudder to the wing, and a 2mm rod was used to create the servo linkage. For the integration of control surfaces, a 3D printed servo linkage was utilized.



Figure 4.36: Empennage assembled with servo attached

➤ Assembly

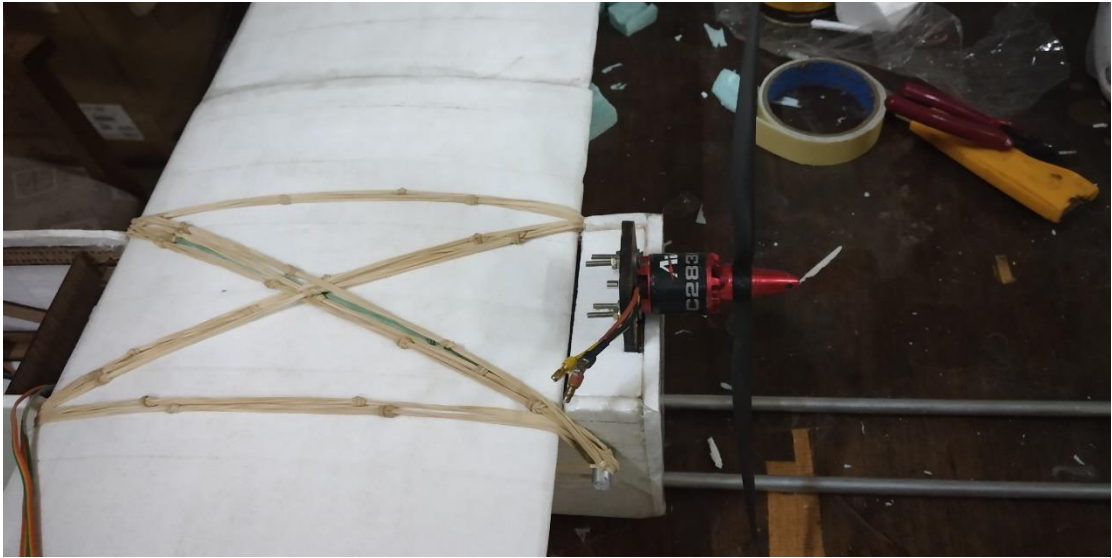


Figure 4.37: Wing and motor mounted on fuselage



Figure 4.38: Final assembled UAS before test flight

4.1.4. Flight Test

After the fabrication of the UAS, manual and autonomous flight tests were performed to ensure its functionality.

➤ **Manual test**

A manual test was performed using a radio controller. A total of three manual tests were performed where a stable flight was obtained in the third flight.

➤ **Autonomous test**

After the success of manual test flight, autonomous test flight was opted. QGroundControl software was used for the flight control and vehicle setup. Telemetry was used to connect the Pixhawk and the ground control system. For the automated flight, the Pixhawk, GPS module and ESC were calibrated at first. Next, the flight path was planned in the QgroundControl and uploaded into the Pixhawk.



Figure 4.39: Initial flight plan for UAS in QGroundControl interface

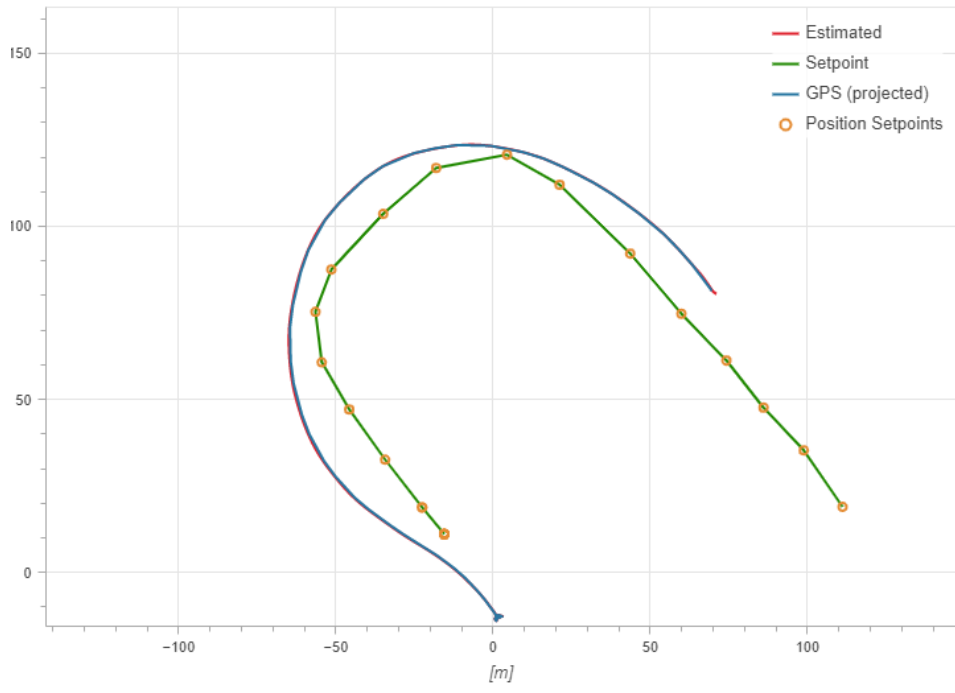




Figure 4.40: UAS path behavior w.r.t. to set waypoint

DHT22	Output: Temperature & Humidity Dimension: 15.1mm x 25mm x 7.7mm Power Supply: 3.3-6V DC Working Temperature Range: -40 to 80°C ±0.5°C accuracy Working Humidity Range: 0-100% with 2-5% accuracy	
Micro SD card Reader	Dimension: 45 x 28mm Power Supply: 4.5V – 5.5V, 3.3V	

4.2.1. Circuit Diagram

The electronic components were initially connected to a breadboard for temporary testing and checks. Once the initial testing was completed, the components were then connected to a matrix board for permanent connection based on the schematic diagram shown below.

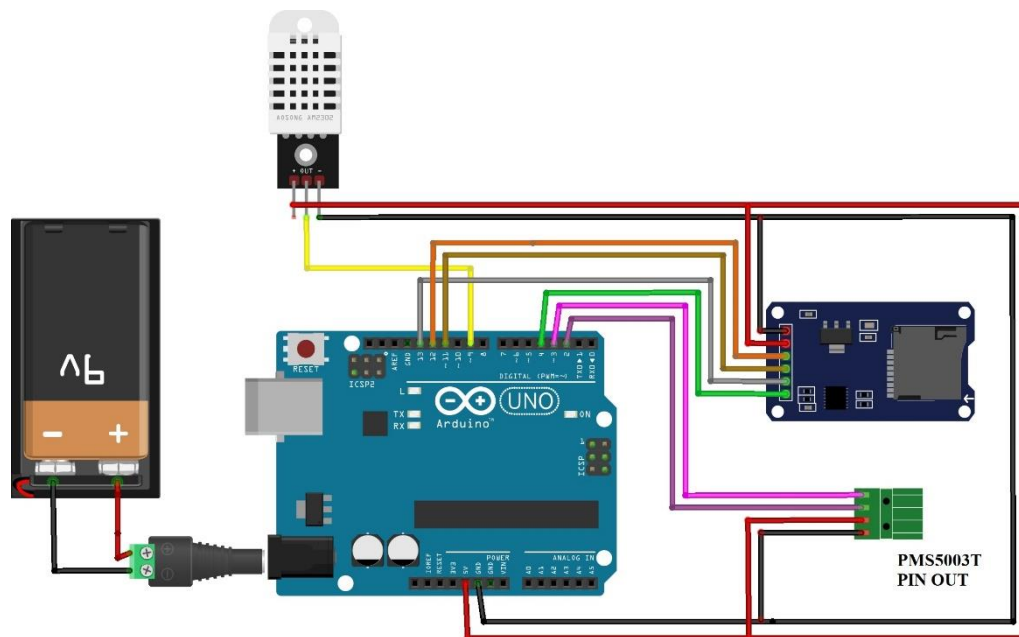


Figure 4.41: Circuit diagram for sensors operation

4.2.2. Sensor Housing and Setup

The Sensor housing was divided into two separate boxes to ensure safety and proper placement of the sensors within the vehicle. The Arduino and SD card module were housed in a 3D printed box and placed beneath the wings, in close proximity to the C.G. position. The placement was carefully selected to ensure optimal balance and stability during flight. Similarly, the PMS5003T and DHT sensors were housed in a separate 3D printed box and placed at the nose of the UAS. This location was chosen to ensure that the air flow to the sensors was clear and undisturbed, allowing for accurate data collection.

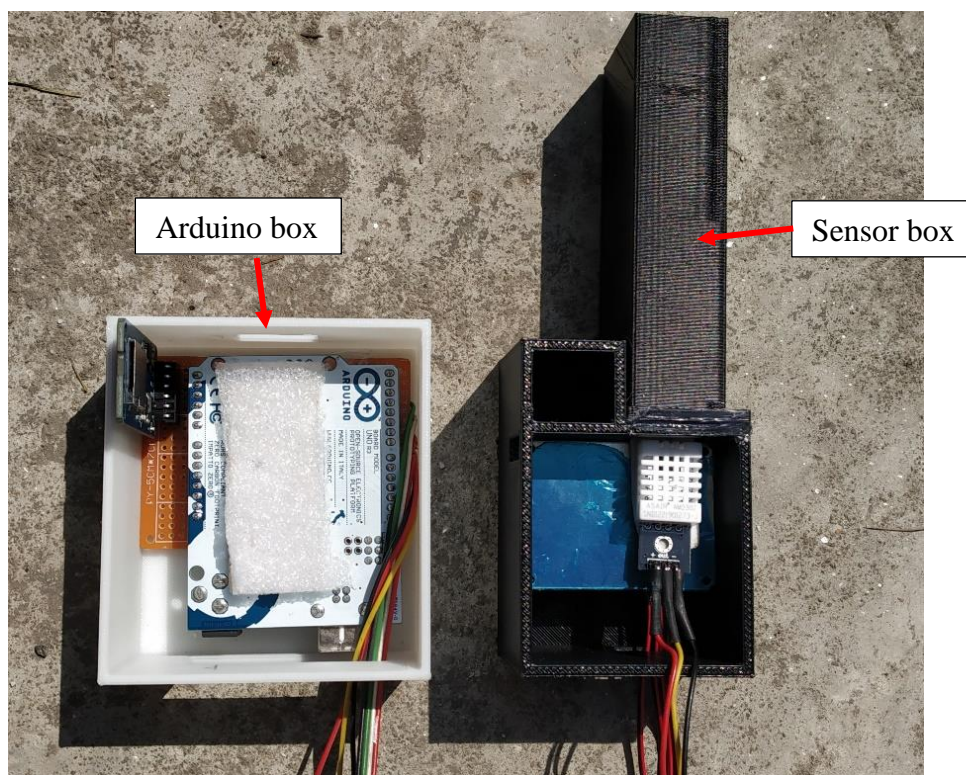


Figure 4.42: Final sensor setup for measurement

5.2.3. Sensor Sensitivity

The value of PM2.5 and PM10 concentration were measured using PMS5003T sensor at three different speeds (8m/s, 11.2 m/s and 14 m/s) to study its sensitivity with respect to the air speed.

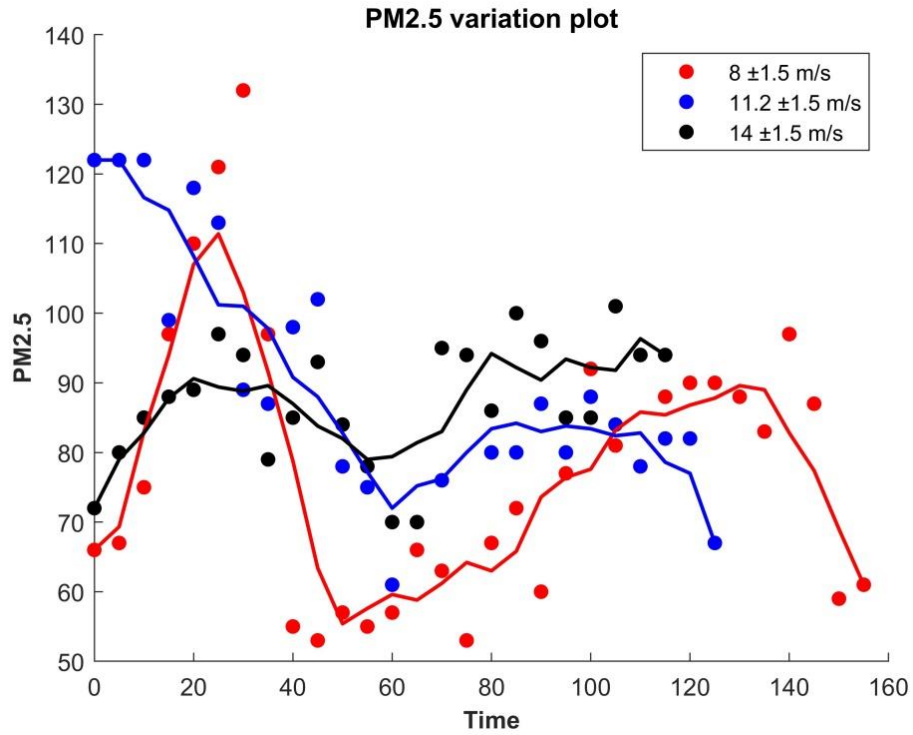


Figure 4.43: Variation of PM2.5 concentration w.r.t. speed

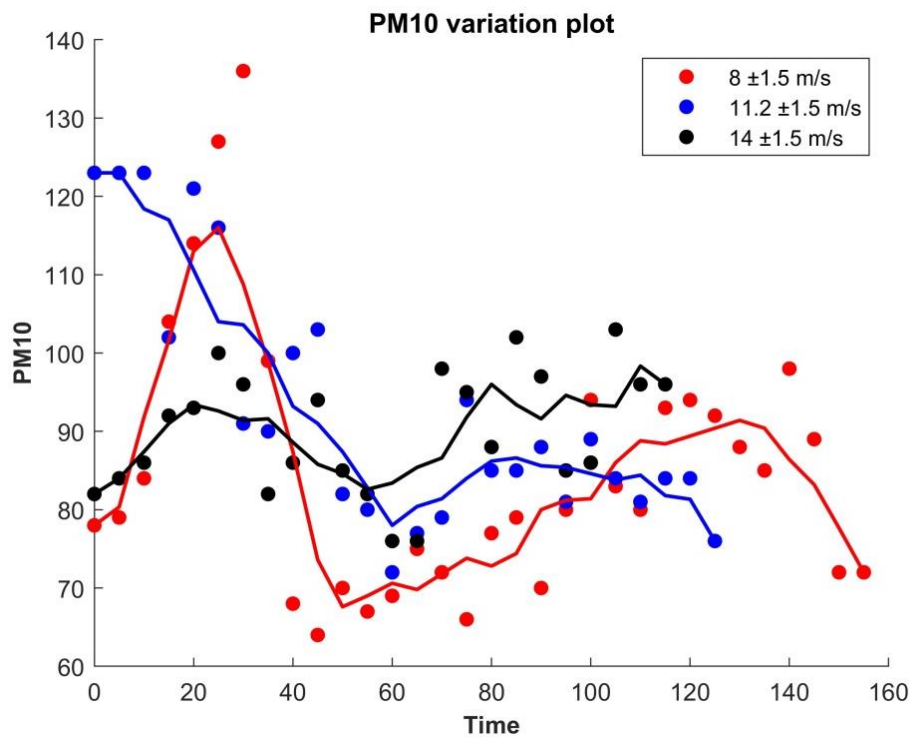


Figure 4.44: Variation of PM10 concentration w.r.t. speed

The graphs illustrate that PM_{2.5} and PM₁₀ concentrations exhibit a similar pattern with respect to flow speed. The PM concentration values were initially higher at flow speed of 11.2 m/s, but the overall trend shows that PM values increase as the flow speed increases.

The sampling capacity and sensitivity of the sensor increases as flow speed increases. At higher flow speeds, more air is drawn through the sensor and more particles are captured, leading to higher PM values while at lower speed less amount of sample air is drawn through the sensor.

It is important to note that the trend of the graphs may be affected by various factors, such as changes in environmental conditions over time. This can result in changes in the composition of the sample air being measured and, subsequently, affect the measured PM values. Therefore, it is important to consider such factors and conduct measurements under controlled conditions to ensure reliable and accurate results.

4.2.3. Sensors Calibration

The calibration of PMS5003T and DHT22 sensors were calibrated using the Laser-egg air quality monitor as a reference instrument. The Laser-egg is an air quality monitoring device that provides the measurements of PM_{2.5}, PM₁₀, Chemicals (TVOCs), Temperature, and Humidity. The calibration setup was located at the building of Aerospace Department, with a data frequency of 1 minute, as the Laser-egg provides data at this interval. The calibration process took approximately 3 and a half hours, with a total of 205 data samples collected from each sensor and the Laser-egg for analysis.

The calibration was performed on the assumption that the air pollution data provided by the Laser-egg are accurate.

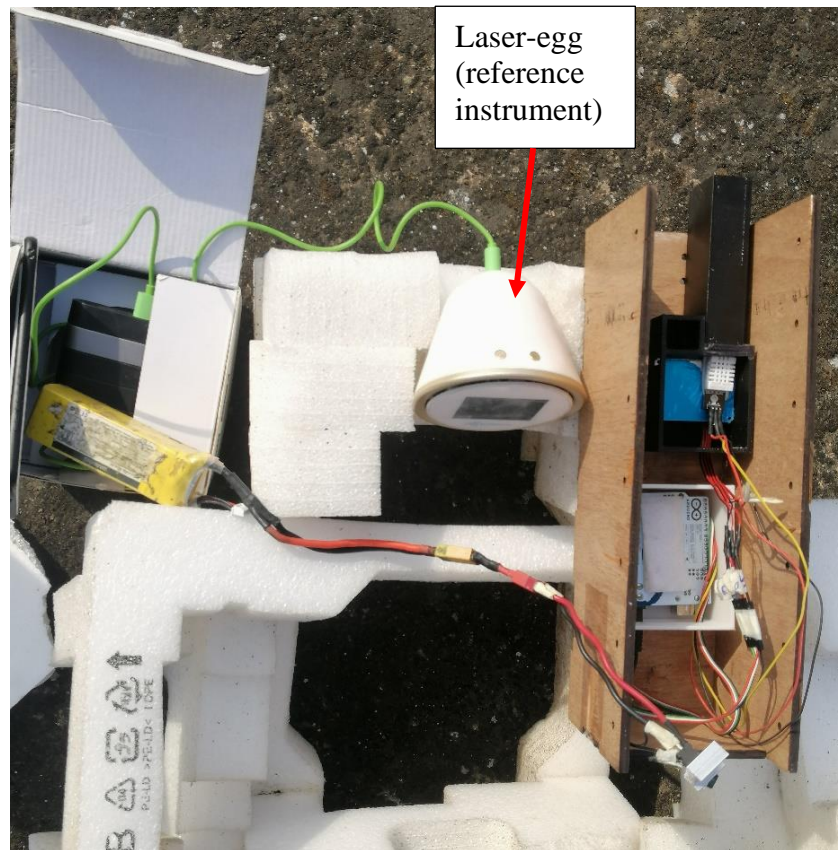


Figure 4.45: Calibration setup

Following the completion of data collection, the following calibration procedures were followed:

- The data collected from the Arduino was saved in a .txt file, while the Laser-egg data was provided in .csv format. To facilitate data analysis, the time scales for both data sets were arranged in a single file.
- A preliminary plot was the created to compare the Laser-egg data to the sensor data.
- A single-point calibration method was used for the calibration. It is the simplest type of calibration and offset is very easy to correct with single point correction.

4.2.3.1. PM2.5 and PM10 Calibration analysis

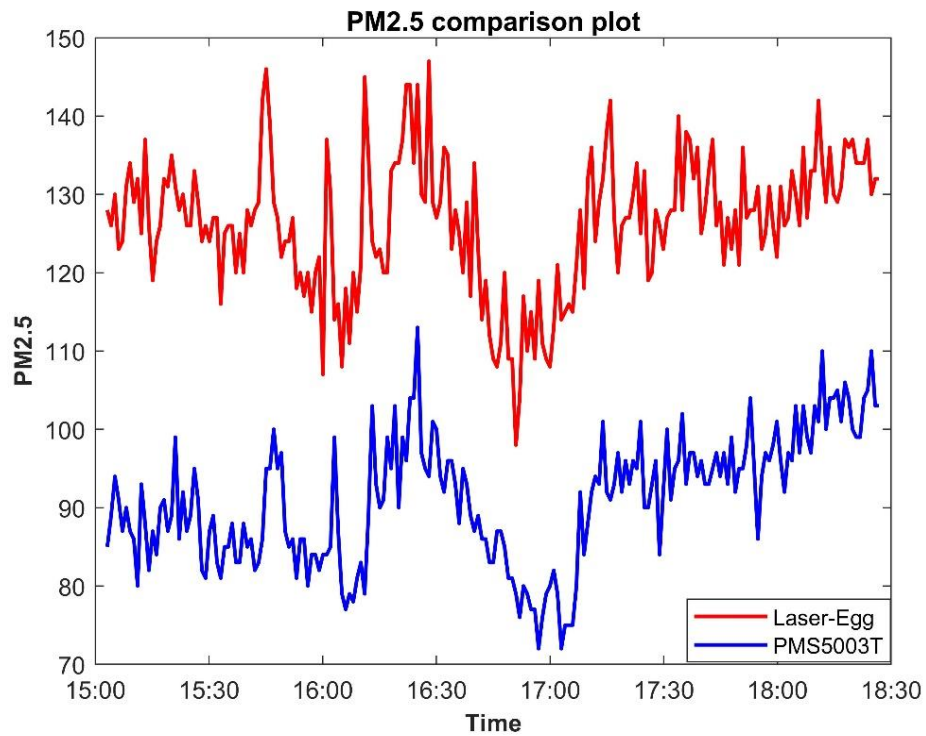


Figure 4.46: Comparison plot for PM2.5

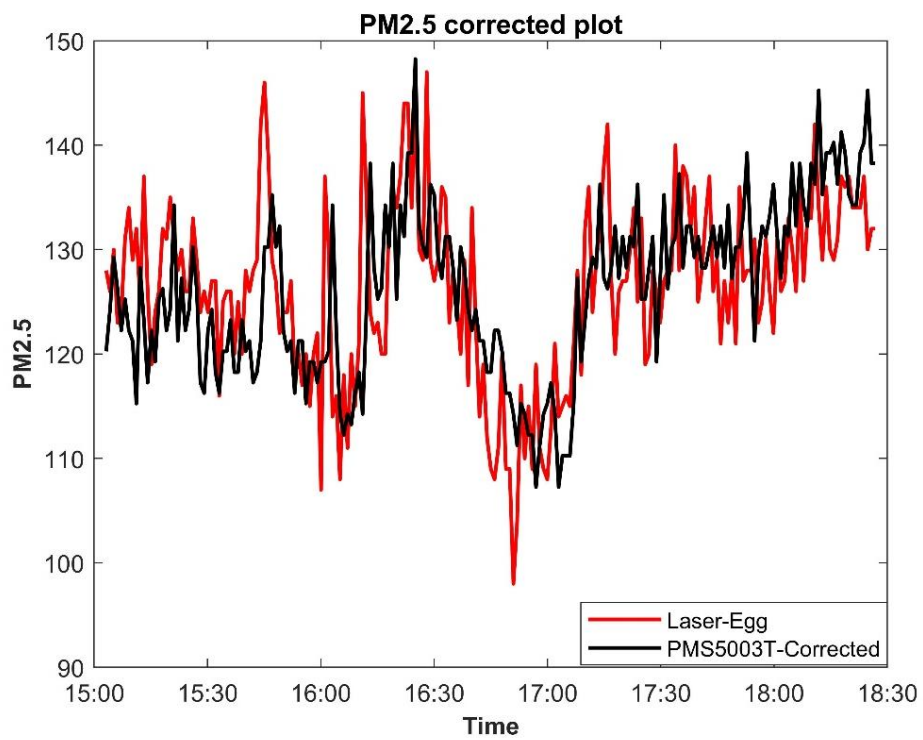


Figure 4.47: Corrected plot for PM2.5

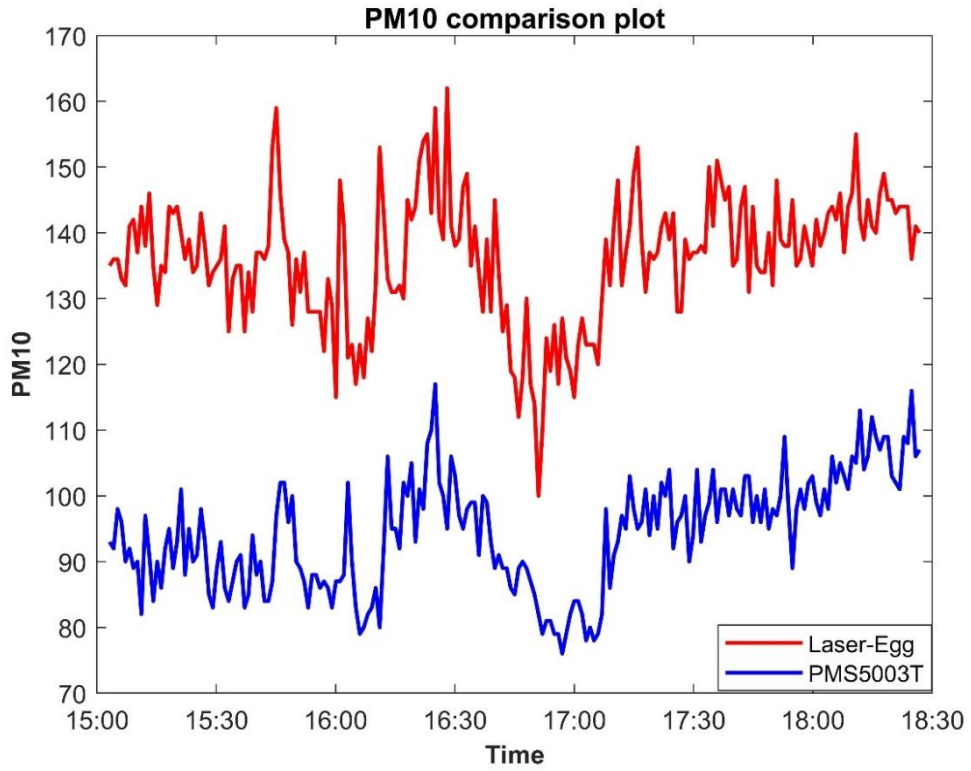


Figure 4.48: Comparison plot for PM10

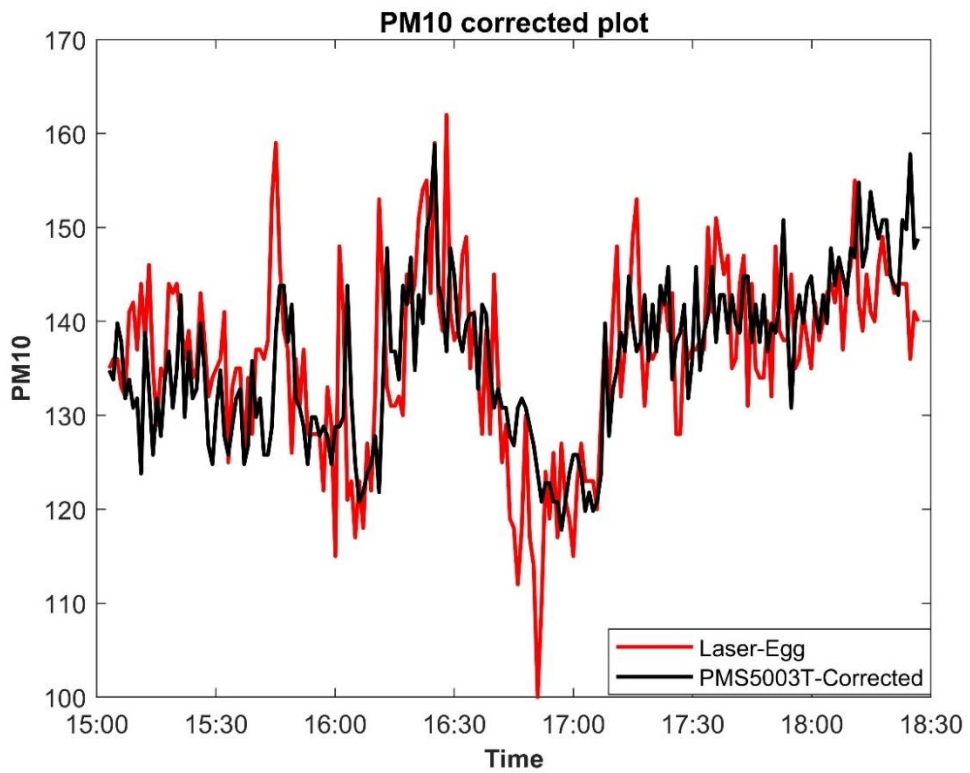


Figure 4.49: Corrected plot for PM10

To establish a relation between the PM2.5 and PM10 measurements obtained from the Laser-egg and PMS5003T sensor, a simple comparison plot was employed. From the figure 4.46 and figure 4.48, it can be seen the deviation between two measurements is relatively linear. A one-point calibration method, which adjusts the offset, was chosen for correction which involved the adjustment of each data point by a constant value. The resulting corrected plots for corrected values of PM2.5 and PM10 are shown in Figure 4.47 and 4.49, respectively.

4.2.3.2. Temperature and Humidity Calibration Analysis

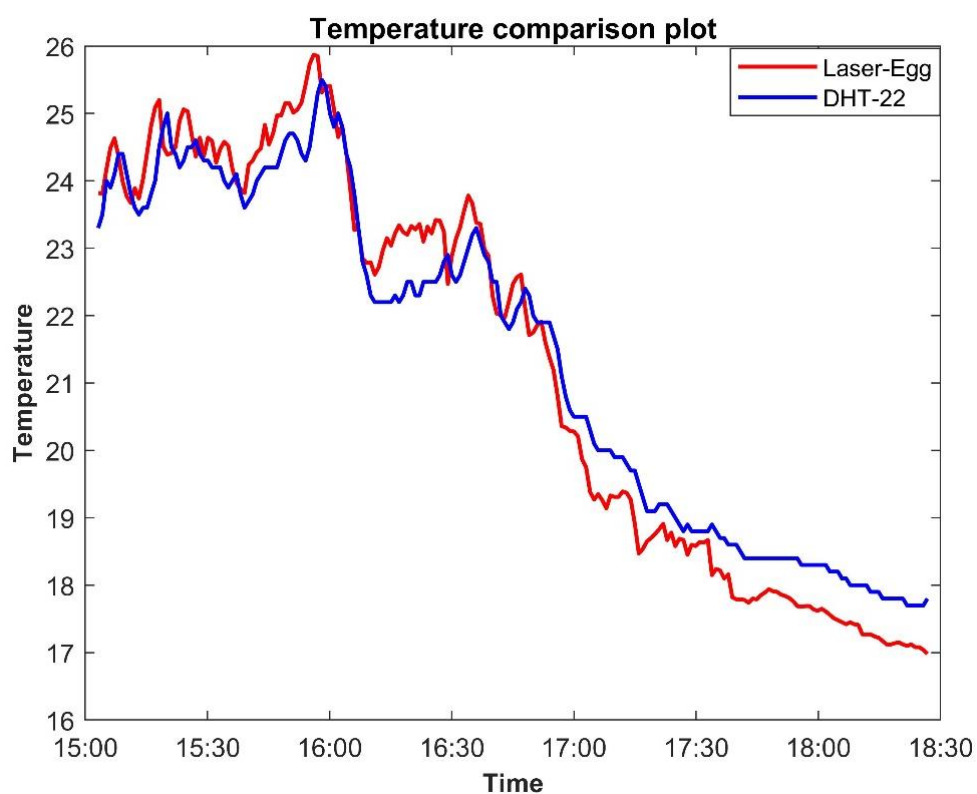


Figure 4.50: Comparison plot for temperature

The comparison plots for temperature and humidity between the DHT-22 sensor and the laser-egg are demonstrated in the figure 4.50 and figure 4.51 respectively. It can be observed that there is less amount of offset in the graphs. The error was around $\pm 5\%$ for temperature and $\pm 10\%$ for the humidity so, no calibration technique was used for the correction of the data.

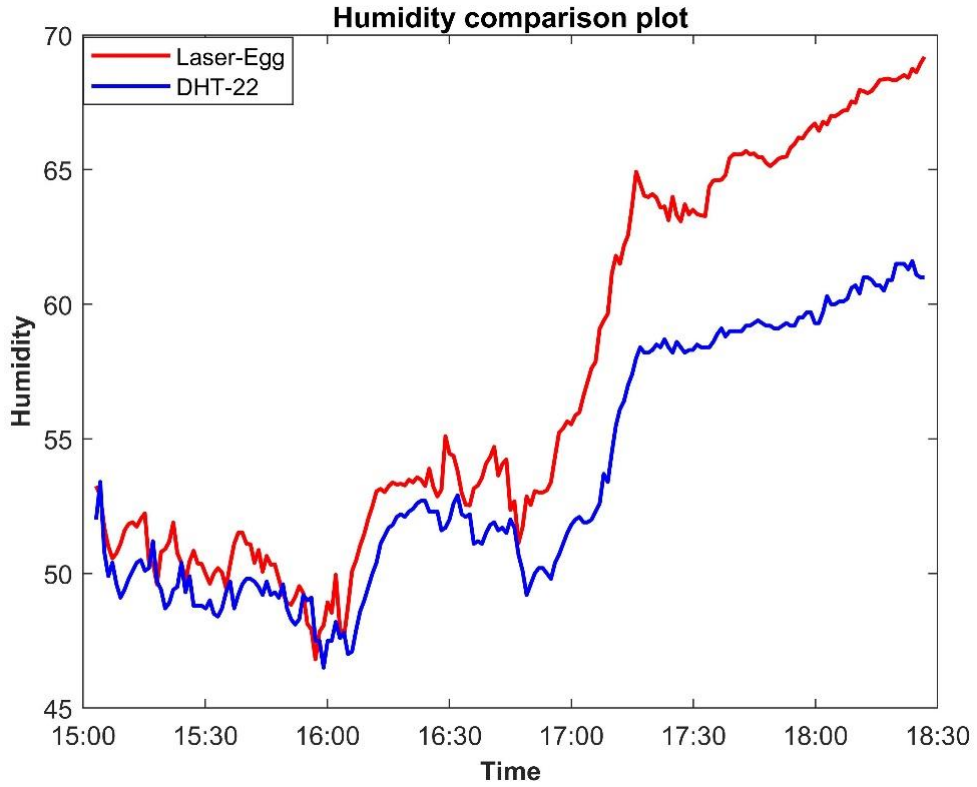


Figure 4.51: Comparison plot for humidity

Table 4.12: Statistics of data used for calibration process

Frequency of data store = 1 min			
No of samples= 205 from each sensor			
	Mean	Median	S.D.
Laser-egg-PM2.5	126.293	127.0	8.642
PMS5003-PM2.5	91.039	92.0	8.168
PMS5003-PM2.5(corrected)	126.293	127.254	8.168
Laser-egg PM10	136.093	137.0	9.824
PMS5003-PM10	94.293	95.0	8.564
PMS5003-PM10(corrected)	136.093	136.800	8.564
Laser-egg-Temperature	21.304	22.11	2.956
DHT22-Temperatre	21.378	22.10	2.517
Laser-egg-Humidity	57.239	53.64	6.998
DHT22-Humidity	53.709	52	4.627

4.2.3.3. Sensors Field Validation

The obtained correction factor was then integrated into the Arduino code to obtain the corrected sensor data. Following this, new measurements were taken from both the sensors and the reference instrument, and the resulting data were plotted for analysis.

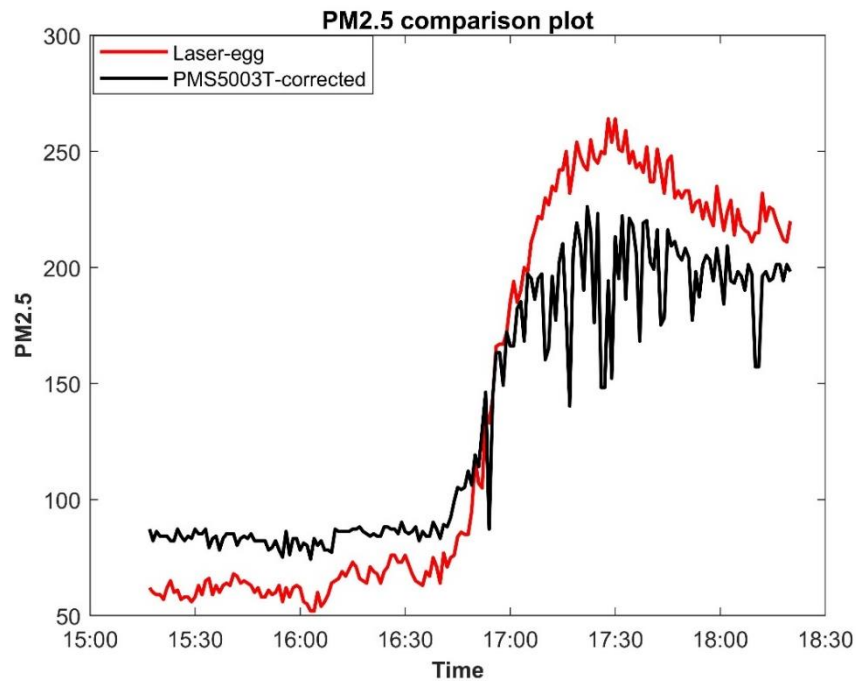


Figure 4.52: Comparison plot for PM2.5 after correction

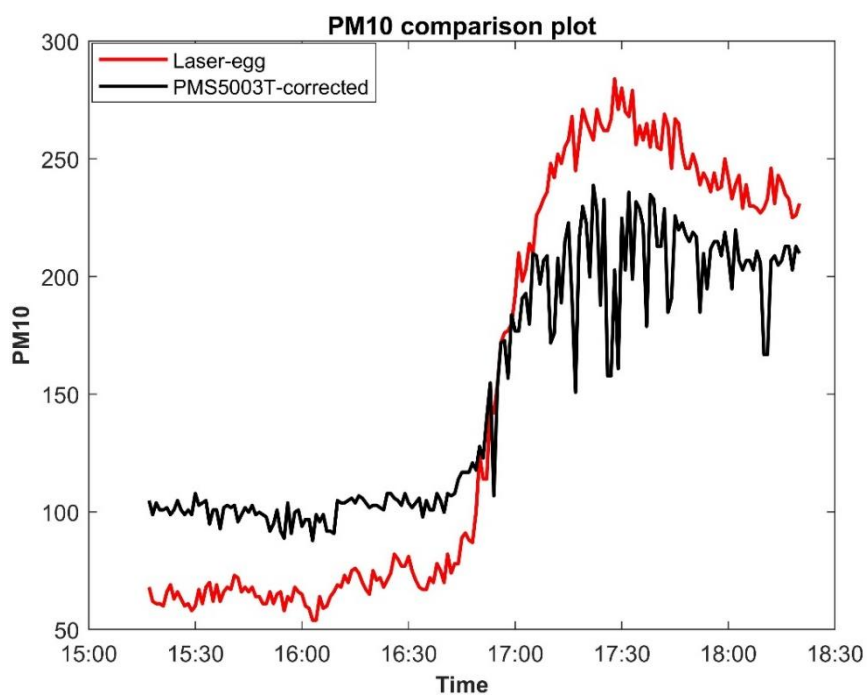


Figure 4.53: Comparison plot for PM10 after correction

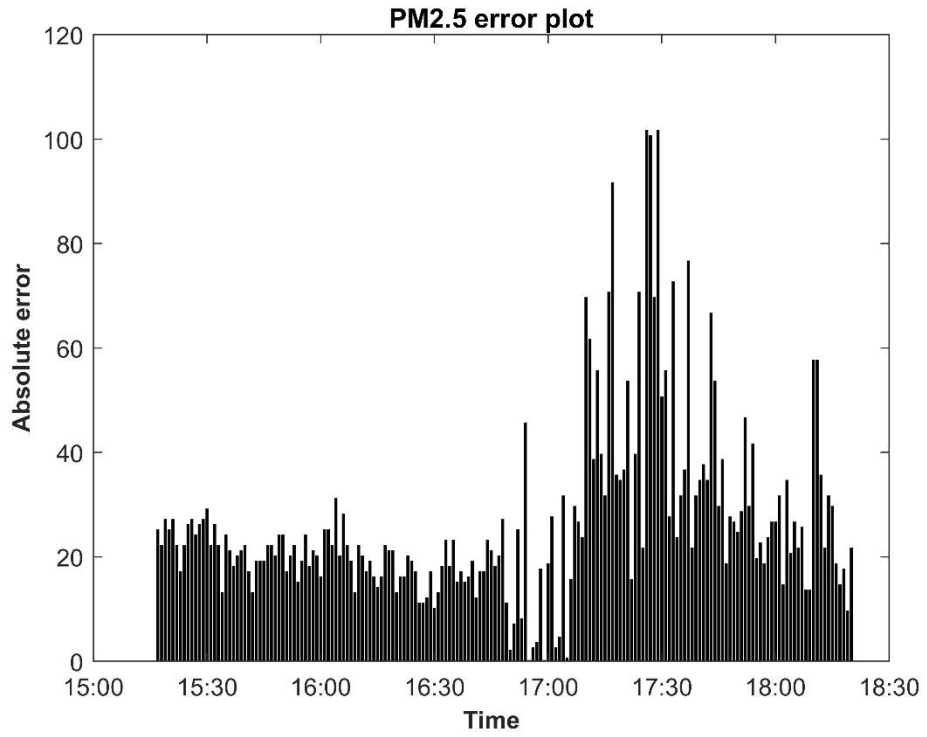


Figure 4.54: Absolute error of PM2.5 vs Time

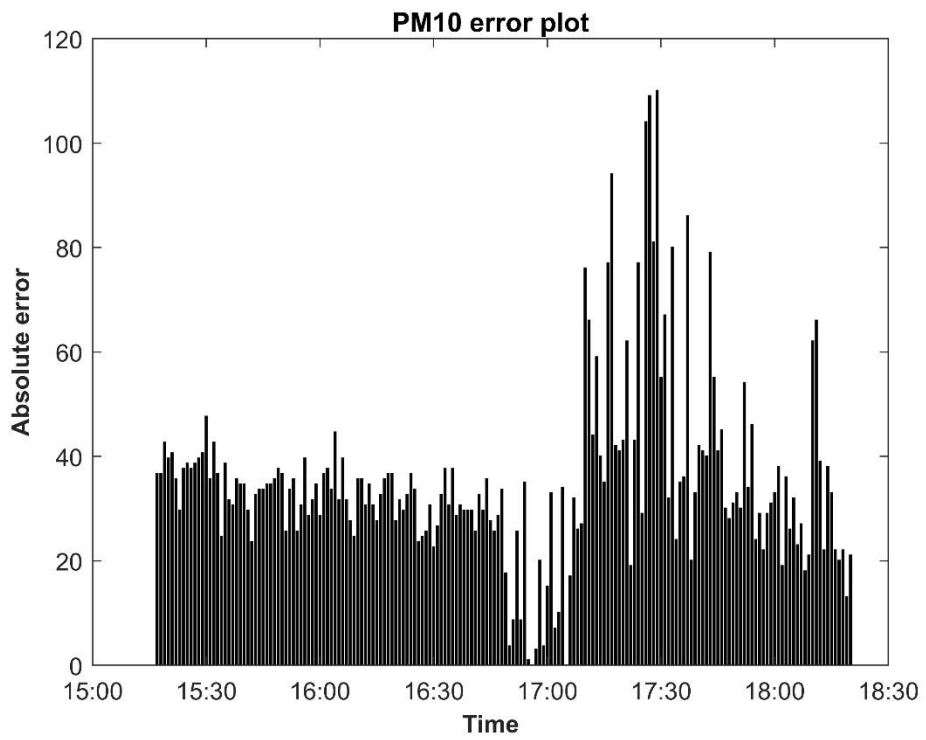


Figure 4.55: Absolute error of PM10 vs Time

It was observed that, despite the correction factor, there was still some discrepancies between the PM concentration data (PM2.5 and PM10) recorded by the PMS5003T sensor and the reference equipment. The mean absolute error was found to be 26.8291% and 35.4598% for PM2.5 and PM10, respectively. As seen in figure 4.56, there is a noticeable increase in the wind speed after 5 PM, which could be the possible reason for the elevated errors seen in the data beyond that time.

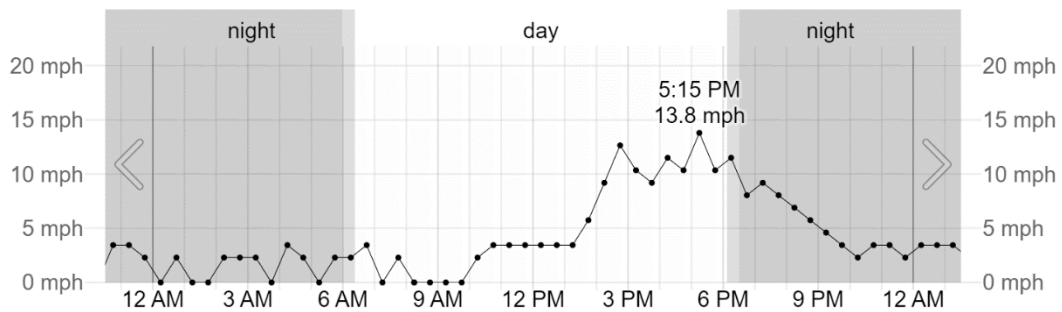


Figure 4.56: Wind speed profile on 7th March (Source: TIA weather data)

Since there was a limited amount of sample data and the measurements were not taken in varying situations such as different seasons and atmospheric conditions, it is uncertain if the calibration process used is entirely accurate. With more sample data and varying conditions, a more accurate correction factor could have been derived. Therefore, it is important to consider such factors and conduct measurements under various conditions to ensure reliable and accurate results.

4.3. Data Acquisition and Processing

Data acquisition process involves the collection of data from various sources, such as sensors and devices, and converting it into a digital format for further analysis and interpretation. This process involves capturing and measuring raw data, which is then processed and digitized.

4.3.1. Working Mechanism

During the flight, the sensors provide the data, which is then processed by the Arduino microcontroller and stored on an SD card module. At the same time, a GPS module connected to the Pixhawk system tracks the UAS's location and stores that information.

Once the flight is completed, the data stored on the SD card and Pixhawk is downloaded and used for post-processing.

4.3.2. Setup

The whole sensor setup was placed within the UAS with a small hole at the front of the nose for air inlet and at the top for air outlet. Once the setup was completed, autonomous flight and manual flight of the integrated system was performed for the data acquisition. QGroundControl software was used for the flight control and vehicle setup.

Telemetry was used to connect the Pixhawk and the ground control system. For the automated flight, the Pixhawk, GPS module, and ESC were calibrated at first. Next, the flight path was planned and uploaded into the Pixhawk. After being set to mission mode, the UAS began its flight, and the process of data collection was initiated.

Likewise, for the manual test the Pixhawk, GPS module, ESC and radio controller were calibrated at first. The Pixhawk and GPS module were used to determine the location of UAS during flight. A random mission was uploaded in Pixhawk and then set to mission mode. Then the UAS was launched and controlled by the radio controller.



Figure 4.57: Flight profile set for autonomous final flight test

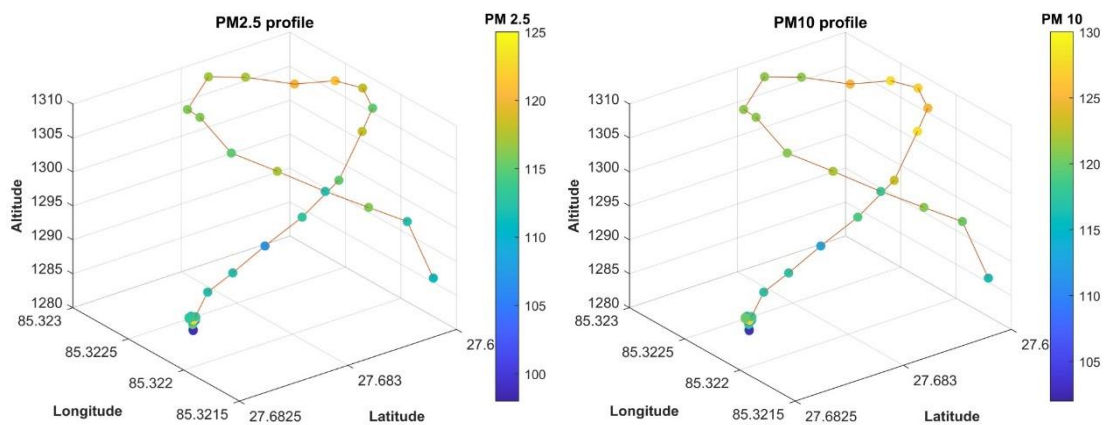


Figure 4.58: Flight profile followed in autonomous final flight test

4.3.3. Data Processing and Analysis

The data obtained from the SD card and Pixhawk were analyzed and plotted to obtain the following results.

➤ Test - one (Autonomous)



(a)

(b)

Figure 4.59: Variations of PM2.5 (a) and PM10 (b) w.r.t. to UAS position

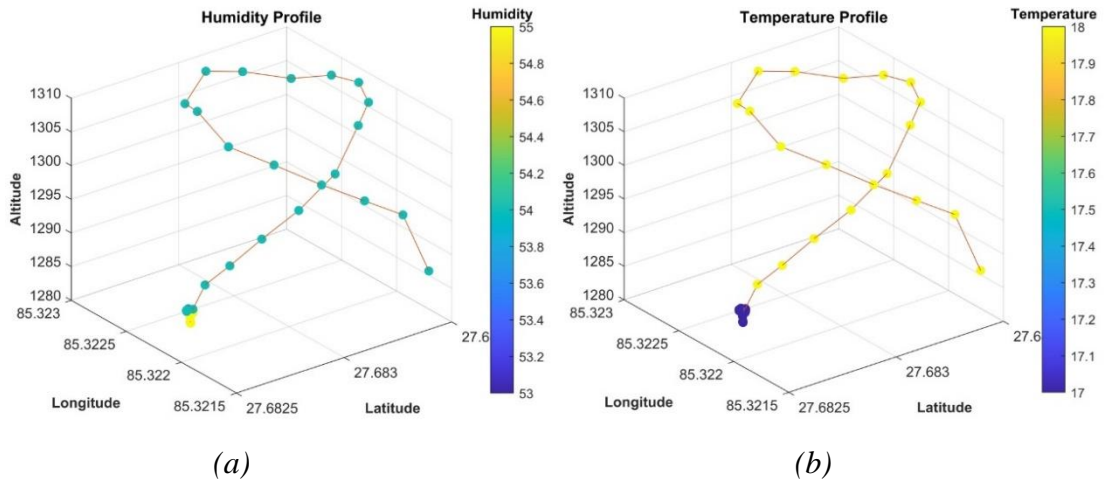


Figure 4.60: Variations of Humidity (a) and Temperature (b) w.r.t. to UAS position

Within the range of the altitude of 25m, the 3D plot provides a clear visualization of how temperature, humidity, PM2.5, and PM10 vary with respect to the UAS's position at different timestamps during the flight. There was not much variation in the values of temperature and humidity. The temperature ranged between 17-18 degrees Celsius, while the humidity ranged between 53-56%. The PM2.5 and PM10 concentration ranged from 100-150 $\mu\text{g}/\text{m}^3$ and 105-150 $\mu\text{g}/\text{m}^3$, respectively.

➤ **Test- two (Manual)**

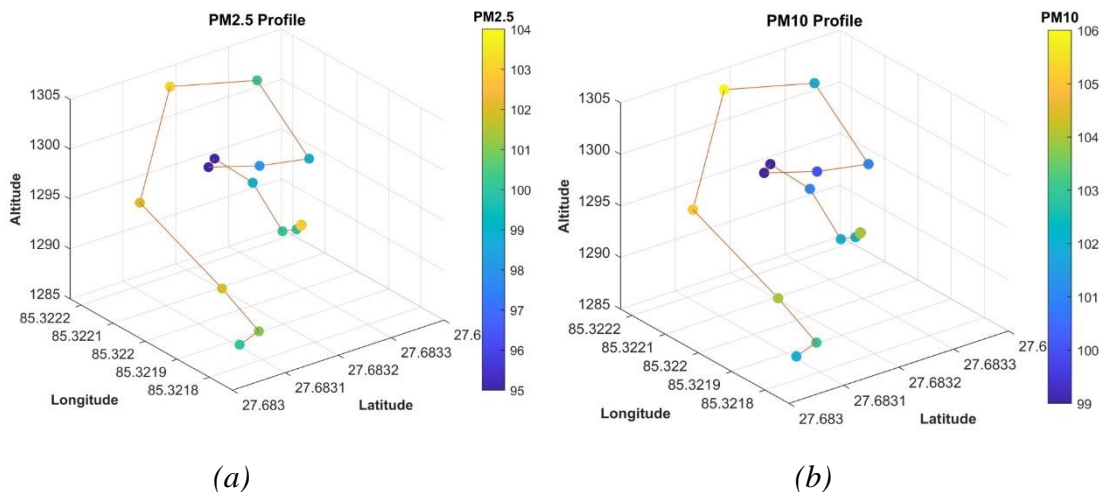


Figure 4.61: Variations of PM2.5 (a) and PM10 (b) w.r.t. to UAS position

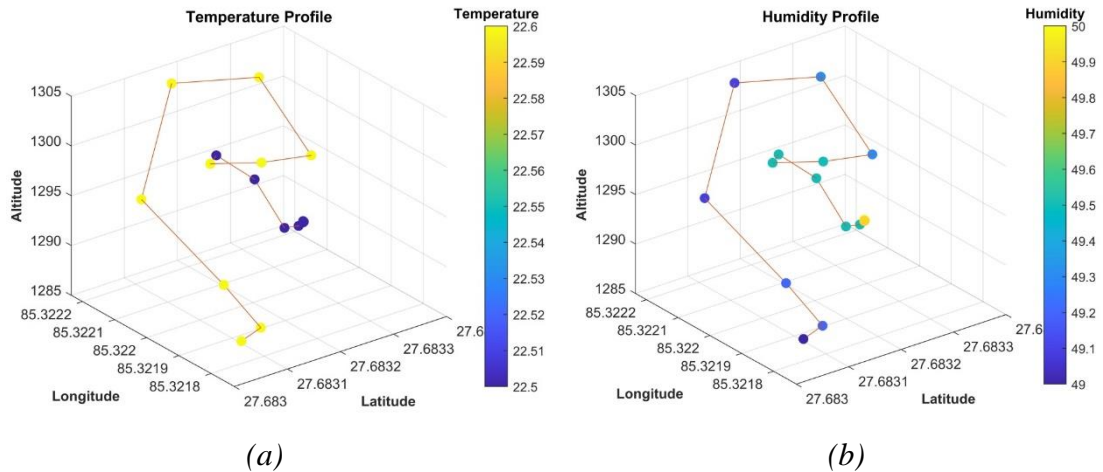


Figure 4.62: Variations of Humidity (a) and Temperature (b) w.r.t. to UAS position

Similarly, the results from manual test were plotted in 3D as shown in figure above. Within the range of 20m, some variations can be seen in the value of PM2.5 and PM10 concentration that ranged from 95-104 $\mu\text{g}/\text{m}^3$ and 99-106 $\mu\text{g}/\text{m}^3$, respectively whereas no variation can be seen in the temperature and humidity value.

There can be seen some slight variations in the value of particulate matter concentrations in the autonomous flight and manual flight. However, the tests were performed on different days and time and there are also other various factors like pollution sources, wind velocity, and atmospheric conditions that can affect the concentration of the particulate matter.

➤ **Variation of PM2.5 and PM10 with respect to altitude**

The scatter plot was generated to analyze the variations of PM2.5 and PM10 with respect to altitude.

➤ **Test-one (Autonomous)**

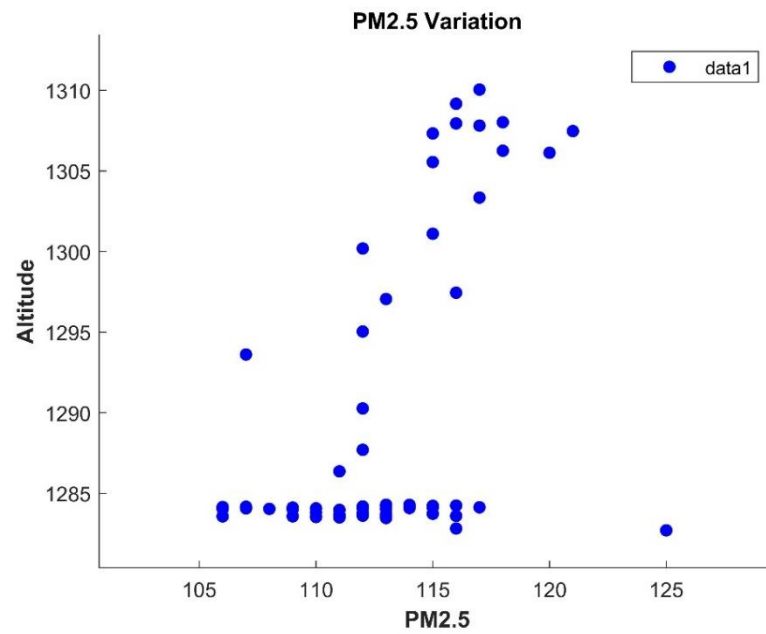


Figure 4.63: Variation of PM2.5 concentration w.r.t. altitude

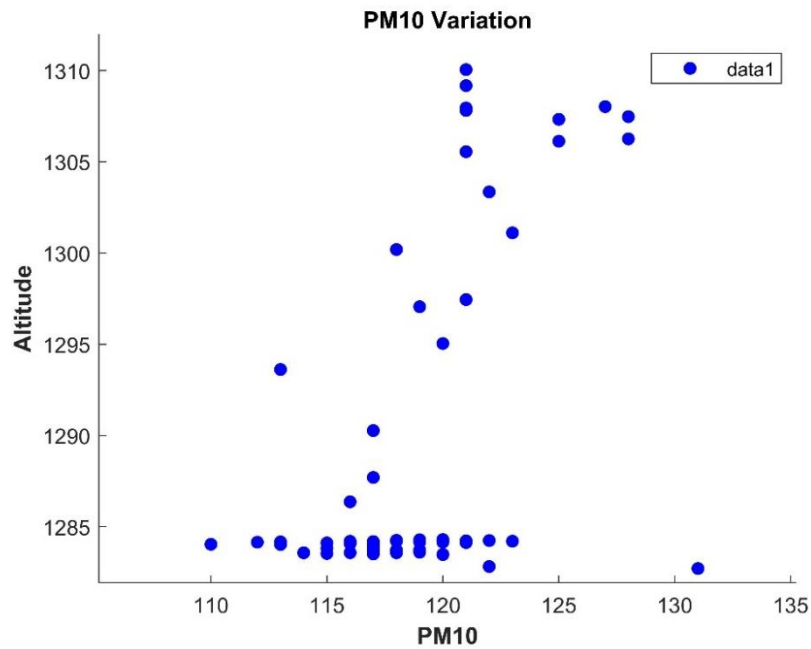


Figure 4.64: Variation of PM10 concentration w.r.t. altitude

➤ **Test-two (Manual)**

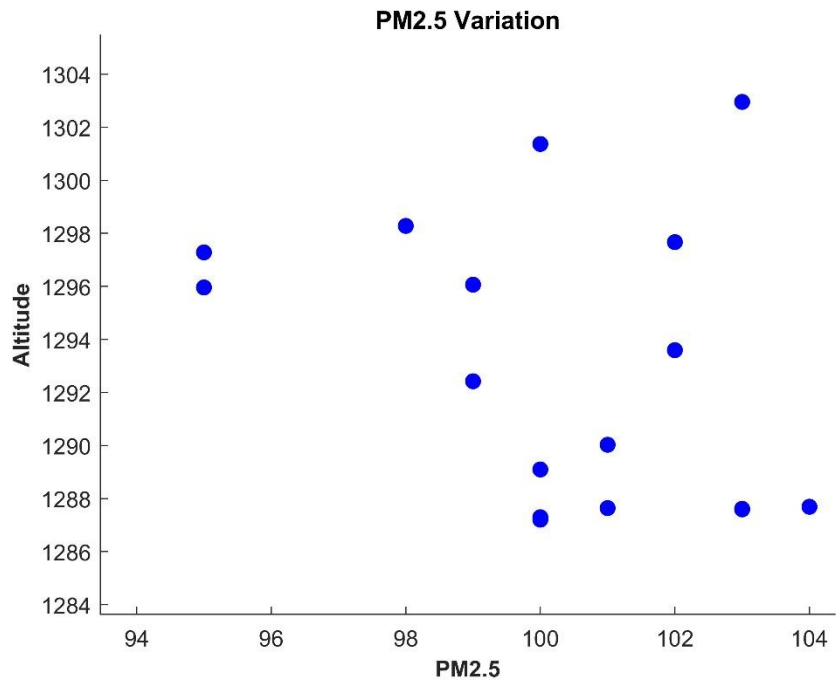


Figure 4.65: Variation of PM2.5 concentration w.r.t. altitude

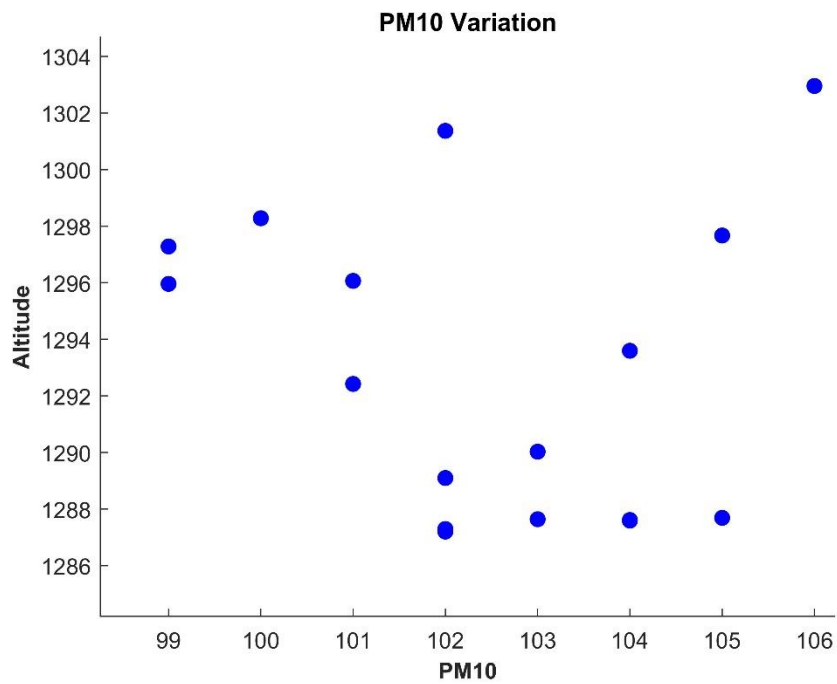


Figure 4.66: Variation of PM2.5 concentration w.r.t. altitude

Similarly, there was no clear pattern observed in changes of value of PM_{2.5} and PM₁₀ with respect to altitude. However, there are many other factors such as time, distinct location (latitude and longitude), wind velocity, and atmospheric conditions that can influence the concentration of particulate matter. Since the UAS was operated at a relatively low altitude of 15-25 meters above ground level, it is unlikely that the altitude difference would have significant influence on variations of PM concentrations.

These results demonstrate the potential of UAS for measuring and visualizing air quality data at any desired location that is within the design criteria.

4.4. Limitations

- The sensor has its own data processing capabilities.
- There was no reliable sources available for calibration and validation of the sensor so the Laser-Egg device was assumed to be accurate and used for calibration.
- The cross-platform discrepancies between X-plane and XFLR5 led to mismatch of results from both software.
- There was certain uncertainty of the GPS, which caused the deviation of the flight path.

4.5. Problems Faced

- The dust sensor available (Sharp GP2Y1010) did not meet our project objective. We were unable to obtain any sources to calibrate or validate the sensor's data on overall dust concentration.
- The number of available devices, such as Pixhawk, Gyroscopes, and Transmitters, was limited with respect to the group using them, causing delays in calibrating them repeatedly.
- Design and manufacturing discrepancies.
- Styrofoam which was available and used was of high density which made the aircraft heavier than calculated.

4.6. Budget Analysis

The overall budget of the project can be illustrated in the tabular form:

Table 4.13: Budget estimation

S.N.	Estimated Materials	Quantity	Cost/Unit (NRS)	Total Cost (NRS)
1.	Pixhawk	1	18,000	18,000
2.	Electronic Speed Controller (ESC)	1	1,000	1,000
3.	Arduino Uno	1	2,000	2,000
4.	Brushless Motor	1	1500	1500
5.	Remote Controller	1	15,000	15,000
6.	Telemetry Module	2	7,000	14,000
7.	GPS Module	1	5,000	5,000
8.	Li-Po Battery	1	4,000	4,000
9.	Battery Charger	1	4,000	4,000
10.	PM 2.5 sensor	1	10,000	10,000
11.	Temperature and Humidity Sensor	1	500	500
12.	Micro Servos	4	500	2,000
13.	SD Card Module	1	500	500
14.	Manufacture and Miscellaneous: Tape, Paper Cutter, Styrofoam, Hot glue gun, adhesive bond, plywood, jumper wire, matrix board, connectors, etc.		28,000	28,000
	Total			1,05,500

CHAPTER 5: CONCLUSION AND FUTURE ENHANCEMENT

5.1. Conclusion

This project aimed to develop a pollution measurement system using a fixed-wing UAS. The project is divided into three parts: UAS design and fabrication, sensor integration and testing. Firstly, a fixed-wing UAS was designed and fabricated. The design process was carried out in three phases: conceptual design, preliminary design, and detail design. During the conceptual design phase, initial aircraft parameters and design constraints were estimated, and wing parameters were calculated using theoretical formulas. A baseline design was then created in XFLR5, and performance and stability analyses were performed in XFLR5 and XPLANE 11, respectively. The final design was developed in CATIA, and the wing, empennage, and fuselage structure were fabricated. Then, each individual components were assembled, and the final model was obtained. After the fabrication, manual and autonomous flight tests were performed to ensure the functionality of the UAS.

Secondly, the sensors selected for the project were PMS5003T for measuring PM1, PM2.5 and PM10 and DHT-22 for the measurement of temperature and humidity. The sensors were calibrated using the reference device Laser-egg 201 in the assumption that the data provided by laser-egg are accurate. Then, a sensor box was fabricated to house the selected sensors. Finally, a manual an autonomous tests were performed with the integrated sensor box at an altitude of about 15-25m. The PM2.5 and PM10 concentration ranged from 100-150 $\mu\text{g}/\text{m}^3$ and 105-150 $\mu\text{g}/\text{m}^3$, respectively during the autonomous test while on a manual test the results of PM 2.5 and PM10 concentration ranged from 95-104 $\mu\text{g}/\text{m}^3$ and 99-106 $\mu\text{g}/\text{m}^3$ respectively. The results demonstrate the potential of using UAS for air pollution measurement.

5.2. Scope for Future Enhancement

There are several potential areas for future enhancements. Firstly, the proper calibration techniques that takes into account a longer sample time as well as various environmental conditions such as seasonal changes, time of day, temperature, and climate could be used to improve the accuracy and reliability of the sensor. Another potential area for enhancement is the integration of additional sensors which would provide the concentrations of other pollutants. Additionally, constructing a duct that reduces the air speed at the sensor inlet, its accuracy could be improved. Similarly, lighter materials, such as balsa wood and carbon fiber rod can be utilized to construct the structure of the UAS, which in turn reduces the weight and increases effectiveness. Furthermore, implementing a real-time data transfer and mapping will allow for more timely and efficient monitoring and analysis of the air quality.

REFERENCES

- [1]“Home | State of Global Air,” *Stateofglobalair.org*, 2019.
<https://www.stateofglobalair.org/>
- [2]World Health Organization, “Air Pollution,” *Who.int*, 2022.
https://www.who.int/health-topics/air-pollution#tab=tab_1
- [3]“Air Quality Monitoring | Nepal,” *pollution.gov.np*.
https://pollution.gov.np/portal/#/home?_k=bu34ve (Accessed Feb. 04, 2023).
- [4] T. Villa, F. Gonzalez, B. Miljievic, Z. Ristovski, and L. Morawska, “An Overview of Small Unmanned Aerial Systems for Air Quality Measurements: Present Applications and Future Prospectives,” *Sensors*, vol. 16, no. 7, p. 1072, Jul. 2016, doi: 10.3390/s16071072.
- [5] W. A. Harrison, D. J. Lary, B. J. Nathan, and A. G. Moore, “Using Remote Control Aerial Vehicles to Study Variability of Airborne Particulates,” *Air, Soil and Water Research*, vol. 8, p. ASWR.S30774, Jan. 2015, doi: 10.4137/aswr.s30774.
- [6] B. J. Nathan *et al.*, “Near-Field Characterization of Methane Emission Variability from a Compressor Station Using a Model Aircraft,” *Environmental Science & Technology*, vol. 49, no. 13, pp. 7896–7903, May 2015, doi: 10.1021/acs.est.5b00705.
- [7] P. Vijayakumar, A. Khokhar, A. Pal, and M. Dhawan, “Air Quality Index Monitoring and Mapping Using UAS,” *IEEE Xplore*, Jul. 01, 2020.
<https://ieeexplore.ieee.org/abstract/document/9182374>
- [8] S. Pochwała, A. Gardecki, and P. Lewandowski, “Developing of Low-Cost Air Pollution Sensor—Measurements with the Unmanned Aerial Systems in Poland,” *Sensors*, vol. 20, no. 12, p. 3582, Jun. 2020, doi: <https://doi.org/10.3390/s20123582>.
- [9] M. Alvarado, F. Gonzalez, A. Fletcher, and A. Doshi, “Towards the Development of a Low Cost Airborne Sensing System to Monitor Dust Particles after Blasting at

Open-Pit Mine Sites,” *Sensors*, vol. 15, no. 8, pp. 19667–19687, Aug. 2015, doi: 10.3390/s150819667.

[10] P. Yadav, T. Porwal, V. Jha, and Prof. S. Indu, “Emerging Low-Cost Air Quality Monitoring Techniques for Smart Cities with UAS,” *IEEE*, Oct. 20, 2020.

[11] J. Burgués and S. Marco, “Environmental chemical sensing using small drones: A review,” *Science of The Total Environment*, vol. 748, p. 141172, Dec. 2020, doi: 10.1016/j.scitotenv.2020.141172.

[12] H. F. Hawari, A. A. Zainal, and M. R. Ahmad, “Development of real time internet of things (IoT) based air quality monitoring system,” *Indonesian Journal of Electrical Engineering and Computer Science*, vol. 13, no. 3, p. 1039, Mar. 2019, doi: 10.11591/ijeecs.v13.i3.pp1039-1047.

[13] Y. Wang, J. Li, H. Jing, Q. Zhang, J. Jiang, and P. Biswas, “Laboratory Evaluation and Calibration of Three Low-Cost Particle Sensors for Particulate Matter Measurement,” *Aerosol Science and Technology*, vol. 49, no. 11, pp. 1063–1077, Oct. 2015, doi: 10.1080/02786826.2015.1100710.

[14] J. E. Thompson, “Improved Measurement Performance for the Sharp GP2Y1010 Dust Sensor: Reduction of Noise,” *Atmosphere*, vol. 12, no. 6, p. 775, Jun. 2021, doi: 10.3390/atmos12060775.

[15] A. Masic *et al.*, “Calibration and Assessment of Low-Cost Dust Sensors Introduction the ECTS system in BH universities View project Investigation of the air pollution in the Sarajevo valley using UAS based measurements View project 29TH DAAAM INTERNATIONAL SYMPOSIUM ON INTELLIGENT MANUFACTURING AND AUTOMATION CALIBRATION AND ASSESSMENT OF LOW-COST DUST SENSORS,” pp. 523-0528, 2018, doi: 10.2507/29th.daaam.proceedings.075.

[16] M. Zusman *et al.*, “Calibration of low-cost particulate matter sensors: Model development for a multi-city epidemiological study,” *Environment International*, vol.

134, p. 105329, Jan. 2020, doi: <https://doi.org/10.1016/j.envint.2019.105329>.

[17] T. Zheng, M. H. Bergin, K. K. Johnson, and S. N. Tripathi, “Field evaluation of low-cost particulate matter sensors in high- and low-concentration environments,” *Atmospheric Measurement Techniques*, vol. 11, no. 8, pp. 4823–4846, Aug. 2018, doi: <https://doi.org/10.5194/amt-11-4823-2018>.

[18] L. Bernd and S. Antonia., “Development of a Calibration Methodology for the SDS011 Low-Cost PM-Sensor with respect to Professional Reference Instrumentation.,” 2017.

[19] Hannaneh Hojaiji, Haik Kalantarian , Alex A.T. Bui , Christine E. King, PhD, Majid Sarrafzadeh, “Temperature and Humidity Calibration of a Low-Cost Wireless Dust Sensor for Real-Time Monitoring,” *IEEE*, 2017.

[20] A. Cavaliere, F. Carotenuto, F. Di Gennaro, B. Gioli, C. Vagnoli, and A. Zaldei, “Development of Low-Cost Air Quality Stations for Next Generation Monitoring Networks: Calibration and Validation of PM_{2.5} and PM₁₀ Sensors,” *Sensors*, vol. 18, no. 9, p. 2843, Aug. 2018, doi:<https://doi.org/10.3390/s18092843>.

[21] N. H. Nguyen, H. X. Nguyen, T. T. B. Le, and C. D. Vu, “Evaluating Low-Cost Commercially Available Sensors for Air Quality Monitoring and Application of Sensor Calibration Methods for Improving Accuracy,” *Open Journal of Air Pollution*, vol. 10, no. 01, pp. 1–17, 2021, doi: <https://doi.org/10.4236/ojap.2021.101001>.

[22] N. Castell, F. R. Dauge, P. Schneider, and M. Vogt, “Can commercial low-cost sensor platforms contribute to air quality monitoring and exposure estimates?,” *Environment International*, vol. 99, pp. 293–302, Feb. 2017, doi: <https://doi.org/10.1016/j.envint.2016.12.007>.

[23] L. Spinelle, M. Aleixandre, and M. Gerboles, “Protocol of evaluation and calibration of low-cost gas sensors for the monitoring of air pollution,” *JRC Publications Repository*, Sep. 12, 2013. <https://publications.jrc.ec.europa.eu/repository/handle/JRC83791> (accessed Mar. 09,

2023).

[24] K. A. Rodriguez-Vasquez, A. M. Cole, D. Yordanova, R. Smith, and N. M. Kidwell, "AIRduino: On-Demand Atmospheric Secondary Organic Aerosol Measurements with a Mobile Arduino Multisensor," *Journal of Chemical Education*, vol. 97, no. 3, pp. 838–844, Jan. 2020, doi: 10.1021/acs.jchemed.9b00744.

[25] J.-I. Hernández-Vega, E. R. Varela, N. H. Romero, C. Hernández-Santos, J. L. S. Cuevas, and D. G. P. Gorham, "Internet of Things (IoT) for Monitoring Air Pollutants with an Unmanned Aerial System (UAS) in a Smart City," *Lecture Notes of the Institute for Computer Sciences, Social Informatics and Telecommunications Engineering*, pp. 108–120, 2018, doi: 10.1007/978-3-319-73323-4_11.

[26] Liang-Yu Chen, Hsiao-Shih Huang, Cheng-Ju Wu, Yi-Ting Tsai, and Yue-Shan Chang, "A LoRa-based Air Quality Monitor on Unmanned Aerial System for Smart City," <https://sci.bban.top/pdf/10.1109/ICSSE.2018.8519967>.

[27] S. Liu, "Development of a UAS-Based System to Monitor Air Quality over an Oil Field," *Graduate Theses & Non-Theses*, Oct. 2018, [Online]. Available: https://digitalcommons.mtech.edu/grad_rsch/187/

[28] A. M. Talib and Dr. Mahdi. N. Jasim, "GIS-GPS based national air pollution monitoring system," *Materials Today: Proceedings*, Jun. 2021, doi: 10.1016/j.matpr.2021.05.445.

BIBLIOGRAPHY

- [1] R. C. Nelson, *Flight stability and automatic control*. Chennai: Mcgraw-Hill Education (India) Private Limited, 2010.
- [2] B. N. Pamadi, *Performance, stability, dynamics, and control of airplanes*. Reston, Va American Institute Of Aeronautics And Astronautics, Inc, 2015.
- [3] J. Roskam, *Airplane flight dynamics and automatic flight control. / Part 1*. Lawrence (Kansas): Dar Corp, 1995.
- [4] D. Raymer, *AIRCRAFT DESIGN: a conceptual approach*. S.L.: Amer Institute Of Aeronautics, 2019.

APPENDIX A

MATLAB CODE:

a) W/S Vs W/P as a function of Stall Speed:

```
clc
y=[0,1.962,0.981,0.654,0.4905,0.3924,0.327,0.218,0.1962,0.1784,0.151,
0.1401,0.0935,0.0892,0.08175,0.07848]; %powerloading
rho=1.0595; %density
vs=9;%stall velocity
Clmax=1.2938;%maximum coefficient of lift (90% of 2D Cl)
for i=1:ly
x1(i)=0.5*(vs.^2)*Clmax*rho
end
plot (y,x1,'g')
plot (y,x1,'g')
ylabel('Wingloading (W/S N/m2)')
xlabel('Powerloading (W/P N/Watt)')
```

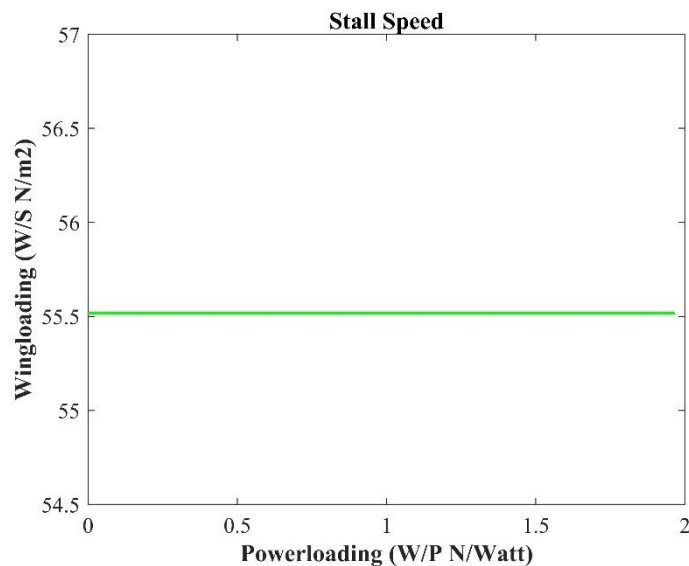


Figure A1: W/S Vs W/P as a function of stall speed

b) W/S Vs W/P as a function of maximum velocity:

```
%Maximum velocity (V max)=20 m/s (80 kph)
%Propeller efficiency (np)=90% (assumed)
%Induced drag factor(k)=0.08 (assumed)
clc
y=[0,1.962,0.981,0.654,0.4905,0.3924,0.327,0.218,0.1962,0.1784,0.151,0.1401,0.0935,0.0892,0.081
75,0.07848] %powerloading
rho=1.0595; %density
vs=9;%stall velocity
vto=1.3*vs;%takeoff speed
vmax=20;%maximum velocity
Cd0=0.022;%zero lift cd (assumed)
K=0.08;%slope
n=0.95;
a=(0.5*rho*(vmax.^3)*Cd0)%mid formula variable
b=((2*K)/(rho*vmax))%mid formula variable
```

```

ly=length(y)
z(1:ly)=1.0
for i=1:ly
x2(i)=((0.90-(0.64-(4*a*b*((y(i))^2))).^0.5))/(2*b*(y(i)))
f(i)=(n/(y(i)*vto));
end
plot (y,x2,'k')
ylabel('Wingloading (W/S N/m2)')
xlabel('Powerloading (W/P N/Watt)')

```

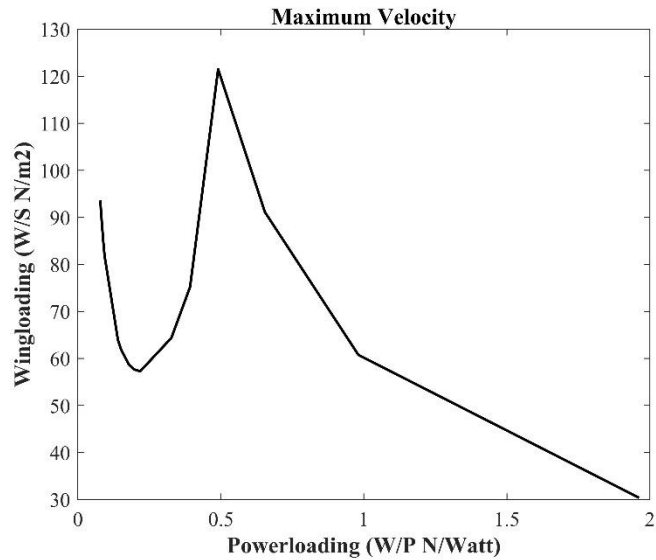


Figure A2: W/S Vs W/P as a function of maximum velocity

c) W/S Vs W/P as a function of takeoff distance:

```

clc
y=[0,1.962,0.981,0.654,0.4905,0.3924,0.327,0.218,0.1962,0.1784,0.151,0.1401,0.0935,0.0892,0.081
75,0.07848] %powerloading
rho=1.0595; %density
g=9.8;
d=30;
U=0.1;
cdg=0.025;%coefficient of drag at ground
clr=1.18;%coefficient of lift at rotation
A=(0.606*rho*g*cdg*d);%midformula variable
v=(cdg clr); %mid formula variable
ly=length(y)
z(1:ly)=1.0
for i=1:ly
x3(i)=A/log((f(i)-U)/(f(i)-U-v))
end
plot (y,x3,'b')
ylabel('Wingloading (W/S N/m2)')
xlabel('Powerloading (W/P N/Watt)')

```

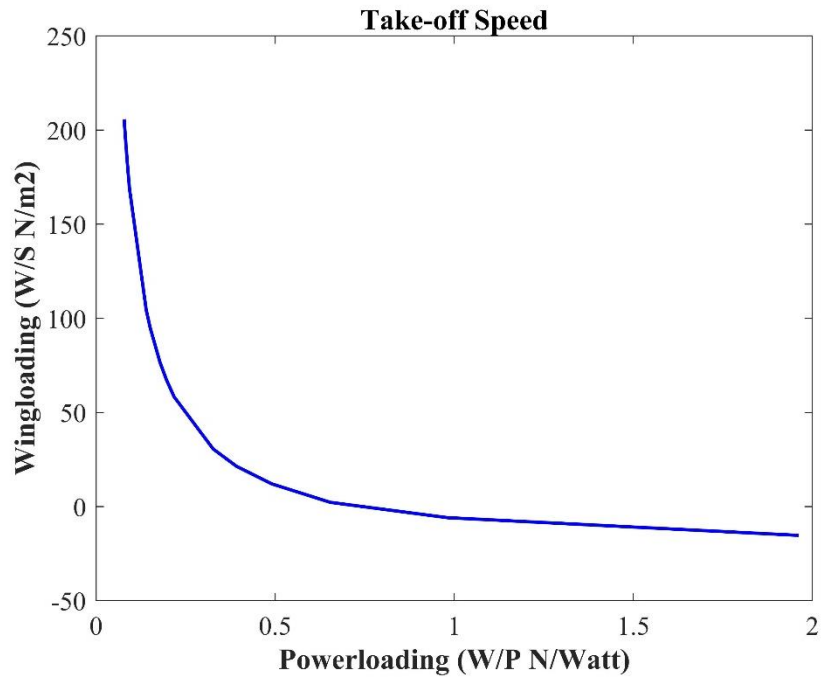



Figure A3: W/S Vs W/P as a function of takeoff distance

d) W/S Vs W/P as a function of Rate of Climb:

```

clc
y=[0,1.962,0.981,0.654,0.4905,0.3924,0.327,0.218,0.1962,0.1784,0.151,0.1401,0.0935,0.0892,0.081
75,0.07848] %powerloading
rho=1.0595; %density
vmax=20;%maximum velocity
Cd0=0.022;%zero lift cd
vc=3.0;
K=0.08;%slope
n=0.9; %propeller efficiency
a=(0.5*rho*(vmax.^3)*Cd0)%mid formula variable
ly=length(y)
z(1:ly)=1.0
for i=1:ly
x4(i)=((0.649e-4)*((a/y(i)).^2)*((n-(y(i)*vc)).^2)*rho*((Cd0/K).^0.5)))
end
plot (y,x4,'m')
ylabel('Wingloading (W/S N/m2)')
xlabel('Powerloading (W/P N/Watt)')

```

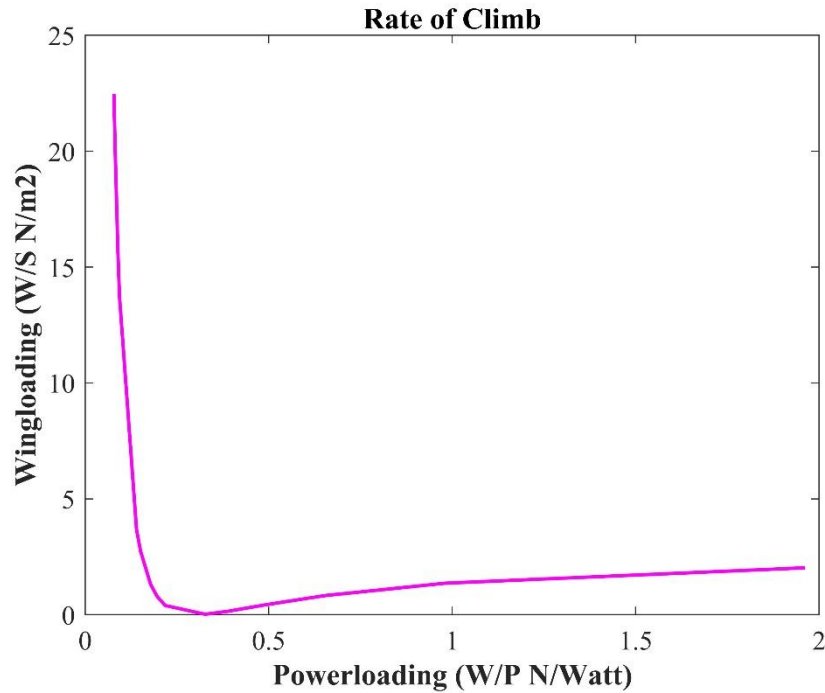


Figure A4: W/S Vs W/P as a function of ROC

e) Overall Constraint Diagram (Wing loading Vs Power loading):

```

clc
y=[0,1.962,0.4905,0.3924,0.327,0.218,0.1962,0.1509,0.1402,0.1227,0.109,0.1033,0.0935,0.0853,0.0
8175,0.07848] %powerloading
rho=1.0595; %density
g=9.8;
d=30;
vs=9;%stall velocity
vmax=20;% maximum velocity
Clmax=1.2938;%maximum coefficient of lift
Cd0=0.022;%zero lift cd
K=0.08;%slope
vto=1.3*vs;%takeoff speed
cdg=0.025;%coefficient of drag at ground
clr=1.18;%coefficient of lift at rotation
n=0.9; %propeller efficiency
U=0.1;%coefficient of friction
v=(cdg clr); %mid formula variable
A=(0.606*rho*g*cdg*d);%mid formula variable
a=(0.5*rho*(vmax.^3)*Cd0)%mid formula variable
b=((2*K)/(rho*vmax))%mid formula variable
ly=length(y)
vc=3.0;
z(1:ly)=1.0
for i=1:ly
x1(i)=0.5*(vs.^2)*Clmax*rho*z(i)
x2(i)=((0.90-(0.64-(4*a*b*((y(i))^2))).^0.5))/(2*b*(y(i)))
f(i)=(n/(y(i)*vto));
x3(i)=A/log((f(i)-U)/(f(i)-U-v))
x4(i)=((0.649e-4)*((a/y(i)).^2)*((n-(y(i)*vc)).^2)*rho*((Cd0/K).^0.5)))
end

```

```

plot (y,x1,'g',y,x2,'k',y,x3,'b',y,x4,'m')
title('Constraint Diagram');
ylabel('Wingloading (W/S N/m2)')
xlabel('Powerloading (W/P N/Watt)')
legend('Stall','Max Velocity','Takeoff','Rate of Climb')

```

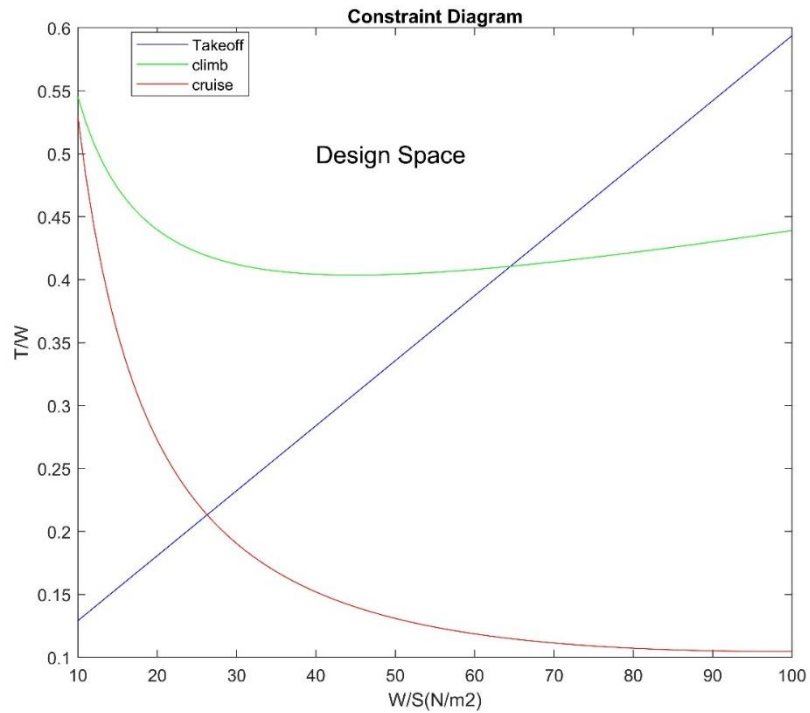


Figure A5: Constraint diagram form T/W approach

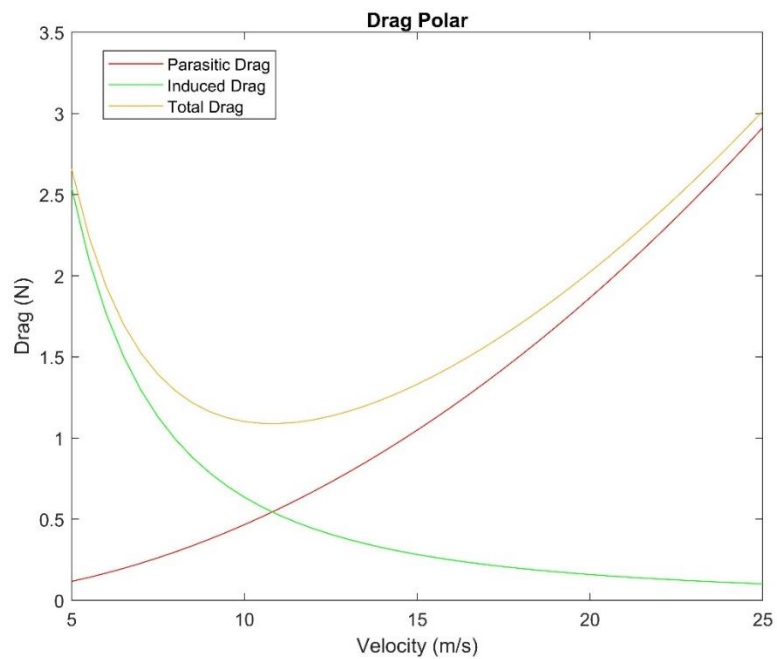


Figure A6: Drag required curve

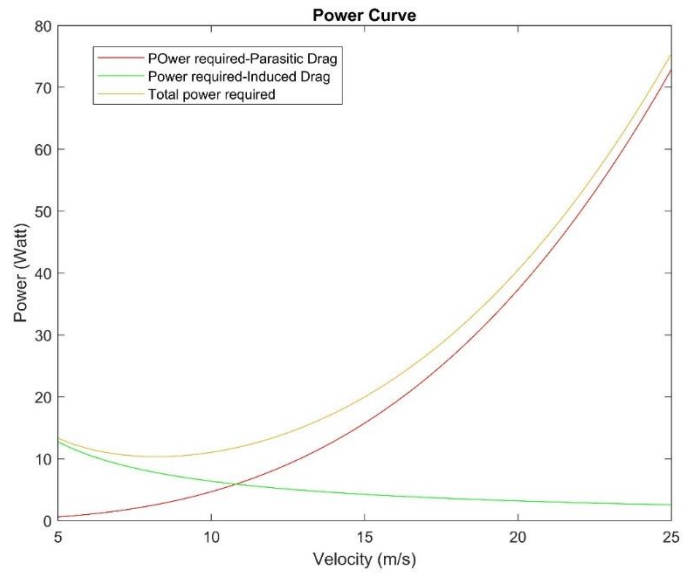


Figure A7: Power required curve

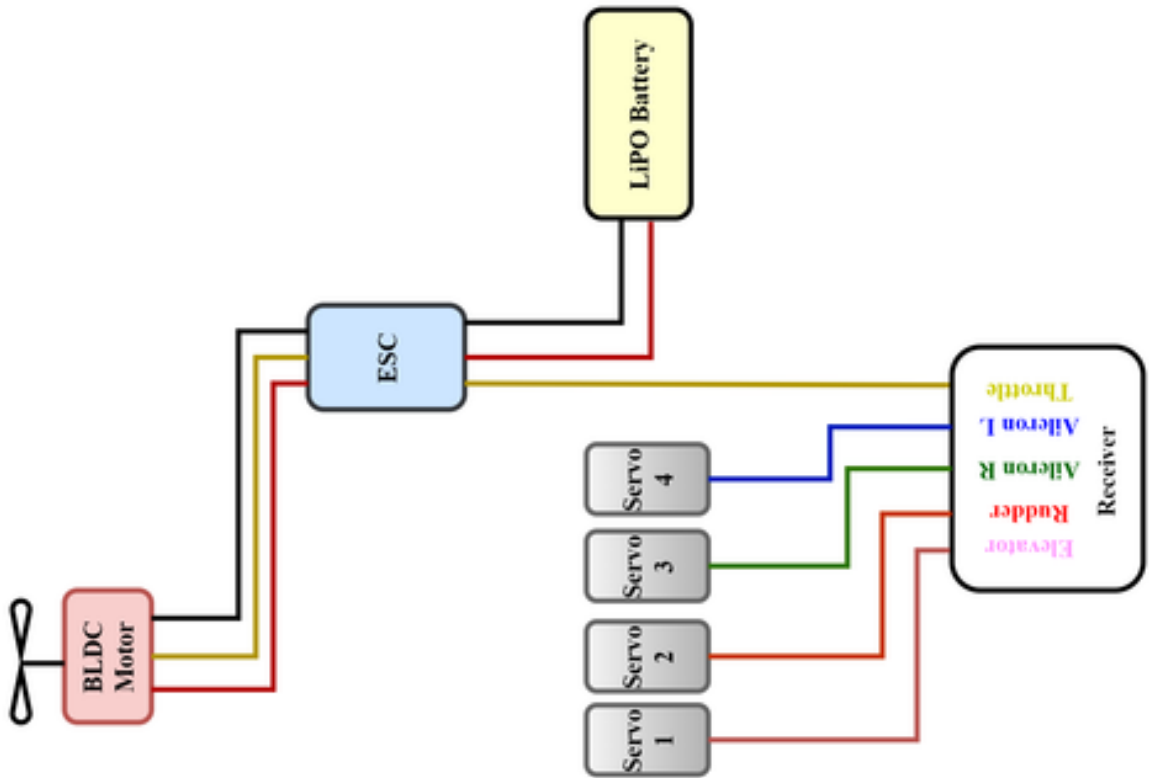


Figure A8: Circuit diagram

APPENDIX B

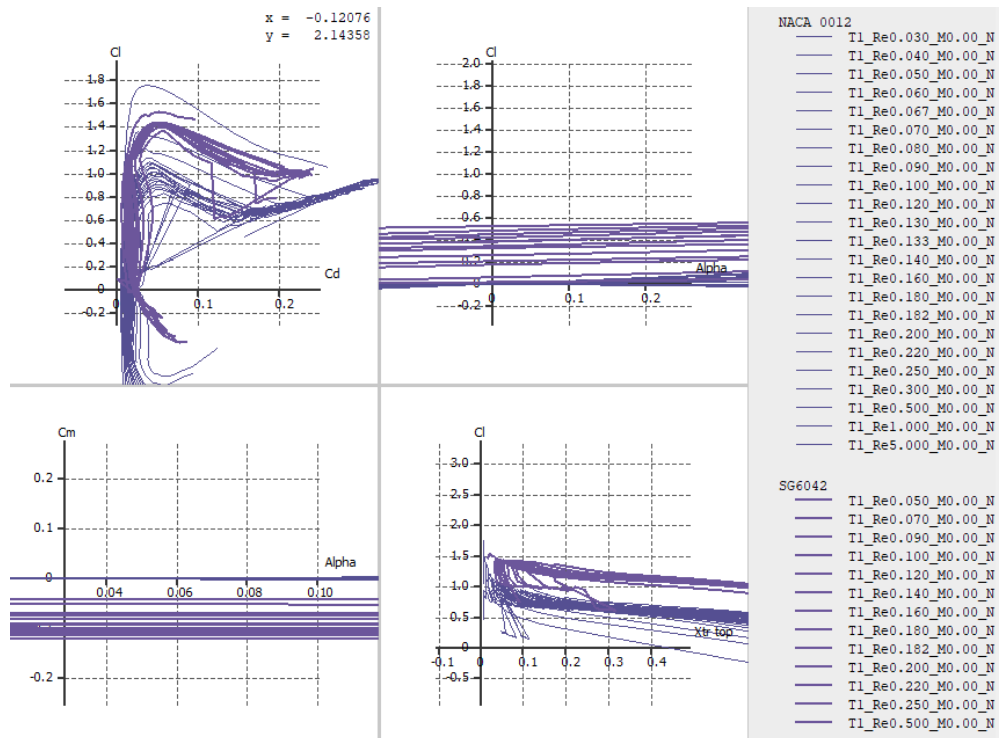


Figure B1: Batch analysis of NACA 0012 airfoil

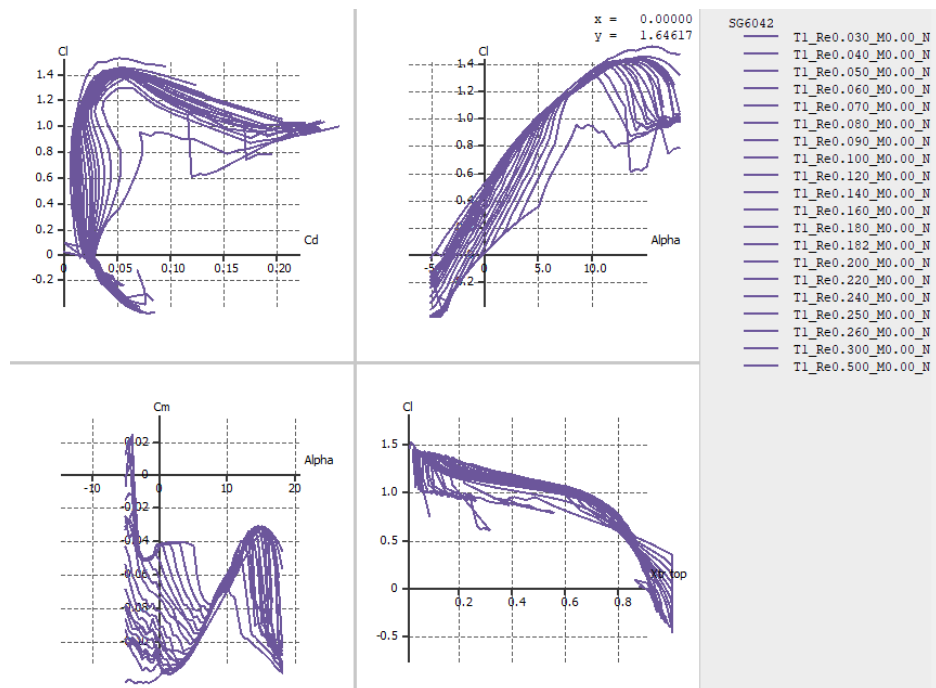


Figure B2: Batch analysis of SG6042 airfoil

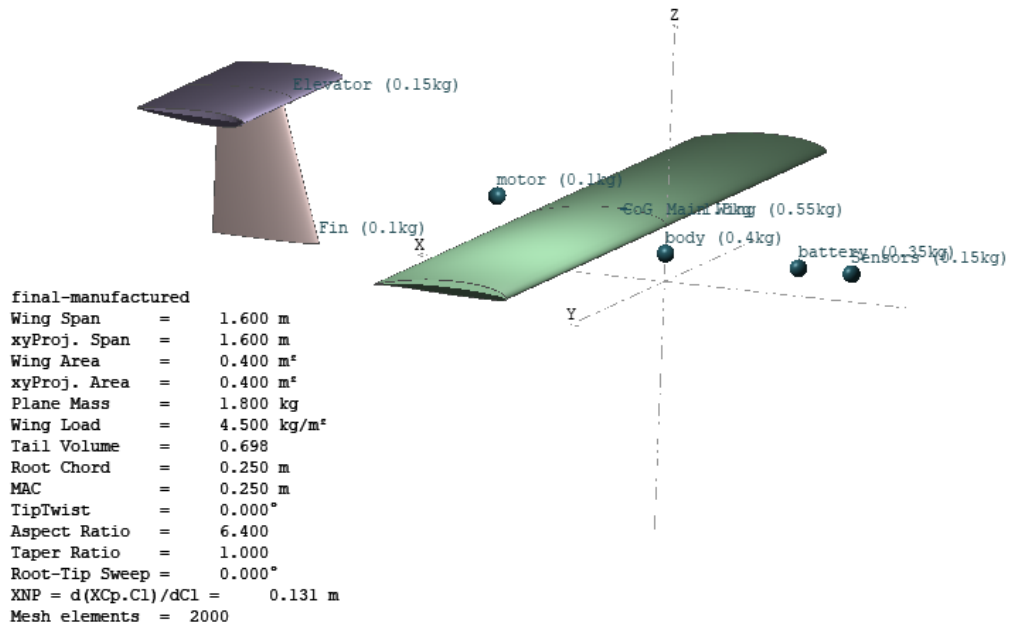


Figure B3: Mass distribution from XFLR5

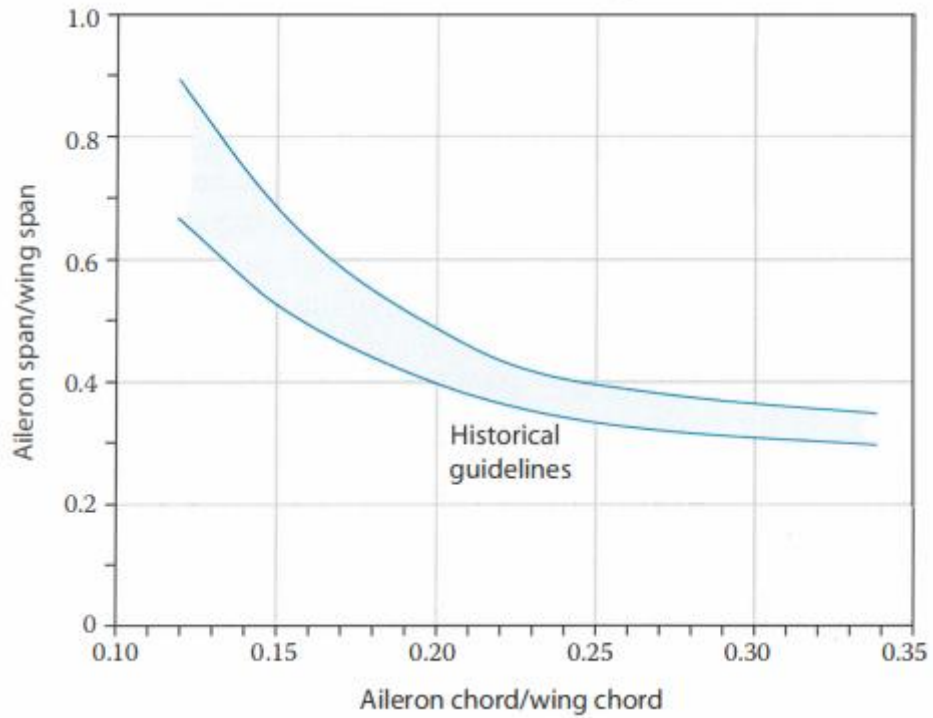


Figure B4: Aileron sizing guidelines (Source: Raymer)

Table B1: Power to weight ratio (Source: Raymer)

Aircraft Type	Typical P/W		Typical Power Loading(lb/hp)
	Hp/lb	Watt/g	
Powered Sailplanes	0.04	0.07	26
Homebuilt	0.08	0.13	12
General aviation-single engine	0.07	0.12	14
General aviation-twin engine	0.07	0.3	6
Agricultural	0.09	0.15	11
Twin turboprop	0.20	0.33	5
Flying boat	0.10	0.16	10

Table B2: Typical values of aspect ratio (Source: Raymer)

Propeller Aircraft	Equivalent Aspect Ratio
Homebuilt	6.0
General aviation-single engine	7.6
General aviation-twin engine	7.8
Agricultural	7.5
Twin turboprop	9.2
Flying boat	8.0

Table B3 Typical values of aspect ratio (Source: Raymer)

	Horizontal Tail		Vertical Tail	
	A	λ	A	λ
Fighter	3-4	0.2-0.4		
Sailplane	6-10	0.3-0.5	1.5-2.0	0.4-0.6
Others	3-5	0.3-0.6	1.3-2.0	0.3-0.6
T-tail	-	-	0.7-1.2	0.6-1.0

Table B4: Typical values of tail volume coefficient (Source: Raymer)

	Typical Values	
	Horizontal c_{HT}	Vertical c_{VT}
Sailplanes	0.50	0.02
Homebuilt	0.50	0.04
General aviation-single engine	0.70	0.04
General aviation-twin engine	0.80	0.07
Agricultural	0.50	0.04
Twin turboprop	0.90	0.08
Flying boat	0.70	0.06
Jet trainer	0.70	0.06
Jet fighter	0.40	0.07-0.12'
Military cargo/bomber	1.00	0.08
Jet transport	1.00	0.09



Figure B5: Laser-Egg 2+ (model LE201) (Source: amazon.com)

ORIGINALITY REPORT

14%

SIMILARITY INDEX

10%

INTERNET SOURCES

7%

PUBLICATIONS

6%

STUDENT PAPERS

PRIMARY SOURCES

1	mech.pcampus.edu.np Internet Source	2%
2	Mohammad H. Sadraey. "Aircraft Design", Wiley, 2012 Publication	1%
3	www.researchgate.net Internet Source	1%
4	eprints.qut.edu.au Internet Source	<1%
5	elibrary.tucl.edu.np Internet Source	<1%
6	www.scirp.org Internet Source	<1%
7	eprints.usm.my Internet Source	<1%
8	www.coursehero.com Internet Source	<1%
9	Submitted to University of Bedfordshire Student Paper	<1%